

CHARACTERIZATION OF SERPENTINE FILLED POLYPROPYLENE

A THESIS SUBMITTED TO
THE GRADUATE SCHOOL OF NATURAL AND APPLIED SCIENCES
OF
MIDDLE EAST TECHNICAL UNIVERSITY

BY

SEMRA CAN

IN PARTIAL FULFILLMENT OF THE REQUIREMENTS
FOR
THE DEGREE OF DOCTOR OF PHILOSOPHY
IN
POLYMER SCIENCE AND TECHNOLOGY

MARCH 2008

Approval of the thesis:

CHARACTERIZATION OF SERPENTINE FILLED POLYPROPYLENE

submitted by **SEMRA CAN** in partial fulfillment of the requirements for the degree of **Doctor of Philosophy in Polymer Science and Technology Department, Middle East Technical University** by,

Prof. Dr. Canan Özgen
Dean, Graduate School of **Natural and Applied Sciences**

Assoc. Prof. Dr. Göknur Bayram
Head of Department, **Chemical Engineering Dept.**

Prof. Dr. Teoman Tinçer
Supervisor, **Chemistry Dept.**

Examining Committee Members:

Prof. Dr. Erdal Bayramlı
Chemistry Dept., METU

Prof. Dr. Teoman Tinçer
Chemistry Dept., METU

Prof. Dr. Cevdet Kaynak
Metallurgical and Materials Engineering Dept., METU

Prof. Dr. Halil İbrahim Ünal
Chemistry Dept., Gazi University

Prof. Dr. Ülkü Yılmaz
Chemical Engineering Dept., METU

Date: 21.03.2008

I hereby declare that all information in this document has been obtained and presented in accordance with academic rules and ethical conduct. I also declare that, as required by these rules and conduct, I have fully cited and referenced all material and results that are not original to this work.

Name, Last name: Semra Can

Signature :

ABSTRACT

CHARACTERIZATION OF SERPENTINE FILLED POLYPROPYLENE

Can, Semra

Ph.D., Department of Polymer Science and Technology

Supervisor: Prof. Dr. Teoman Tinçer

March 2008, 158 pages

In this study, the aim is to prepare polypropylene (PP)/serpentine composites and study their mechanical, thermal and morphological properties. Another objective is to explore whether it is possible to have PP/serpentine nanocomposites with melt intercalation method by using the advantage of the layer silicate structure of serpentine. The most widely used fillers in PP are talc and mica which belong to the phyllosilicates group of silicate minerals. So far, there has been almost no study employing serpentine as filler in either any polymers or PP, although it also belongs to the same group of minerals as talc and mica.

Accordingly, it was planned to divide the work into the study of two groups. In group 1, for the compositions with 2, 5, 10 and 20 wt% serpentine, the particulate filler effects of serpentine both alone and in the presence of surface treatments with hydrochloric acid (HCl) and silane coupling agent (SCA) were investigated. The most impressive results in terms of static and dynamic mechanical properties were achieved with SCA rather than HCl. When the effect of serpentine without

any treatment is considered, reinforcing effect of it can easily be observed without deteriorating the composite properties even at high filler loadings.

In group 2, the nanofiller effects of serpentine in 2 and 5 wt% filled compositions by modification of both the filler and the matrix were aimed to be examined with melt intercalation method. In addition to HCl and SCA treatments, maleic anhydride grafted polypropylene (PP-g-MA) and quaternary ammonium salt (QAS) of cetyl-trimethyl-ammonium bromide were used as compatibilizer and intercalating agent, respectively. While the amount of QAS was kept constant, different percentages of compatibilizer were employed. The presence of QAS and PP-g-MA further improved the properties with respect to group 1 members. Interestingly, the percentage strain at break values did not decrease as much as group 1 compositions with the same filler content. It can be concluded that partial intercalation of group 2 compositions was achieved, according to the X-ray and TEM results.

Keywords: Serpentine, PP/serpentine composites, SCA, PP-g-MA, serpentine nanocomposites

ÖZ

SERPENTİN DOLGULU POLİPROPİLENİN KARAKTERİZASYONU

Can, Semra

Doktora, Polimer Bilimi ve Teknolojisi Bölümü

Tez Yöneticisi: Prof. Dr. Teoman Tinçer

Mart 2008, 158 sayfa

Bu çalışmanın amacı polipropilen (PP)/serpentin kompozitlerinin hazırlanması ve bu kompozitlerin mekanik, termal ve morfolojik özelliklerinin incelenmesidir. Diğer bir amaç ise tabakalı silikat yapısına sahip olan serpentinin bu özelliğinin kullanılarak araya sokma metodu ile PP/serpentin nanokompozitlerinin elde edilip edilemeyeceğini görmektir. PP'nin güçlendirilmesinde yaygın olarak kullanılan talk ve mika silikat minerallerinin tabakalı silikatlar grubuna girmektedir. Serpentin minerali de bu grupta yer almasına rağmen hemen hemen hiç bir çalışmada dolgu malzemesi olarak bir polimerde ve de PP'de kullanılmamıştır.

Bu amaçla, çalışmanın iki grupta toplanması planlanmıştır. Birinci grupta, ağırlıkça %2, 5, 10 ve 20 serpentin içeren kompozisyonlar için serpentinin hem doğal olarak hem de hidroklorik asit (HCl) ve silan bağlayıcı (SCA) uygulamalarıyla dolgu malzemesi olarak etkileri incelenmiştir. Statik ve dinamik mekanik özellikler göz önüne alındığında en etkileyici sonuçlar, HCl uygulamasından ziyade SCA kullanımında elde edilmiştir. Yüksek dolgu maddesi

miktarlarında dahi serpentin doğal haliyle kullanıldığında kompozit özellikleri bozulmadan güçlendirici etki görülmüştür.

İkinci grupta, ağırlıkça %2 ve 5 serpentin içeren kompozisyonların hem dolgu maddesi hem de matrisin modifiye edilmesiyle serpentinin bir nano dolgu maddesi olarak etkilerinin çalışılması amaçlanmıştır. HCl ve SCA uygulamalarının yanı sıra maleik anhidrit aşılınmış polipropilen (PP-g-MA) uyumlaştırıcı, bir kuaterner amonyum tuzu olan setil-trimetil-amonyum bromür ise araya sokma ajanı olarak kullanılmışlardır. QAS miktarı sabit tutularak, PP-g-MA miktarı değiştirilmiştir. Grup 1 kompozitleriyle karşılaştırıldığı zaman QAS ve SCA varlığında, özelliklerin daha fazla iyileştiği görülmüştür. İlgi çekici bir sonuç ise, kırılmadaki yüzde uzama miktarlarının, aynı oranda dolgu maddesi içeren grup 1 kompozitlerine göre daha az miktarda azalmasıdır. Sonuç olarak X ışınları ve geçirimli elektron mikroskopisi analizlerine göre grup 2 kompozisyonları için serpentin tabakalarında kısmi bir araya girmenin olduğunu söylemek mümkündür.

Anahtar Kelimeler: Serpentin, PP/serpentin kompozitleri, silan bağlayıcı, maleik anhidrit aşılınmış polipropilen, serpentin nanokompozitleri

To my mother

ACKNOWLEDGEMENTS

I would like to express my deepest gratitude to my supervisor Prof. Dr. Teoman Tinçer for his support, encouragement and guidance throughout the study.

I am grateful to Prof. Dr. Erdal Bayramlı and Prof. Dr. Ülkü Yılmaz for their valuable discussions during the progress of this study and giving me the opportunity of using the instruments in their laboratories.

I would like to thank to Prof. Dr. Yavuz Topkaya, Prof. Dr. Muharrem Timuçin who let me use the milling equipments and Dr. İbrahim Çam for particle size measurements and helpful comments.

I would like to appreciate Prof. Dr. Asuman Türkmenoğlu for her help in thin section analysis and Prof. Dr. Tayfur Öztürk for his understanding and support during the period of writing of my thesis.

I am thankful to Dr. Mustafa Öztürk from MTA for his help in X-ray analysis and Attila Alkan from Brisa for his help in TEM analysis.

Help of my labmates, Osman Yaslıtaş and Salih Sarıkaya are gratefully acknowledged.

I am truly indebted to my parents and my love Serdar for their endless support, understanding and belief in me.

TABLE OF CONTENTS

ABSTRACT.....	iv
ÖZ.....	vi
DEDICATION.....	viii
ACKNOWLEDGEMENTS.....	ix
TABLE OF CONTENTS.....	x
LIST OF TABLES.....	xiv
LIST OF FIGURES.....	xvi
CHAPTER	
1. INTRODUCTION.....	1
1.1 Silicates: General Definition and Classification.....	1
1.1.1 Nesosilicates.....	3
1.1.1.1 The Olivine Group.....	3
1.1.2 Sorosilicates.....	5
1.1.3 Cyclosilicates.....	5
1.1.4 Inosilicates.....	6
1.1.5 Tectosilicates.....	6
1.1.6 Phyllosilicates.....	7
1.1.6.1 Pyrophyllite-Talc Group.....	10
1.1.6.2 Smectite Group.....	10
1.1.6.3 Vermiculate Group.....	11
1.1.6.4 Mica Group.....	11
1.1.6.5 Brittle Mica Group.....	12
1.1.6.6 Chlorite Group.....	12
1.1.6.7 Palygorskite-Sepiolite Group.....	13
1.1.6.8 Kaolin-Serpentine Group.....	13
1.2 Serpentine.....	13
1.2.1 Antigorite.....	16

1.2.2 Lizardite.....	17
1.2.3 Chrysotile.....	18
1.2.4 Polygonal Serpentine.....	19
1.3 Polymer Composites.....	20
1.4 Polypropylene Composites.....	22
1.4.1 The Use of Talc in Polypropylene.....	24
1.4.2 The Use of Calcium Carbonate in Polypropylene.....	25
1.4.3 The Use of Glass Fiber in Polypropylene.....	26
1.4.4 The Use of Mica and Other Fillers in Polypropylene.....	26
1.5 Polymer Nanocomposites.....	27
1.6 Polymer Clay Nanocomposites.....	29
1.6.1 Clays and Clay Structures.....	31
1.6.2 The Nanocomposite Structures.....	33
1.6.3 Production Methods of Polymer Clay Nanocomposites.....	35
1.6.3.1 In-situ Polymerization.....	35
1.6.3.2 Solution Intercalation.....	36
1.6.3.3 Melt Intercalation.....	36
1.7 Polypropylene Clay Nanocomposites.....	37
1.8 Aim of the Study.....	39
2. EXPERIMENTAL.....	40
2.1 Materials.....	40
2.2 Powder Serpentine Production.....	42
2.2.1 Treatments of Group 1.....	42
2.2.2 Treatments of Group 2.....	42
2.3 Preparation of Compositions.....	43
2.4 Characterization of Serpentine.....	45
2.4.1 Specific Gravity.....	45

2.4.2	X-Ray Analysis.....	45
2.4.3	Scanning Electron Microscopy (SEM).....	46
2.4.4	Differential Thermal Analysis (DTA) and Thermal Gravimetric Analysis (TG).....	46
2.4.5	Thin Section Analysis.....	46
2.4.6	Particle Size Measurement.....	46
2.4.7	Surface Characterization.....	46
2.5	Characterization of Composites.....	46
2.5.1	Impact Testing.....	46
2.5.2	Melt Flow Index (MFI).....	47
2.5.3	Tensile Testing.....	47
2.5.4	Differential Scanning Calorimetry (DSC).....	47
2.5.5	Dynamic Mechanical Analysis (DMA).....	47
2.5.6	X-Ray Analysis.....	48
2.5.7	Scanning Electron Microscopy (SEM).....	48
2.5.8	Transmission Electron Microscopy (TEM).....	48
3.	RESULTS AND DISCUSSION.....	49
3.1	Characterization of As-Received Serpentine.....	49
3.2	Characterization of Powder Serpentine.....	52
3.3	Impact Strength.....	54
3.4	Melt Flow Properties of Composites.....	57
3.5	Tensile Testing.....	60
3.6	Thermal Behavior and Crystallinity of the Matrices.....	69
3.7	DMA.....	72
3.8	X-Ray Analysis.....	86
3.9	Morphology of the Composites.....	92
3.10	TEM Study of QAS Treated Compositions.....	112

4. CONCLUSION.....	117
REFERENCES.....	120
APPENDICES	
A. PORE SIZE DISTRIBUTION GRAPHS.....	129
B. IMPACT STRENGTH DATA.....	139
C. MFI DATA.....	140
D. TENSILE PROPERTIES DATA.....	141
E. DSC THERMOGRAMS.....	147
F. TAN δ vs. TEMPERATURE GRAPHS.....	152
CURRICULUM VITAE.....	157

LIST OF TABLES

TABLES

Table 1.1	Nomenclature of the silicates [3].....	2
Table 1.2	General classification of phyllosilicates related to clay minerals [14].....	9
Table 1.3	Some important polymer clay composite applications [60].....	30
Table 2.1	Some properties of the polymers used in the study.....	40
Table 2.2	Group 1 compositions (X shows the treatment done).....	44
Table 2.3	Group 2 compositions (X shows the treatment done).....	45
Table 3.1	Volume based particle size (μm) data for serpentine powders after 48 hours of milling.....	53
Table 3.2	Tensile properties of group 1 compositions processed and reprocessed at 250 rpm.....	64
Table 3.3	DSC data for group 1 compositions.....	70
Table 3.4	DSC data for group 2 compositions.....	71
Table 3.5	T_g data of group 1 compositions obtained from $\tan \delta$	79
Table 3.6	Storage modulus and T_g data of group 2 compositions.....	85
Table 3.7	Diffraction angle and d-spacing data for all 2 and 5% filler loaded SCA treated compositions of group 1.....	89
Table 3.8	Diffraction angle and d-spacing data for group 2 compositions...	92

Table B.1	The variation of impact strength (kJ/m^2) with respect to group 1 compositions.....	139
Table B.2	The variation of impact strength (kJ/m^2) with respect to group 2 compositions.....	139
Table C.1	MFI (g/10 min) for group 1 compositions.....	140
Table C.2	MFI (g/10 min) for group 2 compositions.....	140
Table D.1	The tensile properties of group 1 compositions.....	141
Table D.2	The tensile properties of group 2 compositions.....	142

LIST OF FIGURES

FIGURES

Figure 1.1	The structure of a $[\text{SiO}_4]$ tetrahedron (\bigcirc : O anion, \bullet : Si cation).....	1
Figure 1.2	Linkage of $[\text{SiO}_4]$ tetrahedra for silicates (a) independent tetrahedron in orthosilicates, (b) double tetrahedral unit in orthosilicates, (c) tetrahedral ring (6-fold) in ring silicates, (d) a single chain in chain silicates, (e) a double chain in chain silicates, (f) infinite tetrahedral sheet in sheet silicates with an infinite two dimensional sheet, (g) infinite tetrahedral network in frame work silicates [5]	4
Figure 1.3	Octahedral sheets (a) trioctahedral, (b) dioctahedral [6].....	7
Figure 1.4	Schematic representations of the way in which (a) 1:1, (b) 2:1, (c) 2:1:1 phyllosilicates are built from T and O sheets [8].....	8
Figure 1.5	The structure of antigorite [8].....	16
Figure 1.6	The structure of lizardite [8].....	18
Figure 1.7	The structure of chrysotile [8].....	19
Figure 1.8	High resolution image parallel to the fiber axis of a polygonal serpentine [34].....	20
Figure 1.9	The structure of a 2:1 clay mineral [73] (\bullet : Si, \otimes : Mg or Al, \bigcirc : O, $\textcircled{\bullet}$: OH).....	32
Figure 1.10	Modification of clay layers with quaternary ammonium salt [74].....	32

Figure 1.11 The arrangements of alkyl ammonium ions in 2:1 layered silicates (a) monolayer, (b) bilayer, (c) paraffin type monolayer, (d) paraffin type bilayer structures [76].....	33
Figure 1.12 The structure of an intercalated nanocomposite.....	34
Figure 1.13 The structure of an exfoliated nanocomposite.....	34
Figure 2.1 The structure of A-1100 (γ -aminopropyl triethoxy silane).....	41
Figure 2.2 The structure of cetyl-trimethyl-ammonium bromide.....	41
Figure 3.1 A view of serpentine piece from Beynam region.....	49
Figure 3.2 X-ray diffraction pattern of as-received serpentine mineral.....	50
Figure 3.3 SEM pictures of as collected serpentine in (a) x2000, (b) x4000 magnifications.....	50
Figure 3.4 DTA/TG curves of serpentine in air and nitrogen.....	51
Figure 3.5 The thin section photographs of serpentine (magnification:40x) (a) a view under plain polarized light, (b) a view under cross polarized light.....	52
Figure 3.6 X-ray diffraction pattern of untreated and treated serpentine.....	53
Figure 3.7 Impact strengths (kJ/m^2) of group 1 compositions	55
Figure 3.8 Impact strengths (kJ/m^2) of group 2 compositions	57
Figure 3.9 MFI values of group 1 compositions.....	58
Figure 3.10 MFI values of group 2 compositions	59
Figure 3.11 Young's modulus (MPa) for group 1 compositions	61
Figure 3.12 Stress at yield (MPa) for group 1 compositions.....	62
Figure 3.13 Stress at break (MPa) for group 1 compositions.....	63

Figure 3.14 Percentage strain at break for group 1 compositions.....	63
Figure 3.15 Young's modulus (MPa) for group 2 compositions.....	65
Figure 3.16 Stress at yield (MPa) for group 2 compositions.....	66
Figure 3.17 Stress at break (MPa) for group 2 compositions.....	68
Figure 3.18 Percentage strain at break for group 2 compositions.....	68
Figure 3.19 Storage modulus versus temperature scan for (a) N, (b) H compositions.....	73
Figure 3.20 Storage modulus versus temperature scan for (a) S, (b) SH compositions.....	74
Figure 3.21 Storage modulus versus temperature scan for (a) S,250, (b) SH,250 compositions.....	75
Figure 3.22 Loss modulus versus temperature scan for (a) N, (b) H compositions.....	76
Figure 3.23 Loss modulus versus temperature scan for (a) S, (b) SH compositions.....	77
Figure 3.24 Loss modulus versus temperature scan for (a) S,250, (b) SH,250 compositions.....	78
Figure 3.25 Storage modulus versus temperature scan for (a) 2,4, (b) 5,10 compositions.....	81
Figure 3.26 Storage modulus versus temperature scan for (a) 2,6, (b) 5,15 compositions.....	82
Figure 3.27 Loss modulus versus temperature scan for (a) 2,4, (b) 5,10 compositions.....	83
Figure 3.28 Loss modulus versus temperature scan for (a) 2,6, (b) 5,15 compositions.....	84

Figure 3.29 X-ray diffraction patterns for (a) 2%, (b) 5% SCA treated normal compositions of group 1.....	87
Figure 3.30 X-ray diffraction patterns for (a) 2%, (b) 5% SCA and HCl treated compositions of group 1.....	88
Figure 3.31 X-ray diffraction patterns for (a) 2,4, (b) 5,10 compositions of group 2.....	90
Figure 3.32 X-ray diffraction patterns for (a) 2,6, (b) 5,15 compositions of group 2.....	91
Figure 3.33 SEM images of impact fractured surfaces of (a) 2-190, (b) 2-190-H, (c) 2-190-S, (d) 2-190-SH.....	93
Figure 3.34 SEM images of impact fractured surfaces of (a) 10-190, (b) 10-190-H, (c) 10-190-S, (d) 10-190-SH.....	98
Figure 3.35 SEM images of impact fractured surfaces of (a) 2-250,2-S, (b) 2-250,2-SH.....	102
Figure 3.36 SEM images of impact fractured surfaces of (a) 2,4-N, (b) 2,4-H, (c) 2,4-Q, (d) 2,4-HQ.....	104
Figure 3.37 SEM images of impact fractured surfaces of (a) 5,10-N, (b) 5,10-H, (c) 5,10-Q, (d) 5,10 HQ.....	108
Figure 3.38 SEM images of impact fractured surfaces of (a) 5,15-N, (b) 5,15-H, (c) 5,15-Q, (d) 5,15-HQ.....	110
Figure 3.39 TEM micrographs of 2,4-Q (a) X 2.5K, (b) X 150K.....	113
Figure 3.40 TEM micrograph of 2,4-HQ X 200K.....	114
Figure 3.41 TEM micrograph of 2,6-Q X 300K.....	114
Figure 3.42 TEM micrograph of 2,6-HQ X 300K.....	115
Figure 3.43 TEM micrograph of 5,10-Q X 200K.....	115
Figure 3.44 TEM micrograph of 5,10-HQ X 300K.....	116

Figure A.1	Adsorption isotherm of 48 hours milled serpentine.....	129
Figure A.2	Adsorption isotherm of 48 hours milled acid treated serpentine..	130
Figure A.3	BET plot of 48 hours milled serpentine.....	131
Figure A.4	BET plot of 48 hours milled acid treated serpentine.....	132
Figure A.5	V-t plot of 48 hours milled serpentine.....	133
Figure A.6	V-t plot of 48 hours milled acid treated serpentine.....	134
Figure A.7	BJH Adsorption plot of 48 hours milled serpentine.....	135
Figure A.8	BJH Adsorption plot of 48 hours milled acid treated serpentine..	136
Figure A.9	HK plot of 48 hours milled serpentine.....	137
Figure A.10	HK plot of 48 hours milled acid treated serpentine.....	138
Figure D.1	Stress-strain plots of (a) N, (b) H compositions.....	143
Figure D.2	Stress-strain plots of (a) S, (b) SH compositions.....	144
Figure D.3	Stress-strain plots of (a) 2,4, (b) 5,10 compositions.....	145
Figure D.4	Stress-strain plots of (a) 2,6, (b) 5,15 compositions.....	146
Figure E.1	DSC thermograms of group 1 compositions.....	147
Figure E.2	DSC thermograms of group 2 compositions.....	150
Figure F.1	Tan δ versus temperature scan for (a) N, (b) H compositions.....	152
Figure F.2	Tan δ versus temperature scan for (a) S, (b) SH compositions....	153
Figure F.3	Tan δ versus temperature scan for (a) S,250, (b) SH,250 compositions.....	154
Figure F.4	Tan δ versus temperature scan for (a) 2,4, (b) 5,10 compositions.....	155

Figure F.5 Tan δ versus temperature scan for (a) 2,6, (b) 5,15
compositions..... 156

CHAPTER 1

INTRODUCTION

1.1 Silicates: General Definition and Classification

The silicates comprise almost over 90% of the accessible crust of the Earth and its body down to the nickel-iron core beginning at 2900 km depth. Olivines, pyroxenes, amphiboles, micas, clay minerals, feldspars, quartz, aluminum silicates and garnets are the mostly found silicate minerals. While feldspars and quartz are greatly abundant in the crust, the upper part of the mantle is composed of mostly olivine and pyroxenes [1]. Many of them are transparent to translucent in thin sections; widely differ in other physical characteristics such as mode, habit, color, hardness, and cleavage [2].

Silicon is the second most predominant element in the Earth's crust that mainly found as silica (silicon dioxide) and as silicate minerals. The silicon tetrahedron, $[\text{SiO}_4]$, formed by tetrahedrally coordinated four oxygen anions around a silicon cation, constitutes the basic unit in silicate structures, as illustrated in Figure 1.1.

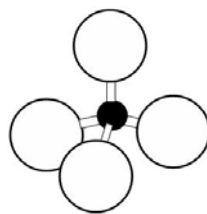


Figure 1.1 The structure of a $[\text{SiO}_4]$ tetrahedron (○: O anion, ●: Si cation)

Besides silicon atom, especially aluminum and magnesium atoms cooperate as cations in these inorganic compounds. Nevertheless, the minor replacements of other elements like titanium, iron, nickel and phosphorus are also possible [3,4]. These cation substitutions are one of the reasons of the presence of large number of silicate varieties [5].

There are different ways to classify the silicate minerals [5]. Although a structural classification is accepted universally, chemical and mineralogical nomenclatures are also widely used. In addition to the isolated $[\text{SiO}_4]$ tetrahedral structures, more complicated chains, two and three dimensional networks may form the crystal structure of the silicates. The dimensionality of silicate anions (D) could be zero, one, two or three; since silicate anions can extend to infinity in all dimensions. Multiplicity (M) is the number of single polyhedra, rings chains and layers that are linked to the anion of the same dimensionality [3]. Table 1.1 shows the chemical and mineralogical naming of the silicates.

Table 1.1 Nomenclature of the silicates [3]

Multiplicity	1	2	3	4	..
Dimensionality					
0	Monosilicates	Disilicates	Trisilicates	Tetrasilicates	..
Oligosilicates	Nesosub silicates	Neso silicates	Sorosilicates		
0	Monocyclo silicates	Dicyclo silicates	Tricyclo silicates	Tetracyclo silicates	..
Cyclosilicates					
1	Monopoly silicates	Dipoly silicates	Tripoly silicates	Tetrapoly silicates	..
(Inosilicates) Polysilicates					
2	Monophyllo silicates	Diphyllo silicates	Triphyllo silicates	Tetraphyllo silicates	..
Phyllosilicates					
3	Tectosilicates				
Tectosilicates					

The silicates with isolated ‘island’ structures are named as nesosilicates (orthosilicates) without oxygen sharing between two tetrahedra [3,5,6].

Sorosilicates (disilicates) are silicates in which sharing of oxygen atom between two silicon tetrahedra takes place. In cyclosilicates (ring silicates), a single tetrahedron shares two corners to form rings of three, four or six tetrahedra. Single or double chain inosilicates (chain silicates) are composed of infinitely long and linear chains [6]. In phyllosilicates (sheet silicates), a tetrahedron shares three corners to form infinite layers. In tectosilicates (frame work silicates), all four corners of a tetrahedron are shared to form three dimensional networks [4]. Figure 1.2 shows the linkage of tetrahedra for silicate structures.

1.1.1 Nesosilicates

The nesosilicates are composed of isolated $[\text{SiO}_4]$ tetrahedra in the absence of corner oxygen atom sharing. The tetrahedra are dispersed evenly between the metal ions resulting in dense close packed structures. They are hard and of high specific gravities than other silicate minerals with stubby, blocky or equidimensional crystals [7].

1.1.1.1 The Olivine Group

The general formula for the olivine minerals is M_2SiO_4 where M is usually Mg, Fe or Ca. The olivine has a hexagonal close packed structure in that M and Si cations occupy one half of the octahedral and one eighth of the tetrahedral sites respectively. Mg_2SiO_4 (forsterite) and Fe_2SiO_4 (fayalite) are the most abundant natural olivines [8].

Orthorhombic olivine crystals are prismatic and tabular in habit. They are generally in the form of rounded, disseminated, glassy grains and granular aggregates. The hardness and specific gravity change 6.5 to 7 and 3.2 to 3.6, respectively. Most are green in color, while for Fe rich compositions the color changes from light green to yellow. Olivine is usually found in mafic and ultramafic igneous rocks. Commonly, it alters to serpentine, magnetite, limonite, magnesite, opal, and garnierite along its grain boundaries. [9,10].

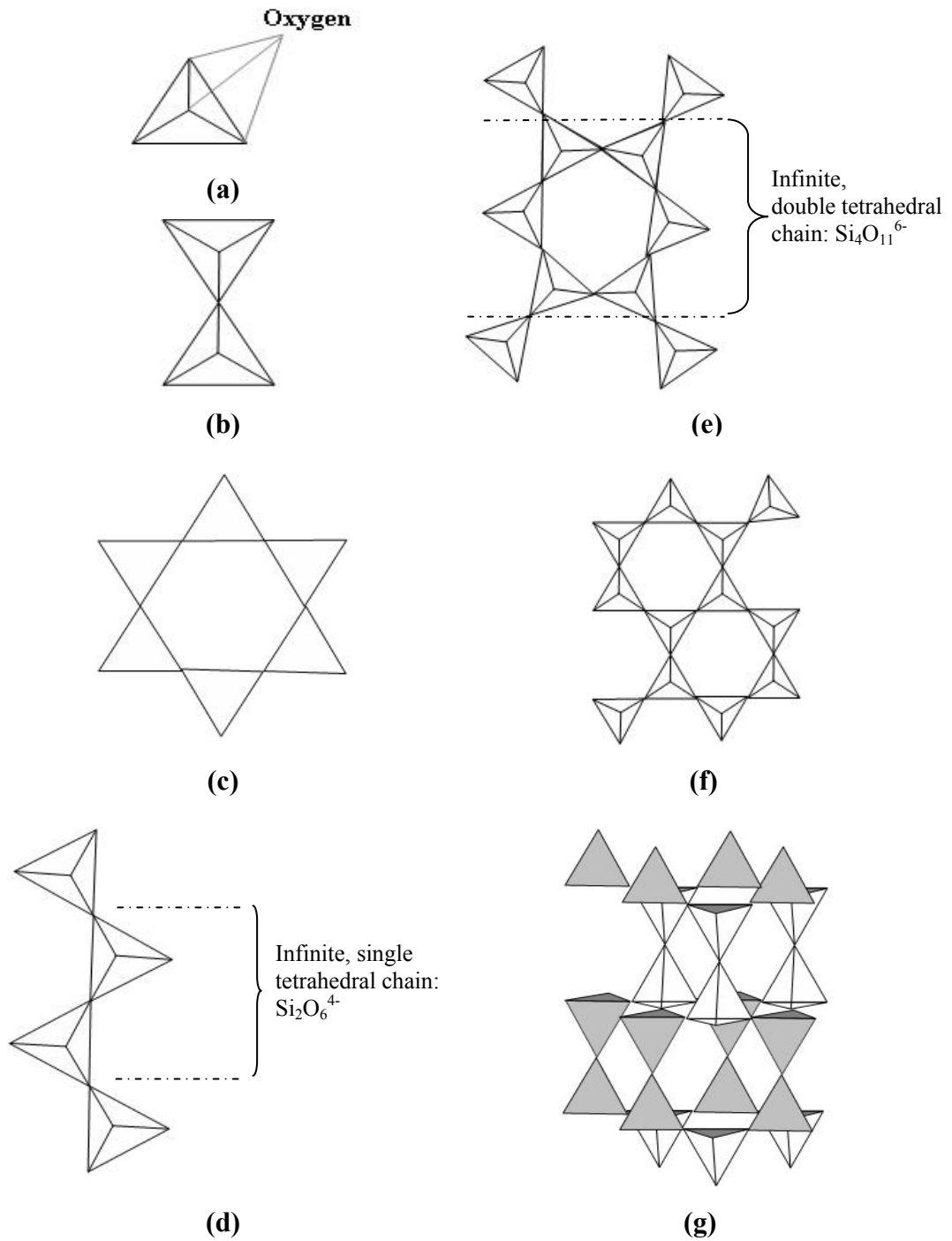


Figure 1.2 Linkage of $[\text{SiO}_4]$ tetrahedra for silicates (a) independent tetrahedron in orthosilicates, (b) double tetrahedral unit in orthosilicates, (c) tetrahedral ring (6-fold) in ring silicates, (d) a single chain in chain silicates, (e) a double chain in chain silicates, (f) infinite tetrahedral sheet in sheet silicates with an infinite two dimensional sheet, (g) infinite tetrahedral network in framework silicates [5]

1.1.2 Sorosilicates

This type of silicates consists of isolated double tetrahedra formed by corner oxygen sharing with silicon to oxygen ratio of 2:7. In these minerals, the connection between the tetrahedra pairs is accomplished by metal and hydroxyl groups and by water molecules. Commonly, in epidote group (zoisite, clinozoisite, epidote, allanite) all silicates have monoclinic crystals. Allanite has a complex silicate structure of which may be derived from the epidote. When some of the Ca ions replace with rare earths and some of the Fe (III) ions with Fe (II), then epidote structure is transferred to allanite. By these replacements, allanite may vary greatly in composition even it may contain radioactive thorium. In epidote group since the structures of the group members are similar, ionic replacements are the key point determining the variability of the crystals [7,11].

1.1.3 Cyclosilicates

This class of silicates is also known as ring silicates due to curved structure of $[\text{SiO}_4]$ tetrahedra to form closed rings where the metallic cations occupy the region between them. Benitoite has a simplest three group triangular ring with hexagonal, euhedral to subhedral crystals having deep blue to pale blue color. Axinite with four group ring is triclinic in structure and usually tabular with overtones of reddish or purplish brown color. Beryl and tourmaline have six group rings that are arranged in flat sheets. Although, some beryl and tourmaline samples crack, usually the easy cleavage is not observed due to the strong bonds holding the ring sheets together. Beryl has lots of varieties named according to the color they have: emerald, pale to dark blue-green; aquamarine, pale blue to medium blue, also bluish-green; morganite, pink, pale violet-pink and pink-orange; goshenite, colorless; golden beryl, yellow. As in beryl, tourmaline varieties are extensive naming schorl, rich in iron; dravite, rich in magnesium, usually brown in color, lithia tourmaline commonly pink, red, green or blue in color [7].

1.1.4 Inosilicates

Inosilicates are formed from indefinitely long, linear either single or double chains. In single chain silicates, two bridging oxygen atoms per a tetrahedron link $[\text{SiO}_4]$ tetrahedra to each other leading to a chain repeat after two tetrahedra. Double chain silicates assume two single chains with corner sharing of three oxygens of half of the tetrahedra and two oxygens of the other half. Pyroxenes for single chain and amphiboles for double chain members are two important subclasses of inosilicates. Both employ mostly monoclinic structures with the same cations and show similar crystallographic, physical and chemical properties. The amphiboles contain OH groups which generally give them slightly lower specific gravity and refractive indices than corresponding pyroxene analogues [11]. While the most common occurrence of pyroxenes is in stubby or blocky crystals, that of amphiboles is in long prismatic and acicular even fibrous habits. For either species, the cleavage pattern may be seemed as another identification tool showing the cleavage angles under magnification [7].

1.1.5 Tectosilicates

Framework silicates or network silicates are used synonymously in place of tectosilicates. In these silicates, four corners of all tetrahedra are shared forming a three dimensional open framework structure. If the structure does not include any cations in place of Si, then the network adopts to SiO_2 composition. In the case where Al replaces with Si, some interstitial cations are needed to satisfy the charge balance. Feldspars are the major constituent for the aluminosilicates whose structures are affected with the change in temperature, pressure and composition [8]. Other than feldspars, silica minerals, kalsilite, cordiorite, feldspathoids, scapolites and zeolites are placed within tectosilicates. When their structures are examined in detail, it is seen that most have different characteristics, e.g. four-membered loops in feldspars and six membered loops in beryl and cordierite. The silica minerals occur in different polymorphs such as quartz, cristobalite and tridymite. Among them, quartz, a constituent of glasses, is the most common form.

The zeolites are very essential minerals with more than 40 varieties in nature and more than 100 synthetic forms in laboratory applications [10].

1.1.6 Phyllosilicates

The phyllosilicates are also named as layer or sheet silicates which are made up of octahedral and tetrahedral sheets, combination of which leads to the formation of layers. Tetrahedral sheets, see Figure 1.2 (f) have a T_2O_5 composition, where T is the tetrahedral cation, generally being Si, Al or Fe ions [6,12]. In the tetrahedral sheets, three basal oxygens per a silicon tetrahedron are shared leading to hexagonal mesh pattern with a chemical formula $Si_2O_5^{2-}$. In the octahedral sheets, octahedral sites that are formed between OH anions are filled by either divalent or trivalent cations. These are Mg, Al, Fe (II or III) ions, but Li, Ti, V, Cr, Mn, Co, Ni, Cu and Zn ions could also be observed. In the case of divalent cations, all three octahedral sites are filled giving a trioctahedral sheet. A dioctahedral sheet is formed when the trivalent cations fill only two of the three sites, as shown in Figure 1.3. The basic building unit of a sheet silicate is formed by different stacking of the layers of octahedral and tetrahedral sheets [5,6,12].

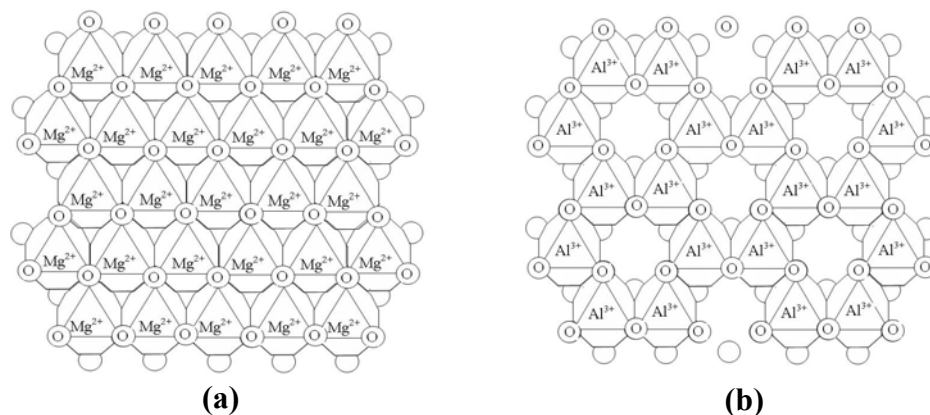


Figure 1.3 Octahedral sheets (a) trioctahedral, (b) dioctahedral [6]

The phyllosilicates can be classified in accordance with how the sheets are combined in three types. In 1:1 or T.O. type, one tetrahedral sheet and one octahedral sheet are combined to make a layer. In 2:1 or T.O.T. type, a layer is formed from two tetrahedral sheets outside of an internal octahedral sheet. The stacking of the layers is maintained with weak van der Waals forces if the interlayers are neutral. Otherwise, in the case of charge imbalance, in either sheet due to substitutions, the cations between the layers hold them together. In 2:1:1 layer silicates, there is an additional octahedral layer between the layers of 2:1 structure, as shown in Figure 1.4. The linkage between the tetrahedral and octahedral sheets brings some misfit. However, there are many substitutions causing variation in mesh sizes of the sheets [8].

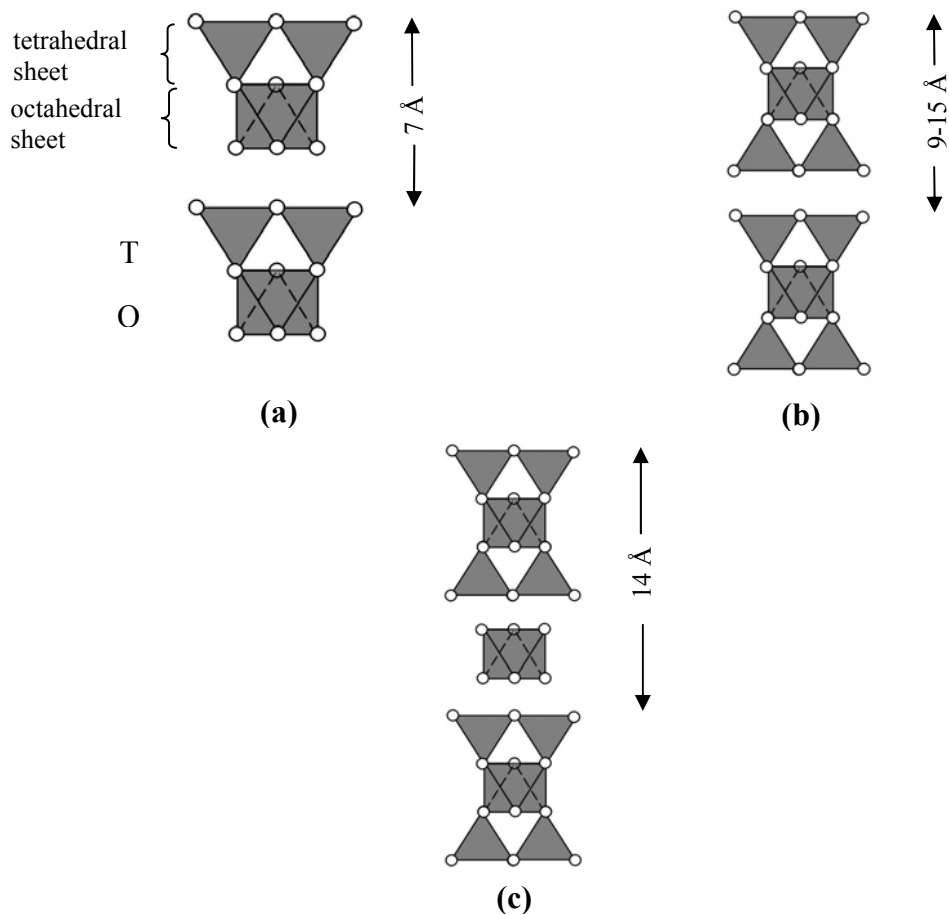


Figure 1.4 Schematic representations of the way in which (a) 1:1, (b) 2:1, (c) 2:1:1 phyllosilicates are built from T and O sheets [8]

The phyllosilicates are categorized into eight groups according to the layer type and layer charge, see Table 1.2. A further division is possible on the basis of octahedral sheet type (dioctahedral or trioctahedral), chemical composition, and the geometry of layer and interlayer superposition. Kaolinites, illites, montmorillonites and vermiculates which constitute the large part of phyllosilicates are included in the clay group [13-15].

Table 1.2 General classification of phyllosilicates related to clay minerals [14]

Layer type	Group	Subgroup	Examples of species
1:1	Kaolin-serpentine (X~0)	Serpentines	Chrysotile, antigorite, lizardite , amesite, berthierine
		Kaolines	Kaolinite, dickite, nacrite
2:1	Pyrophyllite-talc (X~0) Smectite (X~0.2-0.6)	Talcs	Talc
		Phyrophyllites	Phyrophyllite
		Montmorillonites (dioctahedral) Saponites (trioctahedral)	Montmorillonite, beidellite, nontronite Saponite, hectorite, saunonite, stevensite
	Vermiculate (X~0.6-0.9)	Dioctahedral vermiculates	Dioctahedral vermiculate
		Trioctahedral vermiculates	Trioctahedral vermiculate
Mica (X~1.0)	Dioctahedral micas	Muscovite, paragonite, illite, glauconite	
		Trioctahedral micas	Phlogopite, biotite, lepidolite, (illite)
	Brittle mica (X~2.0)	Dioctahedral brittle micas Trioctahedral brittle micas	Margarite Clintonite
(2:1:1)	Chlorite (X variable)	Dioctahedral chlorites	Donbassite
		Trioctahedral chlorites	Chlorite s.s., clinochlore, Chamosite, nimite
		Di, trioctahedral chlorites	Cookeite, sudoite
2:1	Palygorskite-sepiolite (=fibrous clays)	Palygorskites	Palygorskite
Inverted ribbons	(X variable)	Sepiolites	Sepiolite, xylotile

X = layer charge per formula unit. X refers to an $O_{10}(OH)_2$ formula unit for smectite, vermiculite, mica and brittle mica.

1.1.6.1 Pyrophyllite-Talc Group

Pyrophyllite, $\text{Al}_2(\text{Si}_4\text{O}_{10})(\text{OH})_2$, is a soft mineral that occurs generally with quartz and mica in hydrothermal veins and certain alumina rich metamorphic rocks. It usually has lamellar appearance, greasy feel and single perfect cleavage with hardness of 1 to 2 and specific gravity of 2.8 [15,16].

Talc is a hydrous magnesium silicate, $\text{Mg}_3(\text{Si}_4\text{O}_{10})(\text{OH})_2$, occurring mostly in igneous rocks as a byproduct of silicate minerals. The structure may resemble that of pyrophyllite; however talc is a trioctahedral mineral where the octahedral sites are occupied by magnesium. It usually exhibits smooth and greasy feel, pearly luster and perfect cleavage in one direction. Its color and streak are white. The specific gravity and hardness are between 2.7 to 2.8 and 1 to 1.5, respectively [15,16].

1.1.6.2 Smectite Group

Smectites have a 2:1 layer structure with low layer charge ($X < 0.6$) which results in weak linkages between the stacking layers. These minerals have high cation exchange capacity exhibiting considerable water or organic liquid take up into interlayers, which are occupied especially with Na, K or Ca cations and one to several layers of water. They are mostly found in fine grained vermiform, lamellar or spherulitic aggregates [14,16].

Montmorillonites are dioctahedral smectites formed by the alteration of volcanic and basic igneous rocks by replacement of small amount of Al into Si in tetrahedral sheet with a structural formula $(\text{Na})_{0.7}(\text{Al}_{3.3}\text{Mg}_{0.7})\text{Si}_8\text{O}_{20}(\text{OH})_4 \cdot n\text{H}_2\text{O}$. Montmorillonites can be seen as irregular, extremely thin platelets when the aggregation is well oriented. They sometimes exhibit a fibrous texture and more rarely well formed, pseudo-hexagonal plates [16,17].

1.1.6.3 Vermiculate Group

This class of phyllosilicates is found as clay sized vermiculates in sediments as trioctahedral and dioctahedral minerals, although they usually occur as a mixed clay layer. Since most of them are formed by the degradation of other sheet silicates, their properties are dependent upon the starting material. Generally macroscopic vermiculates are obtained from biotite by the removal of potassium and they can be easily recognized. Although these vermiculates mostly contain Mg in the interlayer position, small amounts of Ca, Na and K may present in many samples. In soils, where the weathering conditions are not so aggressive, vermiculate layers are found as interstratified, in which the individual crystals have basic unit layers of two or more types, with mica and chlorite layers. Most of the clay vermiculates occur when K ions are removed from biotite, muscovite and illite and the brucite sheet from the chlorite accompanied by the oxidation of much of the iron in the 2:1 layer. The charge and composition of clay vermiculates may vary widely [17].

1.1.6.4 Mica Group

Mica minerals have monoclinic crystallites of six-sided, flat base tablets which seem to be short and hexagonal prisms. The flat bases of the crystals are shiny cleavage faces and the side faces, of which are much elongated in some crystals, are rough and striated. Besides micas commonly occur as irregular flakes and scales with bright cleavage faces, they are also frequently seen in igneous rocks as rock components. The way that they cleave and their high luster make them differ from other rock forming minerals. For micas, the elasticity of thin lamina is the distinguishing factor from chlorite and talc. While chlorites and talc have flexible flakes, the micas have elastic flakes. The hardness and specific gravity change from 2 to 3 and 2.76 to 3.2, respectively. Chemically, the micas can be divided into two categories as light-colored and dark-colored. Muscovite is the most common variety of the former group, excluding iron and magnesium in its

structure. However these cations are found in biotite mineral which is the most common subclass of dark-colored micas [8].

1.1.6.5 Brittle Mica Group

The brittle micas, which may be found as either dioctahedral or trioctahedral forms, are different from the true micas in that they have high layer charge (-2 per formula unit instead of -1) and bivalent compensation cations other than univalent cations in interlayers. The erosion and alteration of crystalline schists lead to the formation of brittle micas, e.g. clintonite and margarite. They do not often take part in the clay-sized part of sedimentary rocks due to their unavailability at the Earth's surface and resistance to fragmentation [14].

1.1.6.6 Chlorite Group

This group may be considered both as 2:1 and 2:1:1 due to the presence of hydroxide interlayer. Commonly the most of them are monoclinic in their structure where the negatively charged trioctahedral sheets alternate with positively charged octahedral sheets. Typically, trioctahedral chlorites are common having Mg as the main cation in layers and interlayers. Occasionally, chlorites with a dioctahedral type and a combination of dioctahedral layers with trioctahedral hydroxide interlayers are found [14]. In some varieties, aluminum substitutes for magnesium or iron which may replace with chromium, nickel or manganese in appreciable amounts. Due to these extensive substitutions, the chlorite varieties are great in number: penninite, clinochlore, kaemmererite etc. Although the chlorites are not brittle, they are easily cleaved to numerous thin, flexible foliations like mica. The color is dominantly variable green or yellow, violet, brown even white. Chlorites usually form from the rocks which are previously altered iron, magnesium and aluminum containing pyroxenes, amphiboles and biotites [7,15].

1.1.6.7 Palygorskite-Sepiolite Group

These minerals in fact have a needle like morphology and may not seem to be sheet silicates. Since they incorporate chemically absorbed water within their structures and occur in the clay environments, they are called as sheet silicates. The structure is largely two dimensional with shortened layers formed by linking of the octahedral and tetrahedral unit chains in the a-b crystallographic direction and extending semi infinitely in the c direction. The water and exchange ions are found in the inner channels along the interlinked chains. Although their structures are similar to smectites, these minerals experience less cation exchange capacity compared to them. Both minerals occur mostly in certain lacustrine and primarine basins and in the environments with high Si content since they are rich in this cation [17].

1.1.6.8 Kaolin-Serpentine Group

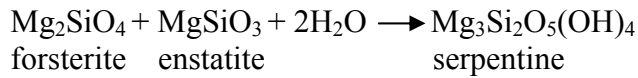
Kaolins are dioctahedral and serpentines are trioctahedral subgroups of the 1:1 layer silicates. Kaolins are hydrous aluminum silicates with small amount of other constituents, always having some MgO and Al₂O₃. Serpentines are hydrated magnesium silicates with small amounts of Al₂O₃ and Fe₂O₃. Kaolinite is the most abundant variety of kaolins formed by the acid leaching of alkaline rocks, e.g. feldspars and micas. Practically, any silicate rock may turn into kaolinite when the conditions are suitable for leaching. [17,19].

1.2 Serpentine

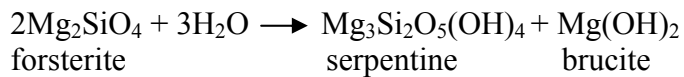
The origin of word serpentine is not exactly known but it may refer to color green. The chemical formula of the principal minerals of the serpentine group is approximately Mg₃Si₂O₅(OH)₄ with a repeating unit distance of almost 7 Å (0.7 nm) [5,6]. Some cation replacements of magnesium and silicon with aluminum, ferric and ferrous ions and sometimes with nickel or cobalt ions are possible [20]. There are basically three types of serpentine varieties: antigorite, lizardite and

chrysotile. The serpentine structures are analogues to kaolin group, although the chrysotile serpentine occurs in silky fibres which are aligned across the veins and their length. Chrysotiles have curved layers along one direction such that they are seemed as either concentric hollow cylinders or rolls parallel to that direction. Lizardites have fine grained and platy morphology when observed under high magnification. Antigorite has alike b dimension and (001) spacing of the unit cell as in chrysotile and lizardite, but has a rather large a dimension, mostly near to 40 Å. When thin sections of massive serpentine are analyzed between crossed polarizers; mesh, window and hour glass structures reflecting the morphology of the previously serpentinized olivine or pyroxenes are seen [21,22].

Serpentines are interesting class of phyllosilicates due to their formation and distribution. The word serpentinite is used if the serpentine minerals constitute almost exclusively of the ultramafic rocks formed through the hydrothermal alteration of pyroxenites, peridotites and dunites [23]. Other components can be magnetite, limonite, chlorite and tremolite. The ores may contain chromite, nickel and often a great amount of soapstone (steatite) as in South Africa and Sudbury, Ontario, Canada. The serpentine minerals are located along the great mountains and island arcs e.g. Great Serpentine Belt of New South Wales, Austria. Another belt starts from the Alps and go through the Asia Minor to the East Indies and the Philippines; they are also associated with the fold mountain ranges of the Americas. Although the origin of these minerals is still unknown, principally they are derived from the ultrabasic rocks. As it can be concluded from the experimental studies, the water vapor charged with silica or carbon dioxide may either remove magnesia or add silica to the original olivines or pyroxenes which are changed through this effect. The temperature is a very important factor in determining the nature of the changes, for example with a decrease in temperature and in the presence of water; olivine may turn into enstatite or enstatite and talc or serpentine [24]. In a study done on the MgO-SiO₂-H₂O system showed that serpentine formation is unlikely above 500°C and it is possible with water vapor on forsterite below 400°C.



According to the same study, it was also noted that the olivine and pyroxene were intruded in their crystalline state without water and subsequently serpentinized in the presence of water below 500°C. The olivine with water vapor is changed to serpentine and brucite below 400°C.



Serpentinization may result from automorphism through the reaction of aqueous residual solutions produced by cooling of olivine rich magmas generally with SiO₂ inclusions.



A possible reaction leading to the serpentinization of olivine requires the addition of silica.



In some cases, reheated peridotite may be serpentinized during the cooling cycle [16,25].



The massive serpentine, translucent and light to dark green in color, can be used as an ornamental stone and building material. It is called as verde antique marble when mixed with white marble showing beautiful coloring. Other serpentine variety bowenite is used a jade substitute. Apart from these usages, serpentine may

be employed in some engineering applications such as a flux in iron and steel production, filler for road pavement and floor material for construction [11,26,27].

1.2.1 Antigorite

Antigorites are given the name of a location where they were first discovered, Valle Antigorio, Italy. This serpentine variety has a slightly different composition than the true polymorphs of serpentine varieties namely chrysotile and lizardite. It has a massive, fine grained, platy form. The Mg:Si ratio of the structure is smaller, in other words the ratio of brucite layers to tetrahedral layers is slightly greater than 1, for this serpentine type according to the ideal composition, although it is not reflected in the formula. Since the mineral has very close resemblance of serpentine silicates both chemically and mineralogically, it is contained in this group [28,29].

Antigorite has a modulated structure which relieves the misfit between the layers most effectively. If the structure is viewed as an extending wave, a continuous octahedral layer bonds to different tetrahedral sheets at each half of the waves, as it can be seen in Figure 1.5, without disturbing the sheet silicate properties. Near the inversion points the concentrations of Mg and OH decrease slightly. That changes the structural formula of antigorite to $Mg_{3m-3}[Si_{2m}O_{5m}(OH)_{4m-6}]$ where m is the number of tetrahedra in the unit cell [28].

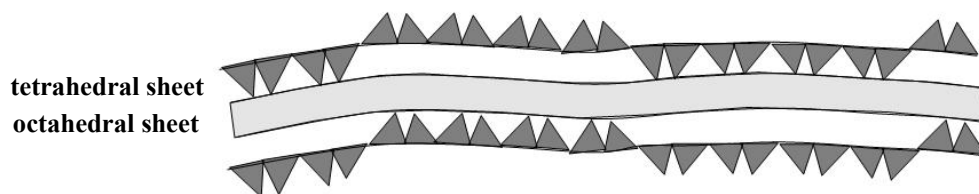


Figure 1.5 The structure of antigorite [8]

Antigorite is the second most abundant type of serpentine polymorph. Although its color changes from light to medium green according to the mineral contained, antigorite samples may have different colors. Usually they are less porous and tougher than other serpentine varieties [12].

Apart from mafic and ultramafic rocks, antigorite is also found in some marbles. It is the alteration product of olivine and to a less extent of bronzite leading to the formation of metamorphic serpentine. It occurs as a secondary mineral in seams and veins of the serpentine rock border. It may also form as an alteration product of diopside and forsterite in crystalline limestones [29,30].

1.2.2 Lizardite

Lizardite and chrysotile are commonly found in nature together, at nearly ideal pressure ranges from surface to almost 400°C [28]. Lizardites are the mostly found serpentine variety especially in retrograde serpentinites. They are extremely fine grained, platy minerals with layers of different orientations. Besides the unit cell is effectively single layered and ortho-hexagonal, lizardite samples may contain a mixture of layers in different orientations [21]. They have a planar structure in which tetrahedral sheet is distorted to match with the corresponding octahedral sheet, see Figure 1.6. The most common polymorph is Lizardite 1T. The replacement of Al for Si in tetrahedral sites and Al for Mg in octahedral sites reduce the misfitting of the sheets. Because of these substitutions tetrahedral sheet expands and octahedral sheet contracts in size [6].

As in other serpentines, it has various shades of green color; however it may have different colors due to association of minerals like hematite or chromite [6].

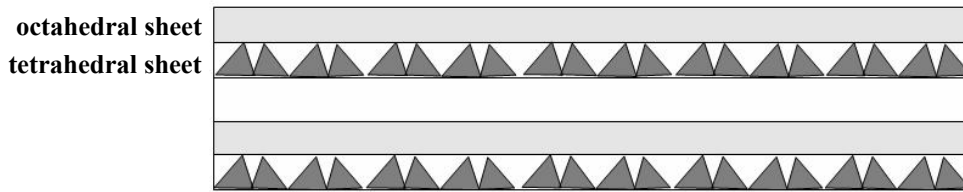


Figure 1.6 The structure of lizardite [8]

1.2.3 Chrysotile

The name chrysotile comes from the Greek, chryso for gold and tilos for fiber. This mineral is the least abundant of serpentine varieties. While it mostly occurs in asbestos deposits as cross fiber, slip fiber and mass fiber, it is also found in a massive, non-asbestiform chrysotile. Although fibrous chrysotile can be easily recognized, non-fibrous form can only be recognized by XRD studies. The color of fibrous chrysotile is usually green in serpentinized ultramafic rocks and that of non-asbestiform chrysotile could be green, pale gray or white [12].

The chrysotile structure resembles that of antigorite. It partially prevents the misfit by having a cylindrical curvature structure along the fiber axis in which expanding layers lead to the formation of fibres, as illustrated in Figure 1.7 [6,12,28]. The fiber axis is parallel to the a axis and growth of the fiber proceeds along the fiber due to the availability of the conditions in that axis finally ending up with an accumulation of curved laths or tubes. While there are some polytypes of chrysotile, 2M_{c1} structure is the most abundant. Clinochrysotile, orthochrysotile and parachrysotile are the three types of chrysotile. Although in clinochrysotile the successive sheets have the same orientation, in orthochrysotile the alternating sheets are reversed right and left successively. In parachrysotile, the sheets curve in the b axis which becomes the fiber axis in this case [31].

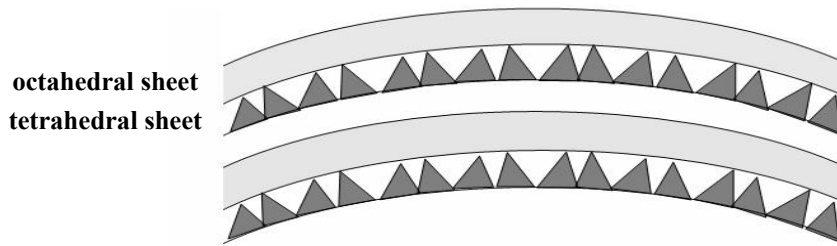


Figure 1.7 The structure of chrysotile [8]

When observed under magnification, the fragments are seen as needles with parallel extinction and positive elongation. Chrysotile is different from antigorite with its fibrous structure and optical properties. Because of its association in serpentine rocks, it is generally distinguished from other fiber forming minerals [30].

1.2.4 Polygonal Serpentine

While polygonal serpentine is not as important as the other serpentine polymorphs, it is worth mentioning. It has a planar structure which forms when the outer diameter of asbestos chrysotile goes beyond a certain point; see Figure 1.8 [28]. It has a polygonal cross section, composed of fibrils with a diameter of about 80-100 nm. The number of sectors in flat layers could generally be either 15 or 30. While the structure is expanding, new Mg octahedra is added to both wedge shaped edges and a $[\text{SiO}_4]$ tetrahedron is added to two per three layers in the same way [32].

Povlen chrysotile is the first name given to the polygonal serpentine which was anomalous to chrysotile having a less curved lizardite pattern. This less-understood form of serpentine is commonly found in serpentine veins, rock-forming serpentines and in kimberlites [12,33].

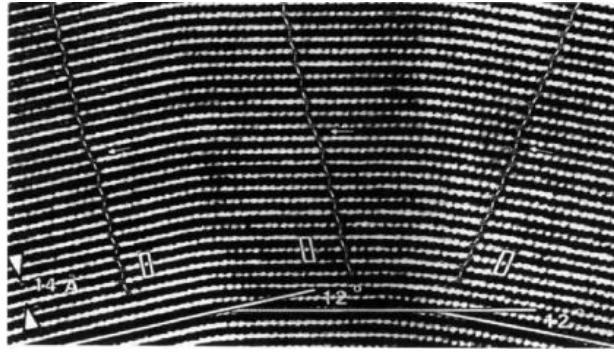


Figure 1.8 High resolution image parallel to the fiber axis of a polygonal serpentine [34]

1.3 Polymer Composites

In a wider sense, composites are two phase materials defined as the combination products of high strength and high modulus fibers with a low modulus matrix. The fibers may be in the form of single fibers or multiple fibers of a yarn or tow. Apart from these long fibers, whiskers, platelets, short fibers and particulate fillers could be embedded into matrix materials as reinforcing constituents. The strength and stiffness of the composites are determined according to the reinforcing material, matrix and the interface between them. In such a combination, a composite has an addition of the properties of the reinforcement and the matrix while they are retaining their identities [35,36]. The composites are categorized as polymer matrix composites, metal matrix composites, ceramic matrix composites, carbon carbon composites, intermetallic composites or hybrid composites [36].

Polymer matrix composites comprise a large and developed class of composite materials, therefore they can find many application areas as engineering structural materials. They can be easily produced in the form of large and complex shapes due to their low processing temperatures. Apart from high strength fibers such as carbon, boron or Kevlar, other reinforcements are applied to satisfy the requirements of high performance function of these composites. In the case of fiber reinforcement, the fiber is the load carrying component giving high strength

and modulus to composites. A matrix keeps fibers in their place, acts as a stress transfer medium and protects them from environmental damages [36].

In polymer matrix composites, the matrix can be either thermoplastic or thermoset. Although thermoset matrix composites are more popular, thermoplastic matrix composites are developing rapidly because of their low cost and high performance characteristics. Major thermoplastic resins are polyether ether ketone, polyphenylene sulfide, polyether ketone, polyether ketone ether ketone ketone, polyether sulfone, polyether imide and polyimide. Thermoplastic matrix composites serve unlimited shelf life and fewer health risks during processing. Besides absorbing low moisture, they can be reprocessed, thermally shaped and welded. Moreover, they show high toughness, good hot-wet properties and environmental tolerance [36,37,38]. Among the thermoset polymers such as epoxy, phenolic, polyester, vinyl ester, bismaleimides and other thermoset polyimides are important resins. Although they have many superior properties, they experience some limitations. The studies have been carried out to find the ways to develop techniques for toughening the resins and obtaining an improved hot-wet performance and lower viscosity systems [36].

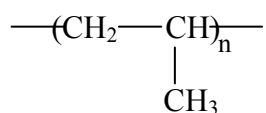
The interface between polymer and reinforcement in composite materials needs considerable attention. In order to improve adhesion and wettability between them, usually filler surfaces are treated and functionalized polymers are used. The interface constitutes a large area in composites, therefore it is important to know what is happening there. The factors affecting the interface such as temperature and diffusion have to be determined for high efficiency [39].

In the case of short fibers and particulates, the composites are formed by mixing them with a liquid resin followed by molding to the final shape. While compression molding is used in thermoset polymers, injection molding, extrusion, calendaring and thermoforming are used in thermoplastic resins as molding methods. In the case of continuous fibers, generally the composites are fabricated

by hand lay-up method in which the unidirectional fibers or woven fabrics are laid into the mold, impregnated with the resin and cured [38].

1.4 Polypropylene Composites

Polypropylene (PP) is a semi-crystalline thermoplastic with a general formula:



Due to its stereoregular (isotactic) structure, it has a special place compared to other polyolefin resins in the family of synthetic stereoregular polymers. It exhibits high stiffness at low density and resistance to higher temperatures in the absence of mechanical stress. It is chemically inert, fatigue and environmental stress cracking resistant and flexible with fairly low softening and melting points. Moreover, ease of machining with commercial processing techniques makes PP a very popular, industrially important polymer [40,41,42].

For PP, to continue its commercial position and compete with the other polyolefins with similar properties, a modification of the resin is essential. The modification includes all kinds of methods even the enhancement of processing conditions and investigation of new ways to improve the applications and develop new ones. Copolymerization and blending are the methods which take a growing percent of share from the total PP production. For example, PP exhibits poor low temperature impact strength due to relatively high T_g , whereas the toughness improvement can be achieved with creation of rubbery domains in PP structure by copolymerization of ethylene or incorporation of a rubber. Stabilizers are essential additives because the tertiary carbon in PP makes it more prone to degradation by oxidation and chain scission [43]. The incorporation of various grades of fillers, pigments, flame retarding agents, colorants etc. are employed greatly in the end use products [40].

The semi-crystalline structure of PP has many effects on its properties. According to sample preparation and processing conditions, PP may contain different amount

of crystallinity, size and distribution of crystallites throughout the polymer. Fillers acting as nucleating agents change the conditions of the crystallization process therefore the polymer will show altered, generally enhanced morphology with a change in the size and amount of crystalline phases [44].

Fillers are not only used to reduce the cost but also to improve the mechanical and thermal properties such as modulus and heat distortion temperature. The modulus of filler affects the rigidity of the composite with respect to its loading and aspect ratio. At low to moderate filler loadings, there is a linear increase in moduli of filler and composite. As the aspect ratio of filler increases, the modulus of composite also increases [42,43].

The filler characteristics have important effects on the composite features. Purity of the filler is important such that insufficient purity may cause discoloration of PP product. Moreover, in the presence of any heavy metal traces, the stability of PP decreases. The filler surface plays an important role in the coupling of the matrix and the filler therefore usually a filler treatment is needed. When nontreated fillers are incorporated into PP, the mechanical properties of the composite are determined basically according to particle properties of the filler. As particle size decreases, strength and sometimes modulus increase, deformability and impact strength decrease. The lower the particle size, the higher the aggregation which causes insufficient homogeneity, rigidity and lower impact strength. In the case of use of large particles, both abrasion properties and appearance may change and deformation and failure characteristics of the composites may be affected adversely [45]. Talc, calcium carbonate, glass fibers and mica are important fillers that are used largely in reinforcement of PP.

1.4.1 The Use of Talc in Polypropylene

Talc is an industrially important mineral which is mainly used as filler for PP due to its low cost, high aspect ratio and ease of availability. It can be readily distinguished by its slippery feel and being the softest of known minerals with a value of 1 on Mohs scale. Some of the properties of talc are dependent upon the features of deposits from where the mineral is obtained and the processing conditions. The crystal structure may change from lamellar and foliated to fibrous or massive. The platy structure gives talc its unique ability to reinforce PP. Although the surface of talc is chemically inert and does not well react with surface modifiers, with some additives such as maleated PP there can be some improvements in surface interactions [43,46].

Talc is used in large amounts in both homopolymer and copolymer grades of PP with 10% to 40% by weight. The efficiency of improvement depends on a number of factors namely, the particle size, its distribution, aspect ratio and purity. The main uses are in automotive, domestic and factory applications such as car heater casing, motor housing, dryer drums, washing machine detergent dispensers and textile bobbins [41].

The main aim of talc application in PP is to increase the stiffness of the composite. The level of stiffness changes parallel to the amount of loading for example, with 20% talc addition the flexural modulus of a homopolymer PP increases from 1.38 GPa to 2.58 GPa and with 40% loading an increase to 4.14 GPa is achieved. In talc filled grades of PP, high heat deflection temperature is also observed since it has a close relation with stiffness. While providing high stiffness, talc has an adverse effect on impact properties. To provide the balance between the stiffness and impact strength, it should be suitable to choose either flexible PP and coarse talc or rigid PP and finer talc. The addition of talc causes reduction in mold shrinkage and thermal expansion coefficient which is reduced by 50% between 50 and 150°C with 30% talc loading [46,47]. Another benefit is an effect on thermal conductivity that is increased from 0.27 to 2.5 W/(m K) with 30% talc addition by volume [48].

1.4.2 The Use of Calcium Carbonate in Polypropylene

After talc, calcium carbonate is the second mostly employed filler for PP. It has a spherical geometry and is a soft mineral with a hardness of 3 on Mohs scale due to exhibiting a perfect rhombohedral cleavage. Although having three polymorphs, calcite is the mostly employed and important one. Calcite mineral can be produced from chalk, limestone and marble. The filler properties vary according to the source from which the filler is obtained [42,43].

In the previous studies, CaCO_3 was used only to decrease the cost of host polymer. It was observed that the mechanical properties of CaCO_3 filled composite didn't seem to be improved due to lack of surface interactions between the polymer and the filler. The improvement has been provided by using surface modifiers, such as stearic acid, titanate and silane coupling agents. It is known that non-coupling fatty acid treatment is a widely used method to improve the surface characteristics of fillers incorporated into PP. The treatment enhances processing by reducing the viscosity and voiding caused by polymer/filler separation under deformation. The matrix-filler debonding let the deformation occur around the particles giving rise to an increase in the ductility of composites. The impact strength of homopolymer PP can be increased by the addition of fatty acid treated natural calcium carbonate depending on the particle size, filler loading and amount of coating due to crack pinning mechanism. The application of monolayer surface coverage at 1% coating level and particle size of 1-2 μm are the best conditions to obtain optimum results [43,49,50]. Even in this case, while impact strength and percentage stain at break improve, tensile strength and stiffness decrease. The filler provides PP with higher fatigue strength, thermal stability and brighter color. Calcium carbonate filled PP composites are used in instrument panels, motor vehicle grills, heater boxes and garden furniture etc. [41].

1.4.3 The Use of Glass Fiber in Polypropylene

There are different grades of glass fibers whose chemical and physical properties vary in accordance with the composition. Among them E and R glasses are incorporated mostly to plastics. To obtain glass reinforced PP composites, PP resin should wet and encapsulate the glass fibers. Usually silane coupling agents and chemically modified PP are used to make these materials compatible. To make the properties even better, some reagents are added such as lubricants, antistatic agents, plasticizers, nucleating agents, antioxidants and surfactants. In fiber reinforced thermoplastics, fiber amount, fiber distribution and alignment, aspect ratio and interfacial bonding between components affect the properties of the composite. Compared to talc and CaCO_3 , its high aspect ratio gives high reinforcing capability to glass fibers. To reach the desired mechanical properties, there is a critical fiber length below which the reinforcing effect of glass fibers is not sufficient. Up to 3 mm fiber length, tensile and flexural strengths increase with a level off after that and up to 6 mm Charpy impact strength increases. The strength of composite increases by the application of glass fibers with small diameters [46,51].

Usually, it is observed that at high glass contents, high tensile strength and flexural modulus are achieved. At 20% or 30% loadings, notched Izod impact strength takes its maximum value depending on the fiber diameter. The flexural modulus and Izod impact strengths of long-fiber/PP composites could be twice that of short-fiber/PP composites. Due to some advantages like low cost and low specific gravity that these composites offer, they become candidates for more expensive engineering composites day by day [46].

1.4.4 The Use of Mica and Other Fillers in Polypropylene

Mica is a high strength, nonflammable, naturally occurring silicate with great abundance. It has excellent thermal stability, corrosion resistance, scratch and mar resistance and high insulating properties. It imparts high flexural modulus than talc

or CaCO₃ to PP composites because of its high aspect ratio [41,52]. The platy shape, in which the dimensions of length and width are similar, provides uniform shrinkage eliminating warpage and a reduction in the flow of gases and liquids through PP leading to good barrier properties. This mineral increases the flexural and tensile moduli, flexural strength and heat deflection temperature when incorporated into PP [46,52]. The composites of mica and PP take great attention because they fulfill the requirements for larger, thinner and strong parts with reduced weight, better surface appearance, higher heat stability and good recyclability [46].

Apart from these reinforcements; there is a great number of fillers used frequently including glass beads [53], perlite [54], magnesium hydroxide [55], wood flour [56] and cellulose [57]. Wollastonite, sepiolite, gypsum, carbon black, clay minerals, metal powders especially aluminum, iron and nickel, steel fibers, silicon carbide, phenolic microspheres and flame retardants are also used [45].

1.5 Polymer Nanocomposites

Nanomaterials are the materials whose at least one dimension is in the nanometer scale. Nanoscience and nanotechnology are based on these materials including clusters, quantum dots, nanocrystals, nanowires, nanotubes and the collections of various nanostructures. Nanomaterials can be distinguished by their different physical and chemical properties with their unique structural and shape characteristics, chemical reactivity, energetics, response, dynamics, electronic structure and catalytic properties. Better understanding and manipulating of these properties will lead to the investigation of new high performance nanomaterials in nanotechnology world [58].

One important application of nanomaterials is in nanocomposites which are a new class of composite materials with polymer, ceramic or metal matrices. They show superior properties over conventional ones because they provide improved chemical resistance, mechanical, thermal and barrier properties. According to the

requirements of the application, fillers of different size and shape can be employed in low concentrations. For example, isodimensional particles are used for optical and electrical conductivity and anisometric particles, e.g. carbon nanotubes, are used as reinforcing fillers to improve mechanical properties [59-61].

During the last decades, polymer nanocomposites have gained popularity among the nanocomposite world. They possess an increased area of polymer filler interface compared to conventional ones which leads to an increased effect on composite properties even at low filler contents. There are different production methods which involves a) direct incorporation of nanosized materials into a polymer melt or solution, b) in situ generation of nanomaterials in a polymer matrix as in the case of vacuum evaporation of metals, thermal decomposition of precursors and reduction of metal ions through an electrochemical procedure, c) polymerization of monomers in the presence of nanomaterials, d) a combination of polymerization and formation of nanomaterials as in the case of sol-gel method and intercalation of monomers into the nanolayered structures with subsequent polymerization [62].

The addition of 1-3 vol% filler could be sufficient to obtain satisfactory results such as transparency, low density, reduced flammability, low permeability and improved mechanical properties. One way to classify them is according to the number of dimensions of fillers within the nanometer ranges as in other nanocomposite types.

- 1. One Dimension:* In the case of layered silicate nanofillers, while the length of sheets can extend to thousands of nanometers, thickness to only one to a few.
- 2. Two Dimensions:* These nanoparticles employ elongated structures like carbon nanotubes, fibers and cellulose whiskers.
- 3. Three Dimensions:* For isodimensional spherical fillers, all three dimensions are nanometer sized as in the case of nanoparticles obtained from sol-gel processing [60].

1.6 Polymer Clay Nanocomposites

Polymer clay nanocomposites comprise an important subclass of polymer nanocomposites, gaining an increasing interest both scientifically and industrially. These nanocomposites show fantastic improvements in strength, modulus, scratch and solvent resistance, barrier, thermal and flammability properties, ionic conductivity and heat distortion temperature [63,64]. Although the main reason of the synergistic improvements in nanocomposite systems is still under consideration, according to the current belief, the factors such as quantum size and columbic charging effects and interfacial interactions related to the ultra fine size and morphology of the nanofillers form the basis for enhancement. Another belief is that the local and global conformations of polymers within the nanolayers of fillers are different than in the bulk, because the polymer chains are confined in the layers and usually there are no polymer surface interactions in the bulk affecting the local and chain dynamics [65].

Intercalated or exfoliated nanocomposites are obtained through the coupling of organically modified clays and polymers. Deintercalated structure formation is possible in a system of aggregated clays and immiscible matrices. In the intercalated nanocomposites, polymer chains enter into the galleries of the layered clay without disturbing the layer ordering. In exfoliated nanocomposites, the layers separate from each other and distribute themselves through the matrix [66]. Both thermoplastic and thermoset resins, including polyamides, polystyrene, polyurethane, phenol and epoxy resins could be applied as matrices whose examples are shown in Table 1.3 [60].

The work done by Toyota research group on nylon 6-montmorillonite pioneered the use of clays in polymer matrices. In this study, the exfoliated clays were homogeneously distributed in the nylon 6 matrix. It was observed that the resultant hybrid composite had improved modulus, strength, thermal, barrier and flame retardant properties compared to neat nylon 6 [67].

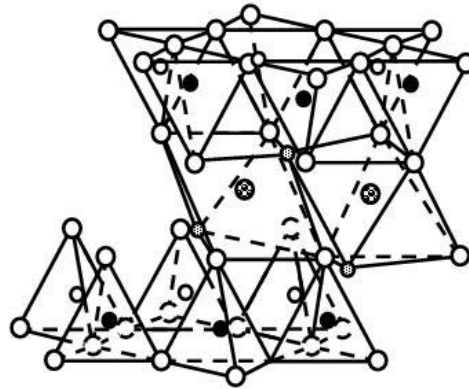
Table 1.3 Some important polymer clay composite applications [60]

Matrix	Manufacturer	Clay	Properties	Applications
Polyamide, esp. (PA-6)	Toyota, AlliedSignal, Ube, Nanocor, Unitica, ShowaDenko, Bayer, BASF, and Solutia-Dow	Exfoliated silicates, e.g., 1-3 vol% Na-MMT	Compared to PA: similar density, transparency, 70°C higher HDT, 70% higher tensile modulus, 130% higher flexural modulus, 50% lower oxygen permeability, 70% lower flammability	Automotive (e.g., truck mirror housing, engine covers), tool housing, garden equipment, telecommunication, aerospace, specialty application, barrier film for food packaging, etc.
Polyolefins, esp. PP and copolymers	Basell, GM, Southern Clay Products Inc., Toyota, Ford, Dow Plastics, and Magna International	Exfoliated smectite ≤ 5 wt%. Compatibilizer is needed; e.g., Toyota uses maleic anhydride modified PP	Low density with stiffness equivalent to composites with 35 wt% talc, dimensional stability, low T impact strength, ductility to -35°C, 75% lower flammability, excellent surface finish	Automotive: body panels, door panels, interior trim, instrument panels, pillars, consoles, etc.
Polyethylene terephthalate (PET)	Eastman, Bayer, BASF, Tetra-Laval	Solution-expanded clay particles present during the polycondensation	Transparency, low permeability, high strength and stiffness, low density	Food packaging, esp. as central layer in co-formed beer, juice and soft drink bottles
Ethylene-vinyl alcohol copolymer (EVAI)	Nanocor, Mitsubishi	Exfoliated smectite clay particles; loading ≤ 5 wt%	NC to be central layer in multilayer, co-formed products	Packaging films, for moisture and oxygen sensitive foods and electronics
Polyoxymethylene or acetal (POM)	Showa Denko, Bayer	Montmorillonite	Low warpage, low shrink, high surface quality, HDT increased by 45°C, 40% higher modulus	Automotive under-hood applications, etc.

1.6.1 Clays and Clay Structures

In the definition of polymer clay nanocomposites, the term layered silicate is used synonymously with clay which belongs to that class of silicates as mentioned before. The typical examples of 1:1 and 2:1 layer silicates are kaolinite and montmorillonite, respectively. While kaolinite (china clay) is generally used in rubber industry, montmorillonite is generally preferred and employed as layered silicate filler due to its availability and ease of surface modification [61]. Montmorillonite is a member of the smectite family occurring as a constituent of bentonite. The crystal structure of the 2:1 clay is shown in Figure 1.9 with an edge shared octahedral sheet between the two corner shared tetrahedral sheets. The layers have lateral dimensions from 100 nm to a few microns and a thickness of about 1 nm depending on the particulate silicate. Isomorphous replacements of ions such as aluminum for silicon, magnesium for aluminum and lithium for magnesium take place within the layers. Since the cations exchange with lower valence substituents, negative charges form with a value of 0.5 to 1.3. The negative charge can be compensated by the adsorption of alkaline cations like lithium, sodium, potassium, calcium and hydrated cations. These exchangeable, charge compensating cations hold the layers together [68,69].

For the layers to function in the formation of a nanocomposite, the layer separation is necessary. To have a sufficient separation, the clay is generally surface modified with quaternary ammonium salts to produce clay-surfactant hybrids, also called organophilic clays or organoclays, through the ion exchange reactions [70]. The clay is modified by exchanging intergallery cations with organophilic cations like alkylammonium and alkylphosphonium ions. The exchangeable cations define the cation exchange capacity (CEC) of the clay which is the number of exchangeable interlayer cations and generally expressed as mEq/100 g. [68,71]. The CEC of the montmorillonites varies between 75 and 115. The exchange reactions are also advantageous in that the basal spacing between the layers of clay increases due to the presence of bulky organic ions, see Figure 1.10 [72].



Interlayer space
Exchange cations and water molecules

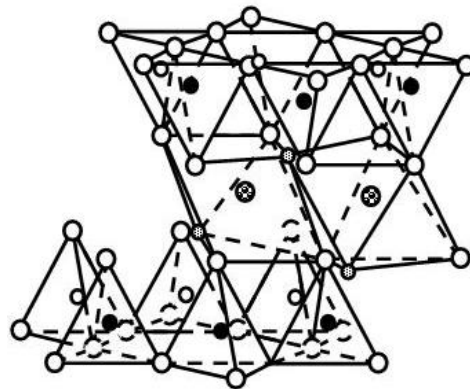


Figure 1.9 The structure of a 2:1 clay mineral [73]
(● : Si, ⊗ : Mg or Al, ○ : O, ⊙ : OH)

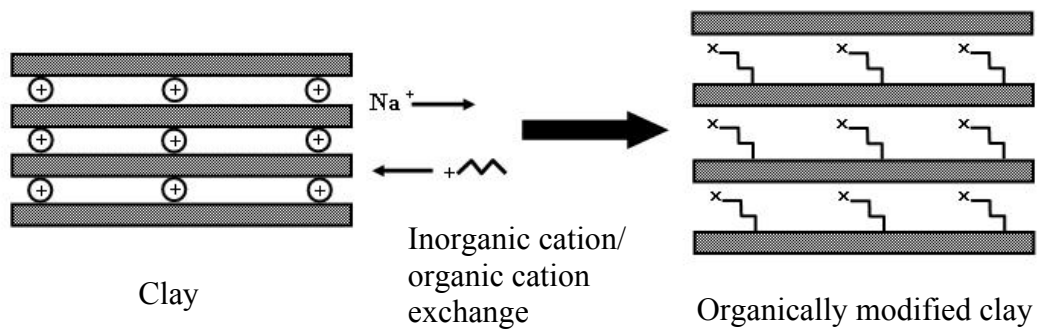


Figure 1.10 Modification of clay layers with quaternary ammonium salt [74]

The alkyl ammonium or alkylphosphonium cations reduce the surface energy of the clay and improve the wetting characteristics with the polymer. The increase in the interlayer spacing results in enhanced interactions between the inorganic and organic components. Moreover, these cations may provide functional groups that can react with the polymer or sometimes initiate the polymerization of monomers. The orientation and arrangement of the alkyl chains in the clay can be determined by X-ray diffraction studies. The chains either lie parallel to the silicate layers forming aggregates of monolayer or bilayer, or have the paraffin type monolayer or bilayer structures in which they may radiate away from the silicate surface depending on packing density, temperature and alkyl chain length, see Figure 1.11[75].

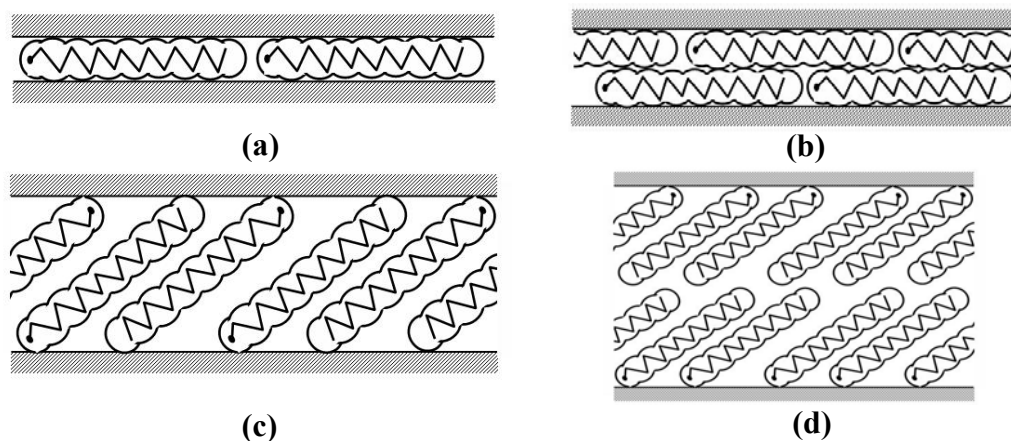


Figure 1.11 The arrangements of alkyl ammonium ions in 2:1 layered silicates (a) monolayer, (b) bilayer, (c) paraffin type monolayer, (d) paraffin type bilayer structures [76]

1.6.2 The Nanocomposite Structures

There are typically two types of polymer clay nanocomposites depending on the strength of interfacial interaction between the polymer and the nanolayer:

1. Intercalated Nanocomposite: Intercalation occurs when the polymer chains enter the gallery between the layers regardless of clay to polymer ratio as illustrated in Figure 1.12. The d-spacing increases and takes the value between 20-80 Å [61, 75].

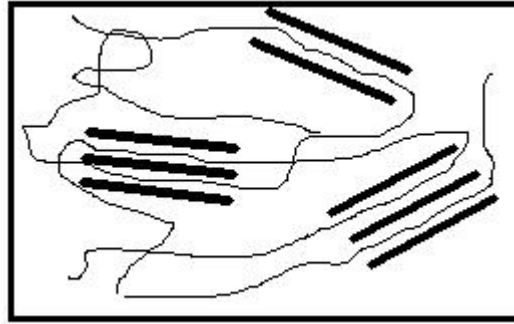


Figure 1.12 The structure of an intercalated nanocomposite

2. Exfoliated Nanocomposite: In exfoliated clay nanocomposites, the clay layers are dispersed through the matrix with an average distance generally 10 nm or more apart, see Figure 1.13. Due to the delamination of the clay layers, d-spacing increases significantly that may contribute much to the improvement of the properties of polymer clay nanocomposites [61].

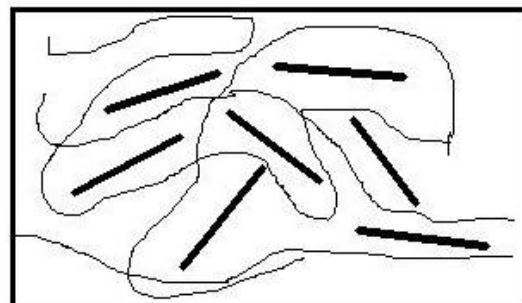


Figure 1.13 The structure of an exfoliated nanocomposite

The nanoscale structure and morphology can be depicted from transmission electron microscopy and X-ray diffraction studies. The shift of (001) peak of the clay to lower angles is considered as an indicative of intercalation. Although there is an increase in interlayer spacing, the ordered structure is kept due to the existence of attractive forces between the clay layers. In exfoliated nanocomposites, the basal peak of the clay disappears due to loss of ordered structure. TEM observations and X-ray pattern confirm the exfoliation of the layers [76].

1.6.3 Production Methods of Polymer Clay Nanocomposites

In general, polymer clay nanocomposites can be prepared by three ways: in-situ polymerization, solution and melt intercalation. While melt intercalation is widely applicable from non-polar and weakly polar to strongly polar polymers, other methods are limited because the monomers and solvents are not readily available and their costs are relatively high. Furthermore, in-situ polymerization and solution intercalation methods are not compatible with most of the polymer processing techniques [76].

1.6.3.1 In-situ Polymerization

This method involves intercalation of monomer between the clay layers with subsequent polymerization initiated by heat or radiation, by the diffusion of a suitable initiator, by an organic initiator or by a catalyst fixed inside the interlayer before monomer addition. This technique is suitable for highly polar polymers such as epoxides. The mechanical properties of epoxy, especially above T_g , can be improved by the addition of clays and layered silicic acids. The length of intercalated organic amine determines the degree of exfoliation in smectite/epoxy nanocomposites. Only epoxy resin or both epoxy resin and curing agent intercalate into the clay layers. The careful control of the curing agent, temperature, time and the ratio of resin to curing agent are essential factors to get exfoliated structures. The approaches similar to epoxy nanocomposites have been tried for

montmorillonite/polyurethane and silicate/ polyester or poly(ethylene oxide) nanocomposites [68,75].

1.6.3.2 Solution Intercalation

In this technique, organoclay and polymer are dispersed through the polar solvent like water or chloroform. The polymer dissolves in solvent and adsorbs onto the swollen and expanded clay layers. Upon the removal of solvent by evaporation, the polymer chains stay as intercalated. Since the intercalation occurs for certain polymer solvent pairs, the selection of a proper solvent is an important criterion to be considered [76].

1.6.3.3 Melt Intercalation

The polymer and the organoclay are mixed above the softening point of polymer with or without shear forces. Nylon-6/Nylon-12/clay nanocomposites are the first hybrids obtained via melt intercalation. Polymer nanocomposites of poly(ethylene oxide), polystyrene and poly(dimethyl silane)s are the other examples of nanocomposites which have been prepared by this method [68].

According to the kink model for melt intercalation, shear causes a kink to form between the layers. While polymer penetrates into the layers, the kink propagates along the layer. The intercalation rate of the polymer is enhanced by the space created by kinking. The flexibility of the layers controls the intercalation such that the kinking occurs with an ease for the layers of low modulus. In accordance with the other models that explain the intercalation in the absence of shear, there should be an optimum interlayer separation and optimum chemical interaction reducing the unfavorable interactions between the polymer and the aliphatic chain. After the intercalation of polymer is achieved, the nanocomposites can be processed with traditional melt processing methods to get a final product form. During this processing, facilitated nanoscale dispersion can lead to clay and/or polymer chain alignment [74].

1.7 Polypropylene Clay Nanocomposites

Along with the matrices mentioned above, PP is a good candidate with low price and balanced properties to be used in polymer clay nanocomposites. PP clay nanocomposites can be produced in two ways: either with the use of functionalized PP and organoclays or with the incorporation of neat PP and semifluorinated silicates, being the former one the most common [77]. However, since PP has a nonpolar chemistry to obtain intercalated or exfoliated nanocomposite is very difficult. Since the clay layers contain polar hydroxyl groups, they have difficulty in dispersing through such a polymer. To improve the adhesion between the clay and PP, generally clays are treated with quaternary ammonium salts, through which the exchange of cations is possible. Nonetheless, such a treatment could not be enough because PP still does not wet these organically modified layer silicates. A polymeric compatibilizer such as maleic anhydride grafted polypropylene (PP-g-MA) can provide delamination of clay layers due to its polar nature [78-81]. García-López et al. reported that the kind of matrix modification is essential in pointing out the clay dispersion and the interfacial adhesion. When the effectiveness's of diethyl maleate (DEM) and maleic anhydride (MAH) as a coupling agent were compared, it was observed that the affinity towards the organoclay was pronounced for MAH due to its high polarity [82]. The choice of surfactant, e.g. quaternary ammonium salt for the clay, is important because its length is an important parameter which affects the degree of exfoliation. Even further enhancement is possible by using proper silane coupling agent [83].

The degree of dispersion can be established according to the X ray and TEM studies. On the X ray pattern, the shape and the intensities of the peaks originating from the clays are used as tools to distinguish two different morphologies. TEM provides information on the internal structure and the spatial distribution of the phases [75]. Melt rheology data are useful in interpreting the state of dispersion in the melt state and the orientation of the clay layers such that the degree of exfoliation can be related to the dynamic viscosity curves. The crystallization behavior of PP is affected from the addition of a compatibilizer and a clay. While

the clay increases the rate of nucleation, PP-g-MA causes a reduction when incorporated separately. The rate of crystallization has an effect on the intercalated nanocomposite structures [83]. Maiti et al. investigated the effect of crystallization on the structure and morphology of PP-g-MA and montmorillonite intercalated nanocomposites. They observed that the extent of gallery spacing increases by raising the crystallization temperature. With the increase in clay content, spherulitic size decreased revealing the role of clay particles as a nucleating agent [84].

In the case of homogeneously dispersed PP nanocomposites, greatly enhanced mechanical properties are obtained at low filler loadings. An improved storage modulus was obtained depending on the degree of intercalation and the aspect ratio of the dispersed clays as reported by Nam et al. [85]. Kawasumi et al. obtained almost complete hybrids when they melt mixed PP, maleic anhydride modified polypropylene oligomers and clays intercalated with stearylammonium. The hybrids showed higher storage modulus compared to PP especially between T_g and 90°C [86]. The increase in storage modulus with the addition of clay particles and even a pronounced increase in the presence of PET (poly(ethylene terephthalate-co-isophthalate) compatibilizer have been reported by Velasco et al. The best dynamic mechanical properties were achieved for the better exfoliated structure which had PP/PET blend matrix with PP-g-MA compatibilizer [87]. A study done by Kodgire et al. showed that the mechanical and thermal properties of the PP/PP-g-MA/clay system significantly enhanced exhibiting 35% increase in tensile modulus and 10% increase in tensile strength. Depending on the dispersion of clay, the thermal degradation temperature raised from 270 to 400°C as a result of clay incorporation [88]. Modesti et al. obtained better results for the thermal and flammability properties of the PP nanocomposites in the presence of PP-g-MA compatibilizer at 5% loading. It was observed that clays brought higher thermal stability to PP in the oxidizing environment and glow wire test emphasized improved flame resistance of the nanocomposites [89]. Villaluenga et al. studied the gas transport properties of PP and modified montmorillonite composite membranes in terms of permeability, diffusivity and solubility of helium, oxygen

and nitrogen for the temperature range of 25-65°C. All filled membranes showed lower gas permeability. It was concluded that for helium, the reduction in permeability was caused by diffusion rather than solubility and for nitrogen and oxygen, diffusivity and solubility were reduced in filled grades [90].

1.8 Aim of the Study

PP is a commodity thermoplastic that has been widely used because of its attractive combination of good processability, mechanical properties, chemical resistance, fatigue resistance, environmental stress cracking resistance, hardness together with processability by injection moulding and extrusion. However PP has some disadvantages most of which could be overcome by proper selection of material, sensible design and good processing. Compounding with inorganic particles is a simple, effective and economical method to improve the mechanical and thermal properties. Among the most widely used fillers for PP, two of them are talc and mica which belong to the sheet silicate mineral group. So far, there has been almost no study employing serpentine as filler in PP, although it also belongs to the same group of minerals as talc and mica. The main purpose of this work is to prepare and characterize serpentine filled PP.

It was aimed to produce composites with 2,5,10 and 20 wt% serpentine and study their mechanical, thermal and morphological properties. Another objective was to explore whether it is possible or not to have serpentine/PP nanocomposites by using the advantage of the layer silicate structure of serpentine with melt intercalation method. Accordingly, the work was planned to divide into a study of two groups. In group 1, up to 20% serpentine addition, the filler effects of serpentine with some treatments were intended to investigate. In group 2, the nanofiller effects of serpentine in 2 and 5% filled samples by modification of both the filler and the matrix were aimed to examine.

CHAPTER 2

EXPERIMENTAL

2.1 Materials

All compositions were prepared by melt compounding of polypropylene (PP) and serpentine in different weight ratios. Some of the compositions were prepared with maleic anhydride grafted polypropylene (PP-g-MA) which acts as a compatibilizer. Properties of PP and PP-g-MA used in the study are given in Table 2.1. Different treatments to serpentine with hydrochloric acid (HCl), silane coupling agent (SCA) of γ -aminopropyl triethoxy silane and quaternary ammonium salt (QAS) of cetyl-trimethyl-ammonium bromide were carried out.

Table 2.1 Some properties of the polymers used in the study

Material	Supplier	Supplier Designation	Specifications	Test Method
PP	Borealis	HE125MO 25308	Density=0.908 g/cm ³ Melt Mass Flow Rate=12.0 g/10 min (230°C/2.16 kg) Tensile Modulus=1551 MPa	ISO 1183 ISO 1133 ISO 527-1,-2
PP-g-MA	Admer®	QF551A	Melt index (230°C)=5.7 g/10 min Density=0.89 g/cm ³ Vicat Softening Point=119°C	D 1238 D 1505 D 1525

Serpentine of Beynam-Ankara region (40 km south of Ankara, on Bala highway), collected as rocks, was employed as filler. Both as-received and powdered forms were characterized by variety of techniques.

The Silane A-1100 which had been supplied earlier by Union Carbide Europe S.A. was used as SCA. Figure 2.1 illustrates the structure of A-1100 (γ -aminopropyl triethoxy silane), which was employed to strengthen the interphase between PP and serpentine.

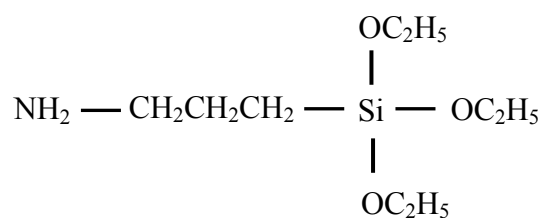


Figure 2.1 The structure of A-1100 (γ -aminopropyl triethoxy silane)

Cetyl-trimethyl-ammonium bromide, a product of The British Drug Houses Ltd., was used as an intercalating agent for serpentine. Its structure is shown in Figure 2.2.



Figure 2.2 The structure of cetyl-trimethyl-ammonium bromide

2.2 Powder Serpentine Production

Collected rocks were hammered to small pieces, ground, rolled and pulverized to produce powder serpentine. Pulverized powders were wet sieved with ethanol by 400 mesh (<38 μm) sieve. After removal of ethanol, ball milling was employed to obtain serpentine powders as small as possible in size without using any dispersants. Wet milling was performed in a 1800 ml hardened porcelain jar containing stainless steel balls with ethanol at B/P of 10 by holding the weights of filler and balls as 350 g and 3500 g, respectively for 48 hours.

All work was divided into a study of two groups according to the filler amount, processing conditions and type of treatments. After milling and the removal of ethanol the treatments pointed out below were carried out.

2.2.1 Treatments of Group 1

1. **Normal:** The powders were kept in muffle furnace for three days at 350°C for drying.
2. **HCl Treatment:** Serpentine powders were kept in 2M HCl for one week and washed with distilled water by suction filtration before they were dried in muffle furnace.
3. **SCA Treatment:** The treatment was employed to both normal and HCl treated serpentine powders after drying in furnace. SCA was dissolved in diethyl ether and serpentine was added with well mixing at a 1:46 weight ratio of SCA to serpentine. After removal of diethyl ether, the powders were dried overnight at 100°C.

2.2.2 Treatments of Group 2

SCA treatment was performed at a 1:46 weight ratio of SCA to serpentine to all serpentine powders of group 2 which had been dried in muffle furnace and treated

as described below. Following the SCA treatment, the powders were dried overnight at 100°C.

- 1. Normal:** Except SCA, no additional treatment was applied to dried serpentine.
- 2. HCl Treatment:** The treatment involved continuous stirring of filler for 5 days in 2M HCl solution which was renewed with freshly prepared one everyday.
- 3. QAS Treatment:** The treatment was employed to both normal and HCl treated serpentine powders which were dispersed in water by stirring overnight. The pH of the solutions was maintained at 3 with concentrated HCl. Then, cetyl-trimethyl-ammonium bromide salt was added to the solution (serpentine/cetyl-trimethyl-ammonium bromide salt=10/3 by weight) and the mixture was continued stirring at 70°C for one day. Before vacuum filtering, additional mixing was employed about 5 hours without heating.

2.3 Preparation of Compositions

Compounding of PP and serpentine was achieved by Thermoprism TSE 16 TC, corotating, intermeshing twin screw extruder (D = 16 mm, L = 384 mm) for both groups. The barrel temperatures were 220°C from hopper to die and the feed rate was 20 g/min. In group 1, compositions having 2, 5, 10 and 20 wt% filler were processed at a screw speed of 190 rpm. Additionally, processing and reprocessing of 2 and 5% SCA treated samples were done at 250 rpm. A one-step extrusion was employed; while PP was fed into the extruder from the main feeder, serpentine was fed from the side feeder. After pelletizing and drying at 80°C, extruded samples were shaped by Arburg Allrounder 220-90-350 type single screw injection molding machine. The barrel temperatures were adjusted to 200, 220, 240 and 250°C. In group 2, 2 and 5 wt% filled samples were melt blended at 190 rpm. For each composition, two sets of experiments were conducted with PP-g-

MA to serpentine ratio of 2:1 and 3:1 by weight. All samples were prepared in a two-step extrusion process. In the first step, PP-g-MA and serpentine were compounded in accordance with the desired ratio. Then, these masterbatches were dry mixed with PP, fed into the main feeder and extruded at the same conditions as in group 1. After pelletizing and drying at 80°C, extruded samples were molded by Microinjector, Daka Instruments type laboratory scale injection molding machine at a barrel temperature of 220°C. The studied PP-serpentine systems with their preparation conditions and designations are given in Table 2.2 and 2.3.

Table 2.2 Group 1 compositions (X shows the treatment done)

Sample Group Designation	Sample Designation	Filler Content (wt%)	Screw Speed	Reextrusion	SCA Treatment (A-1100)	HCl Treatment
Pure PP	Pure PP	-	-	-	-	-
N	2-190	2	190	-	-	-
	5-190	5	190	-	-	-
	10-190	10	190	-	-	-
	20-190	20	190	-	-	-
H	2-190-H	2	190	-	-	X
	5-190-H	5	190	-	-	X
	10-190-H	10	190	-	-	X
	20-190-H	20	190	-	-	X
S	2-190-S	2	190	-	X	-
	5-190-S	5	190	-	X	-
	10-190-S	10	190	-	X	-
	20-190-S	20	190	-	X	-
SH	2-190-SH	2	190	-	X	X
	5-190-SH	5	190	-	X	X
	10-190-SH	10	190	-	X	X
	20-190-SH	20	190	-	X	X
S,250	2-250-S	2	250	-	X	-
	5-250-S	5	250	-	X	-
	2-250,2-S	2	250	X	X	-
	5-250,2-S	5	250	X	X	-
SH,250	2-250-SH	2	250	-	X	X
	5-250-SH	5	250	-	X	X
	2-250,2-SH	2	250	X	X	X
	5-250,2-SH	5	250	X	X	X

Table 2.3 Group 2 compositions (X shows the treatment done)

Sample Group Designation	Sample Designation	Filler content (wt%)	PP-g-MA content (wt%)	PP content (wt%)	HCl treatment	QAS treatment
2,4	2,4-N	2	4	94	-	-
	2,4-H	2	4	94	X	-
	2,4-Q	2	4	94	-	X
	2,4-HQ	2	4	94	X	X
5,10	5,10-N	5	10	85	-	-
	5,10-H	5	10	85	X	-
	5,10-Q	5	10	85	-	X
	5,10-HQ	5	10	85	X	X
2,6	2,6-N	2	6	92	-	-
	2,6-H	2	6	92	X	-
	2,6-Q	2	6	92	-	X
	2,6-HQ	2	6	92	X	X
5,15	5,15-N	5	15	80	-	-
	5,15-H	5	15	80	X	-
	5,15-Q	5	15	80	-	X
	5,15-HQ	5	15	80	X	X

2.4 Characterization of Serpentine

2.4.1 Specific Gravity

Specific gravity of serpentine was measured by electronic densimeter MD-300S.

2.4.2 X-Ray Analysis

X-ray analysis was employed to powder serpentine by Rigaku D/Max 2200/PC X-ray diffractometer by employing CuK α radiation with $\lambda=1.54 \text{ \AA}$, 40 kV and 40 mA source. The diffraction pattern was recorded at a scanning rate of 1 $^\circ$ /min and steps of 0.01 $^\circ$.

2.4.3 Scanning Electron Microscopy (SEM)

The morphological character of powder serpentine was analyzed by JEOL, JSM-840A SM.

2.4.4 Differential Thermal Analysis (DTA) and Thermal Gravimetric Analysis (TG)

DTA/TG analysis was conducted in air and nitrogen atmospheres at a heating rate of 10°C/min between 50 and 850°C by Setaram Labsys TGA/DTA instrument.

2.4.5 Thin Section Analysis

Thin section of a serpentine sample was examined by Olympus BH-2 type microscope at a magnification of 40x.

2.4.6 Particle Size Measurement

The particle size measurement after milling was carried out by Malvern Mastersizer 2000 in ethanol medium.

2.4.7 Surface Characterization

Surface area and pore volume distribution were studied with gas (N₂) adsorption technique by Quantachrome Corporation Autosorb-1-C/MS.

2.5 Characterization of Composites

2.5.1 Impact Testing

Unnotched Charpy impact testing was employed on injection molded samples of 70mmx7mmx2mm in size by Pendulum Impact Tester type Coesfeld Material

Test machine according to ASTM D256. For each composition average result of at least seven samples was reported at room temperature.

2.5.2 Melt Flow Index (MFI)

Melt flow index measurements were carried out by Coesfeld Material Test, Meltflicker LT at 230°C with 2.16 kg load application according to ASTM D1238. Injection molded samples were cut into small flakes and fed into the barrel of the instrument. After complete melting, the extruded samples were cut at every 60 seconds and the results were reported as g/10 min.

2.5.3 Tensile Testing

Tensile testing was performed by Instron Tensile Testing Machine (TM1102) on standard dumbbell shaped injection molded samples according to ASTM D638. The drawing rate and gauge length were 50 mm/min and 7.5 cm, respectively. Testing was performed on at least seven samples for each composition and average results were reported at room temperature.

2.5.4 Differential Scanning Calorimetry (DSC)

Thermal analyses were carried out between 20 and 200°C under nitrogen atmosphere with a heating rate of 10°C/min by Dupont Thermal Analyst 2000 DSC 910 S.

2.5.5 Dynamic Mechanical Analysis (DMA)

The dynamic mechanical properties of the injection molded samples were studied by Perkin Elmer Pyris Diamond DMA in the tensile mode according to ASTM D4092. The samples were tested from -60 to 70°C at a frequency of 10 Hz and oscillating amplitude of 5 μm with a heating rate of 5°C/min.

2.5.6 X-Ray Analysis

The X-ray analysis of 2 and 5% serpentine filled group 1 composites was carried out by Rigaku D/Max 2200/PC X-ray diffractometer employing CuK α radiation with $\lambda=1.54 \text{ \AA}$, 40 kV, 40 mA source. The diffraction pattern was recorded between 5 and 30° 2 θ ranges at a scanning rate of 1°/min and steps of 0.01°. D8 Advance Bruker X-ray diffractometer in mineralogy laboratory of MTA Genel M \ddot{u} d \ddot{u} rl \ddot{u} g \ddot{u} (General Directorate of Mineral Research & Exploration) was used for the X-ray analysis of group 2 samples under the same conditions as group 1 compositions.

2.5.7 Scanning Electron Microscopy (SEM)

SEM analysis was employed on impact fractured surfaces of samples by FEI Quanta 400 FESEM and JEOL, JSM 6400 SM to study morphological properties.

2.5.8 Transmission Electron Microscopy (TEM)

To investigate the nanometer scale distribution and micro morphology of filler layers transmission electron microscopy analysis was carried out by Jeol JEM-2000FX STEM on the specimens cut from the middle portion of injection molded samples. LKB CryoNova Cryoultramicrotome was used to take ultra thin sections of nearly 100 nm. Then they were placed on formvar carbon coated copper grids (300 mesh) and analyzed under an accelerating voltage of 200 kV. The analysis was carried out in BRİSA Bridgestone Sabancı Lastik Sanayi ve Ticaret A.Ş. (BRISA Bridgestone Sabanci Tire Manufacturing and Trading Inc.)

CHAPTER 3

RESULTS AND DISCUSSION

3.1 Characterization of As-Received Serpentine

It was observed that the serpentine of Beynam Forest has deep green and brown color with an oily luster as seen in Figure 3.1. Its specific gravity was measured as 2.5.



Figure 3.1 A view of serpentine piece from Beynam region

The mineralogical identification was carried out by X-ray analysis. The X-ray diffraction (XRD) pattern of powder samples (as-received) displayed characteristic peaks belonging to serpentine minerals. As the pattern in Figure 3.2 indicates the serpentine contains lizardite and chrysotile together.

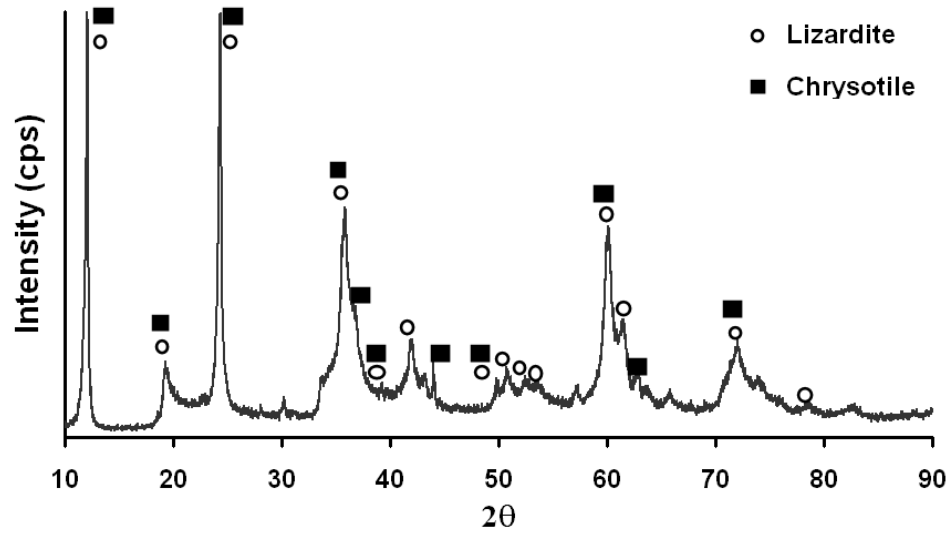


Figure 3.2 X-ray diffraction pattern of as-received serpentine mineral

The morphology of powder serpentine was studied by SEM analysis. As depicted from the SEM pictures in Figure 3.3, as-collected pieces have platelet morphology confirming the lizardite based structure. Long fibers of asbestiform chrysotile were not observed in the serpentine samples.

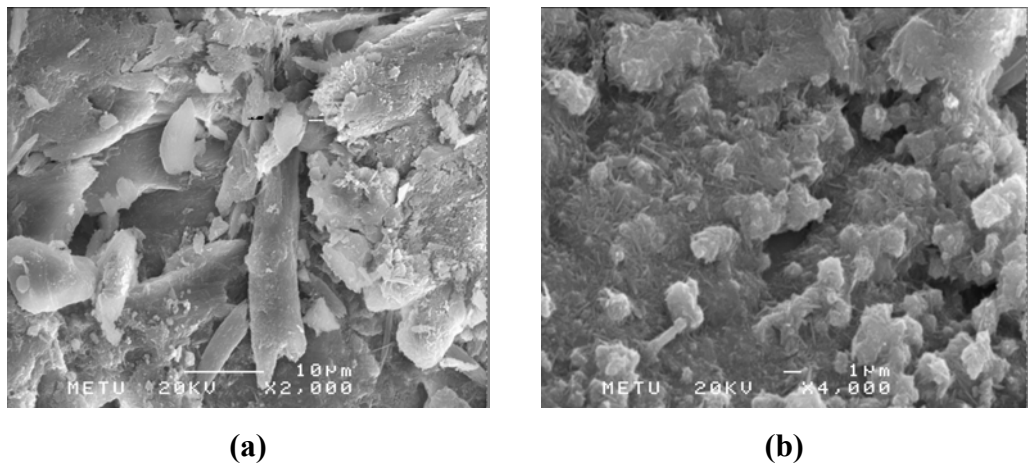


Figure 3.3 SEM pictures of as collected serpentine in (a) x2000, (b) x4000 magnifications

DTA/TG analysis was conducted in air and nitrogen atmospheres. Analysis of DTA curves shows three endothermic peaks at about 200°C and 400°C due to the release of adsorbed water and at about 650°C due to serpentine dehydroxylation, see Figure 3.4. Further heating caused serpentine to show additional exothermic peak at about 820°C due to forsterite crystallization [6].

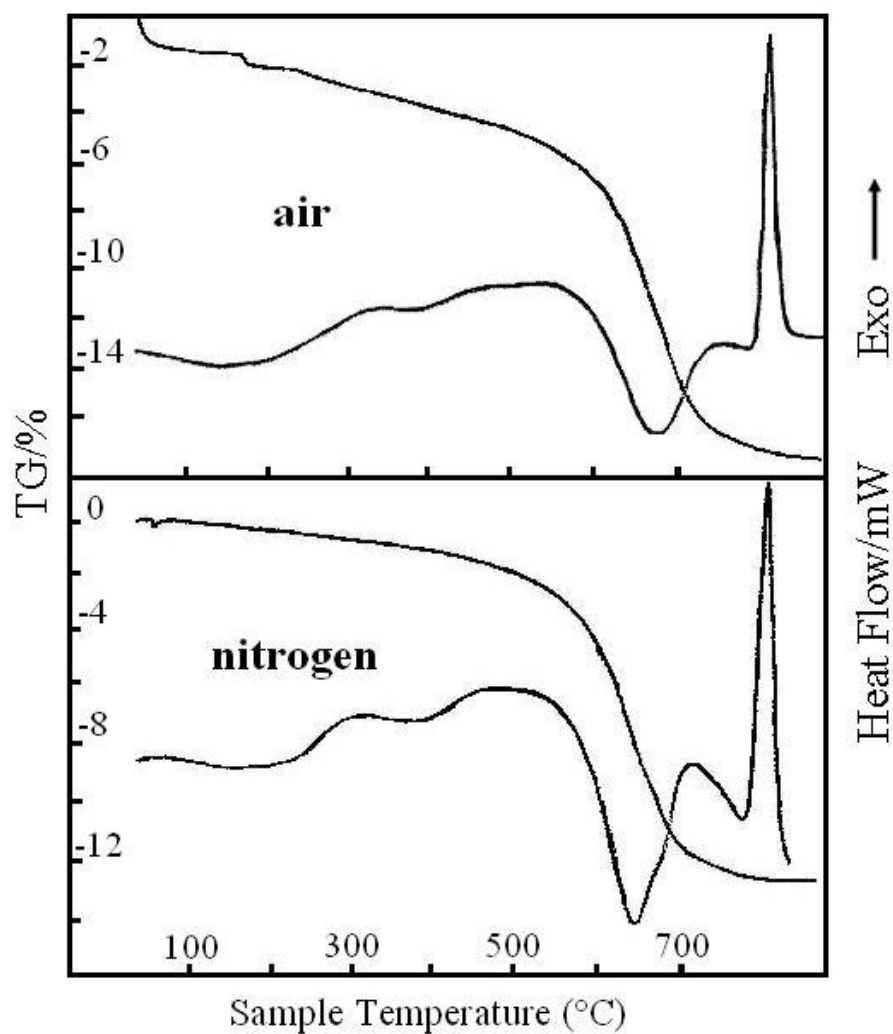


Figure 3.4 DTA/TG curves of serpentine in air and nitrogen

Thin section of a serpentine sample was examined under a microscope. The mineral can be observed in its natural color as brown with dark iron oxide regions in Figure 3.5 (a). The other photograph shows the mesh texture with characteristic birefringence colors of serpentine.

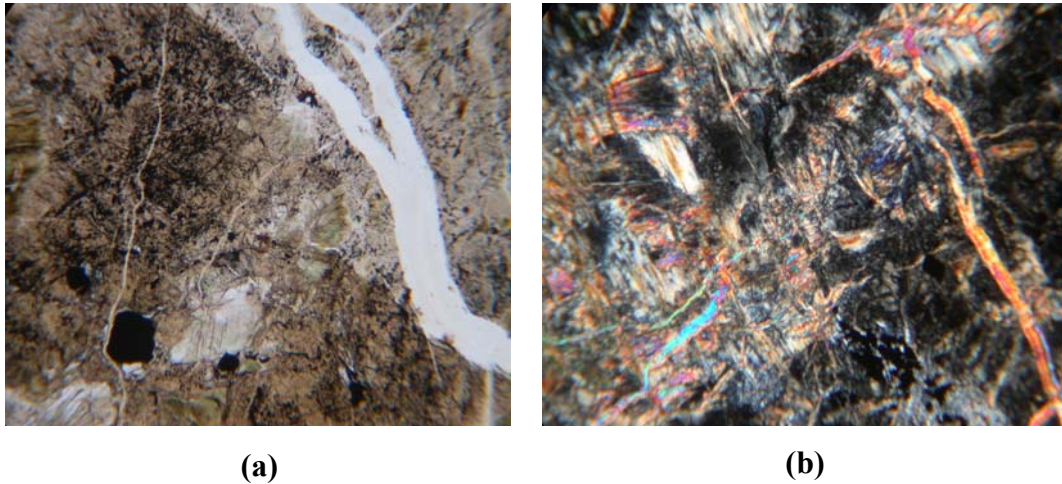


Figure 3.5 The thin section photographs of serpentine (magnification:40x) (a) a view under plain polarized light, (b) a view under cross polarized light

3.2 Characterization of Powder Serpentine

X-ray analysis was done on group 1 serpentine samples of HCl treated and untreated samples after they were dried in muffle furnace (ready to be used for processing) to see the effect of ball milling on the crystal structure of serpentine. The analyses were employed to three serpentine powders over 2θ ranges of $5-30^\circ$, since the most important and representative peaks of the mineral are found in this region. Treated and untreated powders are compared with the as-received one in Figure 3.6. It can be concluded that after such a long period of milling duration, the crystal structure of the powder kept the original form.

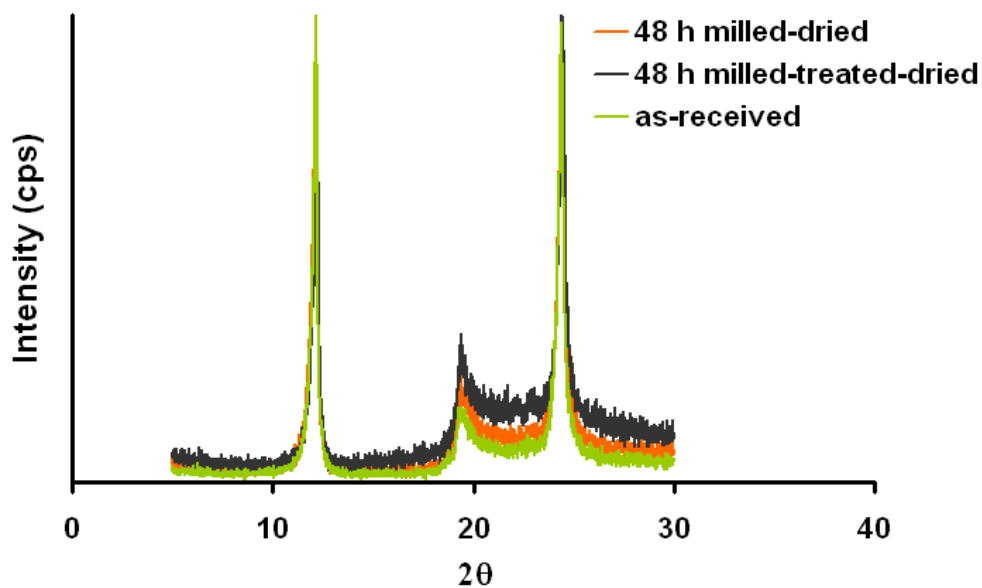


Figure 3.6 X-ray diffraction pattern of untreated and treated serpentine

The particle size of powder serpentine after milling was measured. The average particle size data (average of 7 measurements) are given in Table 3.1.

Table 3.1 Volume based particle size (μm) data for serpentine powders after 48 hours of milling

d(0.1)	d(0.5)	d(0.9)
1.19 \pm 0.18	3.25 \pm 1.08	8.15 \pm 2.62

According to the table average diameter of the filler is 3.25 μm i.e. about 50 vol% of serpentine is under 3.25 μm . Similarly 10 vol% and 90 vol% of the filler are smaller than 1.19 μm and 8.15 μm , respectively. Surface area and pore volume distribution were studied with gas (N_2) adsorption technique. The adsorption-desorption isotherms were obtained for 48 hour milled normal and acid treated serpentine samples at relative pressures (P/P_0) between the range 0.0-1.0. From V-t plots (volume vs. de Boer statistical thickness) and isotherms (volume vs. relative

pressure, P/P_0) of two samples, it can be said that the samples mainly consist of micropores and mesopores. The comparison of the V-t plots of two samples shows that the volume of adsorbed gas was higher for HCl treated serpentine at the minimum de Boer statistical thickness value. This indicates the increase in the number of micropores in the presence of acid treatment. Between 0.05 and 0.3 relative pressure values, BET multilayer adsorptions of nitrogen on the surface of serpentine were measured as 61.23 m²/g and 132.99 m²/g for normal and treated samples, respectively. Note that, acid treatment doubled the specific surface area of milled serpentine. By acid treatment, number of micropores increased which led to high surface area measurements for treated samples. In the BJH adsorption plots (Barret-Joyner-Halenda scheme for mesopore size distribution) the maximum pore diameter was obtained below 10Å which coincides with the HK (Horvath-Kawazoe) method presenting the micropore volume distribution, see Appendix A.

3.3 Impact Strength

The resistance to impact loading was measured by unnotched Charpy impact testing. Figure 3.7 presents the results for group 1 compositions. It is generally true that incorporation of mineral fillers to polymers do not improve the impact strength of matrices. Accordingly, overall view of the results shows that parallel to filler increase, impact strength decreased. However, it seems that serpentine even at high loadings (10 and 20%) didn't reduce the impact strength of the composites much.

During the preparation of serpentine powder, one of the objectives was to obtain the powders as near as possible to submicron ranges with narrower particle size distribution since these parameters have profound effect on mechanical properties of the composites. Particles with submicron dimensions impart toughening mechanism to the matrix leading to high impact strength. Therefore milling was performed for long time durations starting with the powders passing through 400 mesh sieve. Another point to consider related with the filler

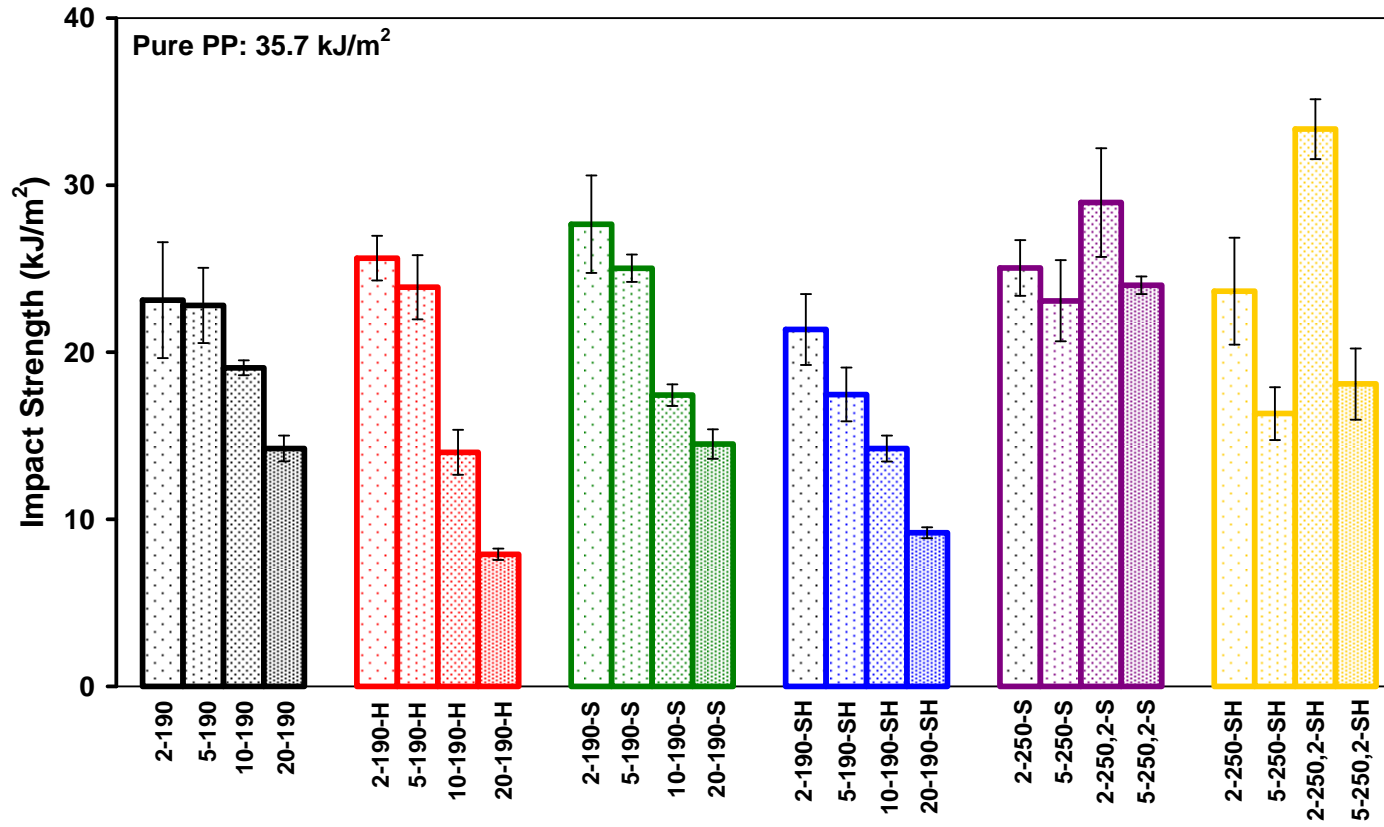


Figure 3.7 Impact strengths (kJ/m²) of group 1 compositions

is the particle shape. Due to possible stress concentration sites brought by the platelet geometry of the serpentine impact strength of the compositions might have been affected adversely.

For normal, HCl or SCA treated samples at high-filled compositions; impact strength values were low as expected due to limited deformation ability of the matrix. There was an apparent increase in impact strengths of SCA treated normal samples especially at low loadings (2 and 5%). Upon the treatment, 2-190-S composition showed 20% increase in impact strength compared to 2-190. This may be attributed to the decreased stress concentration sites in the samples with better distribution throughout the matrix.

The acid treated samples during the hydrolysis might have suffered from the layer formed on the surface preventing the interaction between the filler and the matrix. This may lead to low impact strength evident especially for 10 and 20% loaded compositions. The SCA treatments on these acid treated samples were not effective as opposed to normal samples.

The highest impact strengths among the studied compositions were obtained for 2-250,2-S and 2-250,2-SH formulations. For 2% loaded samples second extrusion seems to improve the impact strength at 250 rpm which may be attributed to the better dispersion through the second extrusion process.

There was significant change in the impact strengths of group 2 compared to group 1 compositions, as illustrated in Figure 3.8. The average for all compositions is near to 50 kJ/m² compared to 35.7 kJ/m² for pure PP. The reason for the increased impact strength is the presence of tougher PP-g-MA in the matrix along with PP.

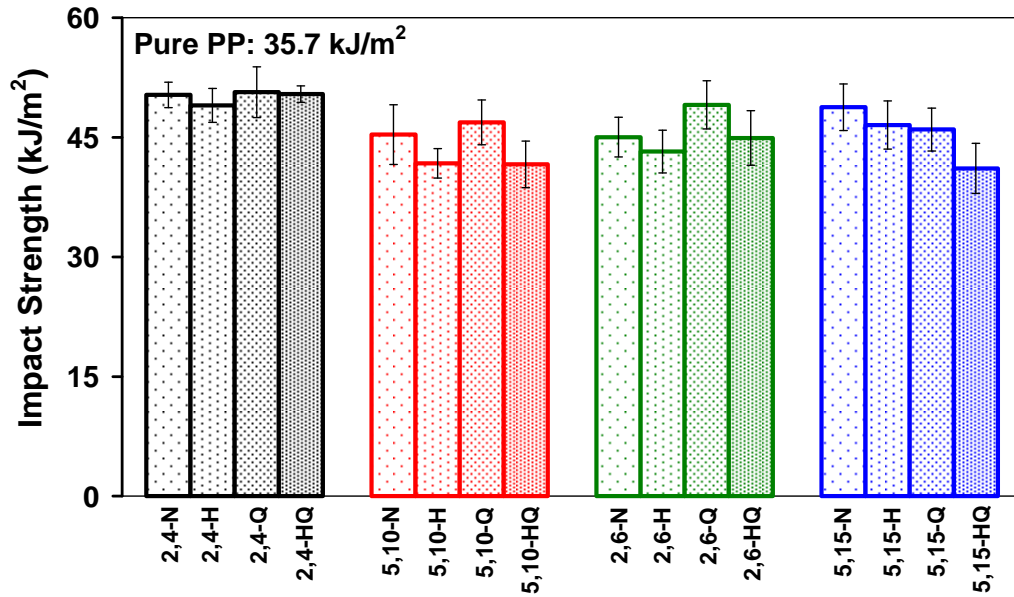


Figure 3.8 Impact strengths (kJ/m²) of group 2 compositions

3.4 Melt Flow Properties of Composites

The MFIs of the group 1 compositions are given in Figure 3.9. For all formulations melt flow decreased with increasing filler loading. The MFIs of 2% filled systems are higher than those of 5% filled ones since the former compositions suffer less from agglomeration than high-filled counterparts. At high loadings, due to increased filler amount, aggregation increases which may bring enhanced filler-filler interaction with flow hindrance.

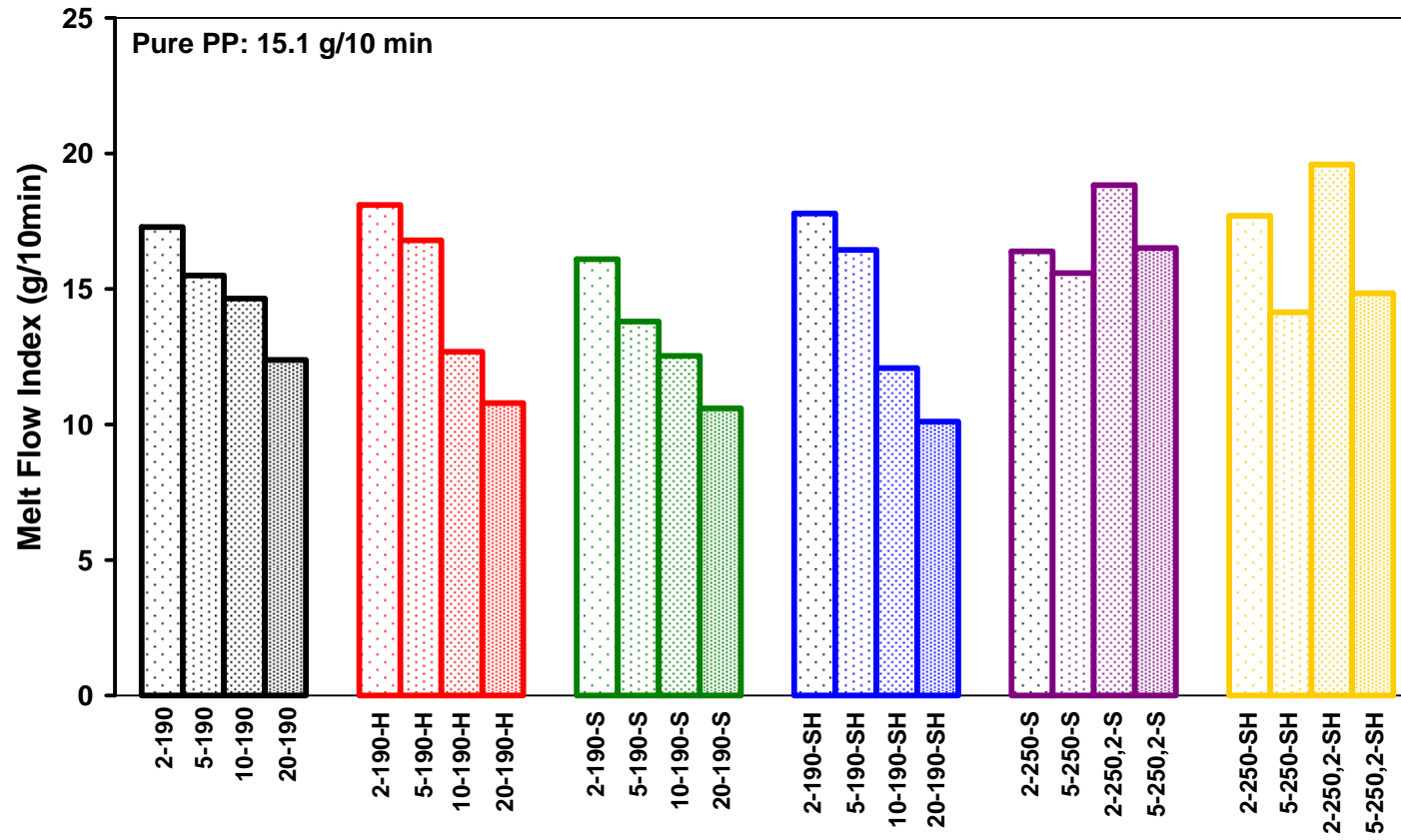


Figure 3.9 MFI values of group 1 compositions

The reduction of the MFIs through SCA treatment may be attributed to the coupling effect of SCA imparted to serpentine and PP. During the flow due to improved polymer-filler interaction, PP and serpentine may hold on to each other leading to retardance of flow. At this point, it is probable that there is no plasticizing effect induced by the SCA, but improved interaction. If there were any, there would be easy flow due to slippage of the polymer chains leading to higher MFI or lower viscosity values.

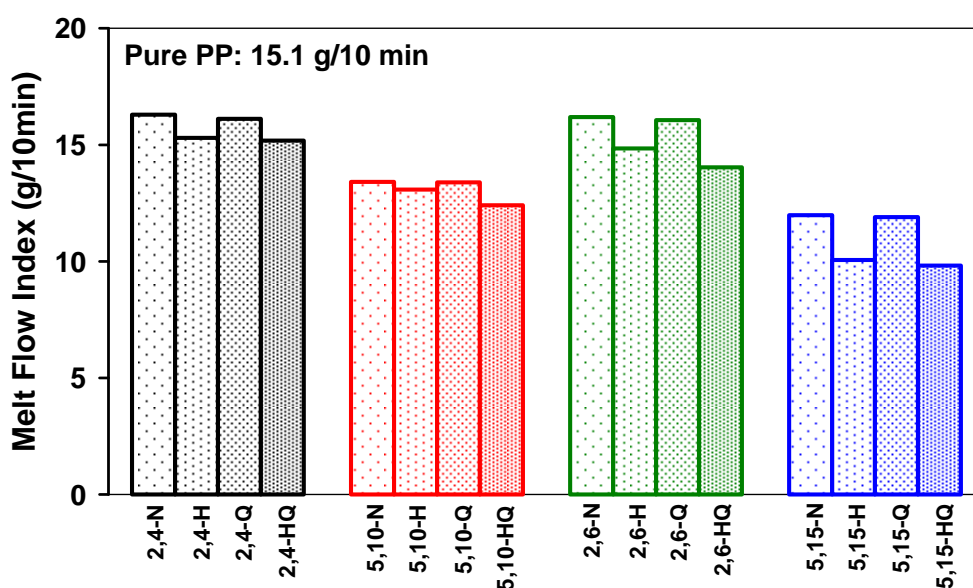


Figure 3.10 MFI values of group 2 compositions

The melt flow behaviors of group 2 samples are analyzed in Figure 3.10. The MFI of PP-g-MA was measured as 5.5 g/10 min. The presence of bulky anhydride groups in the structure of PP-g-MA makes melt flow index lower than pure PP under the same conditions.

In group 1, when the comparison is made between 2 and 5% filled S and SH compositions, it is observed that SH samples have higher MFI. However in group 2, treated samples whether with HCl or QAS exhibited higher melt viscosity than

their normal counterparts. Here, the comparison of normal and HCl treated samples at the same loading shows the effect of compatibilizer. It may be said that compatibilizer may be more effective in HCl treated samples than normal ones due to more hindered melt flow of the former. The same logic may be valid for QAS treated normal and acid treated formulations. As the amount of compatibilizer increased melt flow index decreased upon the comparison of the compositions with the same filler and different compatibilizer contents, especially for 5,10 and 5,15 compositions the decrease was more pronounced. The QAS treatment had nearly no effect on the flow properties of normal samples since there is no observable change in MFI values.

3.5 Tensile Testing

The tensile properties of the composites were derived from load vs. elongation plots in which Young's modulus, stress at yield, stress at break and percentage strain at break were then calculated. Figure 3.11 presents the modulus data for group 1 compositions. Young's modulus increased with the filler content as expected. The mobility of the polymer chains are restricted due to the constraints imposed by the filler layers leading to high modulus values. When the results are compared with the modulus of pure PP which is 710 MPa, for normal samples 60%, HCl treated 62%, SCA treated 87% and both SCA and HCl treated 71% increase can be observed on the average. It seems that acid treated filler showed no effect on stiffness of the composites when it is compared to untreated one.

As seen from the figure, SCA treated normal compositions (i.e. S) exhibited higher modulus than N and H composites. This increase could be attributed to the enhanced filler-matrix interaction such that, the presence of SCA may increase the amount of constraints to mobility leading to high modulus values. In contrast to S, in SH compositions the coupling agent was not able to show the same effect, i.e. they showed lower modulus than S composites.

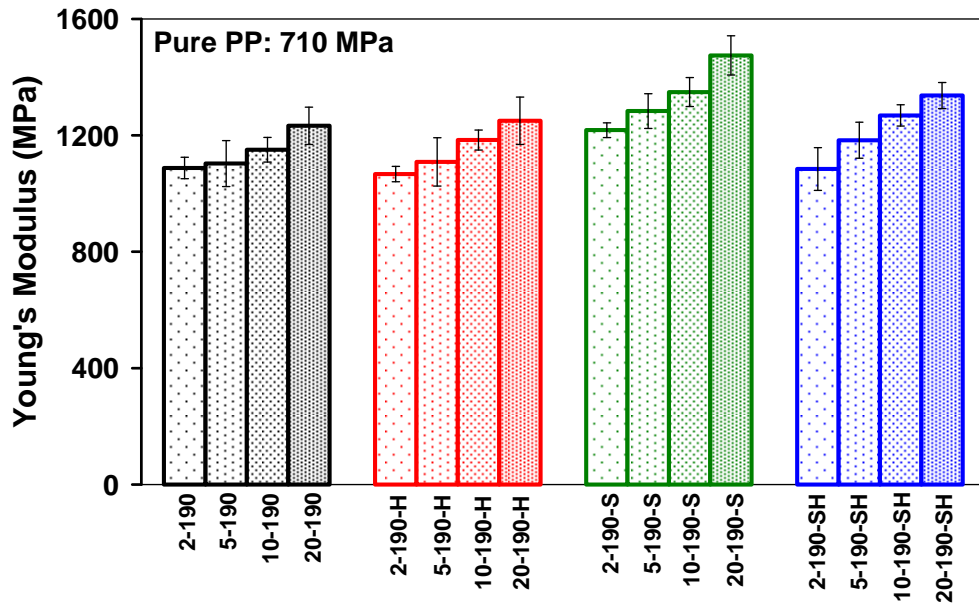


Figure 3.11 Young's modulus (MPa) for group 1 compositions

The effect of serpentine addition on the yield stress of composites is illustrated in Figure 3.12. As the filler content increased the yield stress decreased gradually but even at the highest filler content the yield stress was found to be well above that of unfilled PP. The reason behind that could be the better interaction between serpentine and PP even in the absence of SCA. Although, the bonding between filler and the matrix is important parameter for both yield stress and modulus, the effect is much more pronounced in the case of yield stress [92,93]. Since the incorporation of coupling agent into the matrix further improved the interaction at the interface, higher yield stress values are obtained for S compositions.

While the composite is mechanically loaded, stress concentration occurs unavoidably at the interphase followed by yielding of the material. As the concentration of filler increases, the amount of total interphase area between matrix and the filler also increases which may lead to higher stress concentration and lower yield stress values.

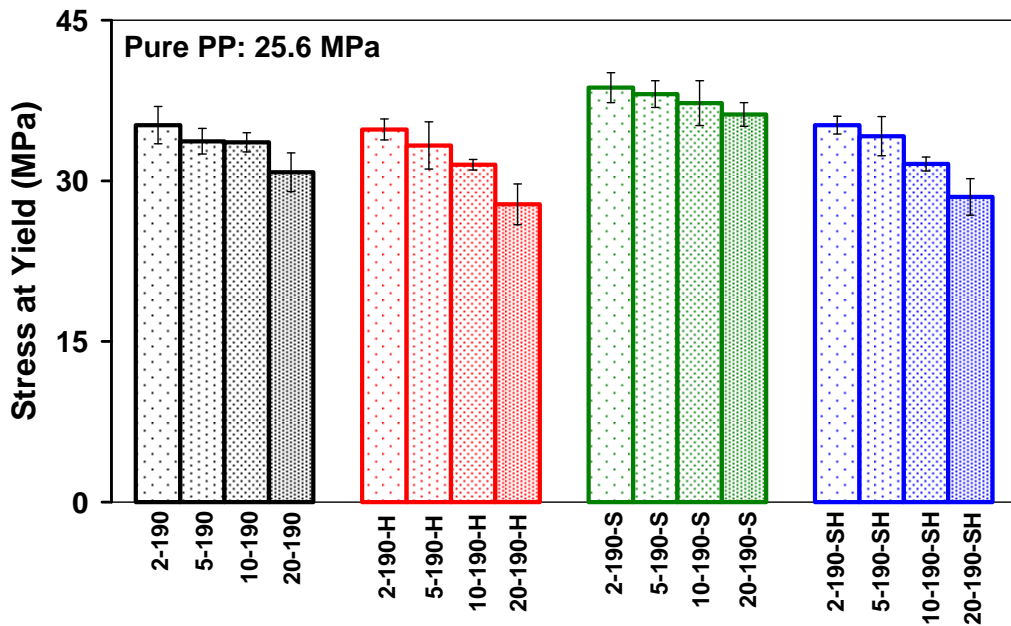


Figure 3.12 Stress at yield (MPa) for group 1 compositions

Figure 3.13 shows the variation of stress at break with composition. Similar to yield stress behavior, the stress at break values are higher than that of pure PP. A decrease in values proportional to the filler loading can be explained in a similar manner as in yield stress. The highest stress at break values were attained in the case of SCA treated compositions.

Drastic reductions in elongation at break of composites are shown in Figure 3.14. Percentage strain at break decreased with the increase in filler content in comparison with a value of 367.6 for pure PP. In the presence of SCA, elongation at break values further decreased compared to normal compositions which may be attributed to the strong coupling. Due to high constraints on the mobility PP/serpentine composites showed resistance to plastic deformation.

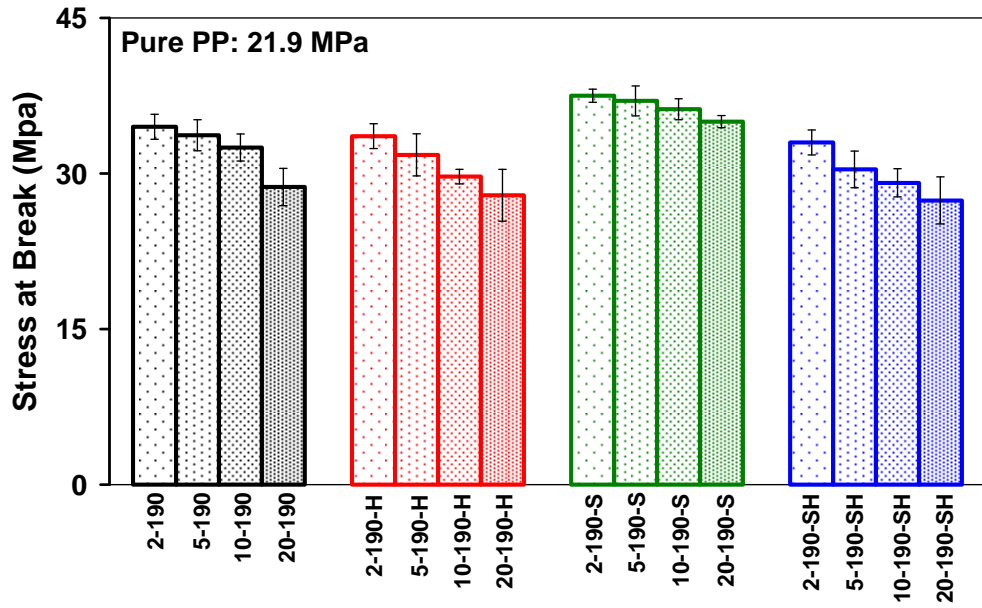


Figure 3.13 Stress at break (MPa) for group 1 compositions

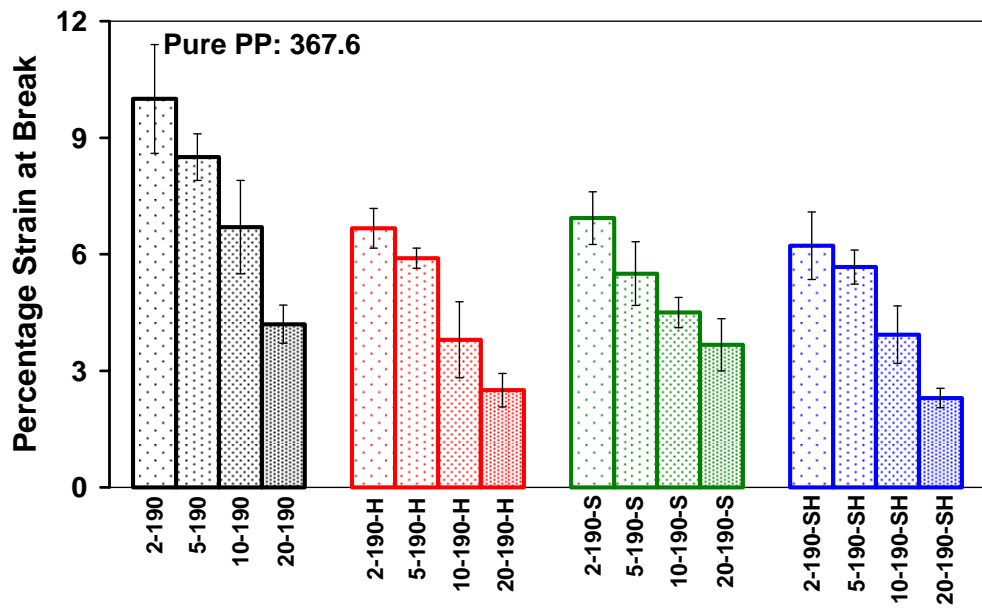


Figure 3.14 Percentage strain at break for group 1 compositions

In the overall scheme, at high-filled composites tensile properties are not much different from low-filled composites leading us to think that the composite properties are somewhat independent of filler content. If the addition of filler is concerned in a way its effect in reducing the production cost, then it seems to be a proper choice to use serpentine as filler in PP composite systems.

Table 3.2 Tensile properties of group 1 compositions processed and reprocessed at 250 rpm

Compositions	Young's Modulus (MPa)	Stress at Yield (MPa)	Stress at Break (MPa)	Percentage Strain at Break
2-250-S	843±97	26.0±1.5	22.9±1.7	7.1±0.7
5-250-S	1012±52	31.6±0.7	28.5±0.6	7.5±1.3
2-250,2-S	721±55	23.7±3.7	17.2±2.1	8.3±1.0
5-250,2-S	942±73	30.9±1.0	14.3±2.4	9.2±0.4
2-250-SH	732±62	25.9±1.2	22.7±2.8	6.5±0.2
5-250-SH	1150±50	32.1±1.6	29.4±1.1	6.7±0.5
2-250,2-SH	727±82	24.8±0.7	21.1±3.0	7.0±1.4
5-250,2-SH	1055±70	31.7±0.9	27.2±1.9	7.9±0.8

The effects of extrusion rate and reprocessing on tensile properties for low filler contents are given in Table 3.2. Although, among 2% filled compositions 2-250-S has the highest modulus, it is lower than those of any moduli of the same filler content given in Figure 3.11. Moduli of 2-250,2-S, 2-250-SH and 2-250,2-SH are nearly the same with pure PP. As the filler loading increased to 5%, in the first extrusion the Young's modulus increased due to filler effect but the increase is higher compared to their 190 rpm processed counterparts while there is a slight decrease in the second extrusion. It seems that reprocessing had negative effect on stiffness of S,250 and SH,250 compositions.

Note the similar trend in the yield stress values of the corresponding composites. Here, bonding between the matrix and the filler may be affected adversely leading

to low stress at yield. Furthermore, under these processing conditions stress at break of the composites also experienced a reduction. In the overall, the tensile properties of these composites are inferior to samples processed at 190 rpm. Processing at 250 rpm and applying second extrusion had unfavorable effect on tensile properties due to the chain scission of PP. Due to increased shear force the composites may have experienced degradation brought by chain scission.

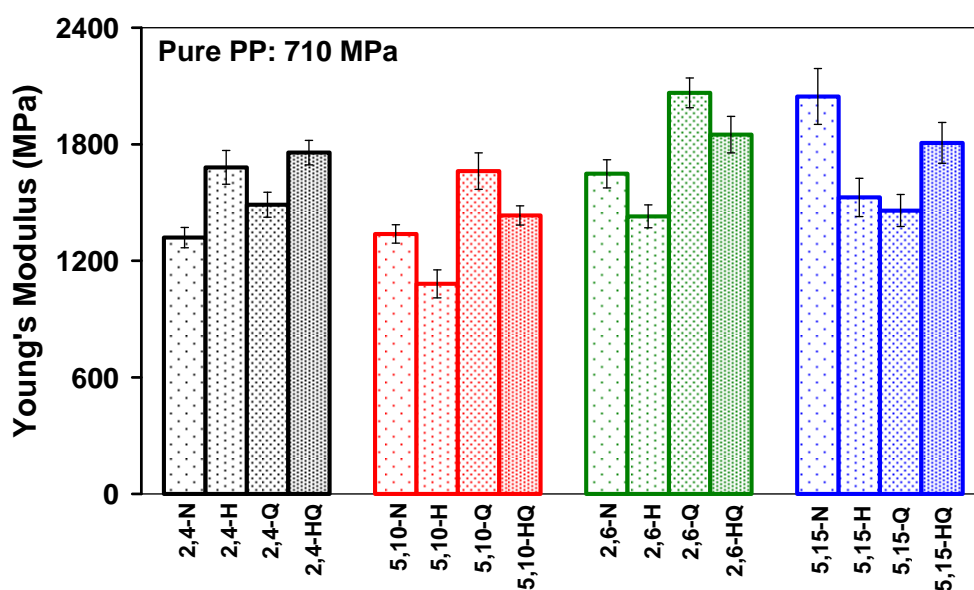


Figure 3.15 Young's modulus (MPa) for group 2 compositions

The role of the introduction of PP-g-MA to the PP matrix and QAS treatment of normal and acid treated serpentine on the tensile properties were investigated. Figure 3.15 shows the Young's modulus data for group 2 compositions. Incorporation of compatibilizer further increased the modulus for the neat formulations namely 2,4-N, 5,10-N, 2,6-N and 5,15-N (for abbreviations please refer to experimental part). Among them the maximum modulus was reached at 2046 MPa corresponding to 5,15-N which means that 188% and 59% increase compared to pure PP and 5-190-S, respectively. Hence it is obvious that the presence of PP-g-MA in the matrix improved the stiffness. According to the results

obtained in group 1 and group 2 compositions, it can be said that the acid treatment decreased the coupling effect of SCA. When the effect of QAS is considered, Young's modulus values increased with respect to neat compositions except for 5,15-N and 5,15-Q. The modulus of 2,4-Q is 2 times and 5,10-Q is 2.3 times greater than that of pure PP. The maximum improvement was achieved in the case of 2,6-Q which is 2.9 times higher compared to pure PP. QAS was also effective in increasing the modulus of acid treated compositions. In the case of QAS treated compositions there may be some intercalation of the layers in which case the stiffening effect of the layers further increases due to the increased surface area of the layers.

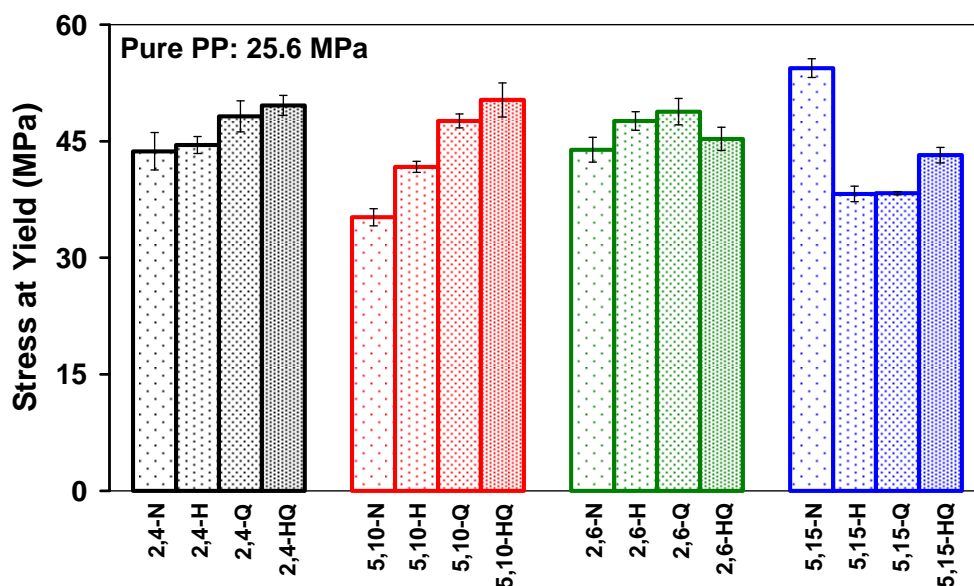


Figure 3.16 Stress at yield (MPa) for group 2 compositions

The variation of the yield stress with group 2 compositions is illustrated in Figure 3.16. General view shows additional improvement for neat formulations excluding 5,10-N composition in comparison to the corresponding group 1 composites. The maximum yield stress was achieved for 5,15-N at 54.4 MPa. The reason can be attributed to the high amount of PP-g-MA compared to 5,10-N formulation which

has the lowest yield stress of group 2, since compatibilizer may not compensate the filler effect at that composition. As an indication of high yield stress, PP should have better interfacial adhesion to serpentine in the presence of PP-g-MA. Except 5,15-N and 5,15-Q, QAS treatment further increased the yield stress which reached a maximum at 48.8 MPa for 2,6-Q.

While the similar behavior is observed with yield stress, the differences between compositions are pronounced for the stress at break as shown in Figure 3.17. Refer to the figure, the increase is 49%, 14%, 29% and 19% for 2,4-Q, 5,10-Q, 2,6-Q and 5,15-Q, respectively in comparison to their neat formulations. Both 2,4-HQ and 5,10-HQ showed further increase in stress at break values which can be perceived as an indication of high interaction at the interphase. 5,15-N composition showed interesting behavior; although its yield stress is maximum, it experienced very low stress at break. 2,6-Q has the highest value among QAS treated compositions, at the same time it had higher modulus and yield stress.

Figure 3.18 demonstrates the variation of elongation at break with compositions of group 2. The compositions of this group behaved differently compared to group 1 which experienced very drastic reduction in elongation at break compared to pure PP even at the smallest filler content. Here, in spite of the decrease in percentage strain at break with filler addition, the reduction was not in the extreme limits. Evidently, addition of compatibilizer was not harmful to the deformability of the matrix. 2,4-N and 2,6-N compositions exhibited very high values of elongation 324.9 and 327.7, respectively which can be comparable to 367.6 for pure PP. As seen from the figure for high loadings namely 5,10-N and 5,15-N compositions, the reduction in values is observed as expected. Generally the lowest values were obtained for acid treated samples parallel to filler loading. 2,4-Q and 2,6-Q exhibited slightly lower elongation at break compared to 2,4-N and 2,6-N, respectively.

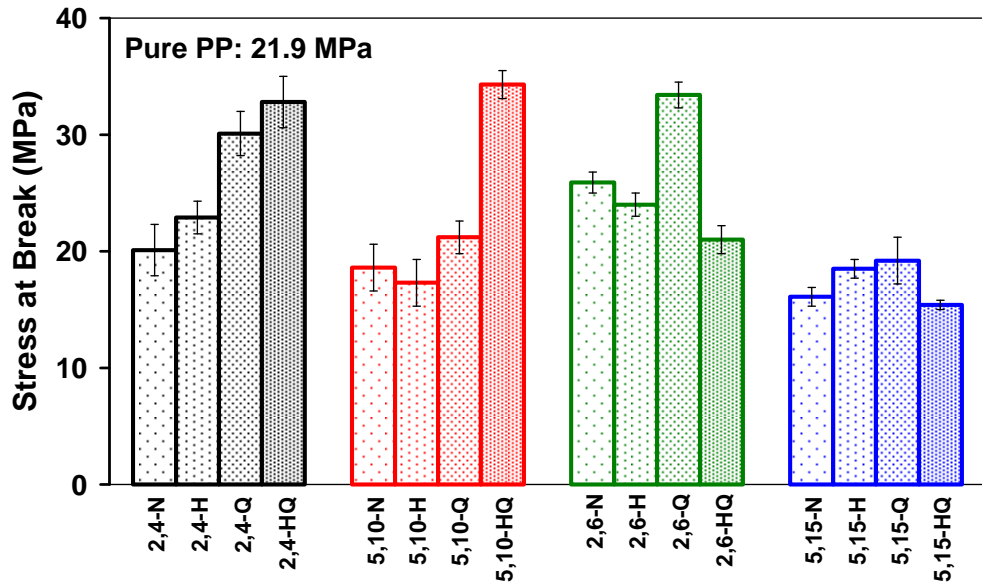


Figure 3.17 Stress at break (MPa) for group 2 compositions

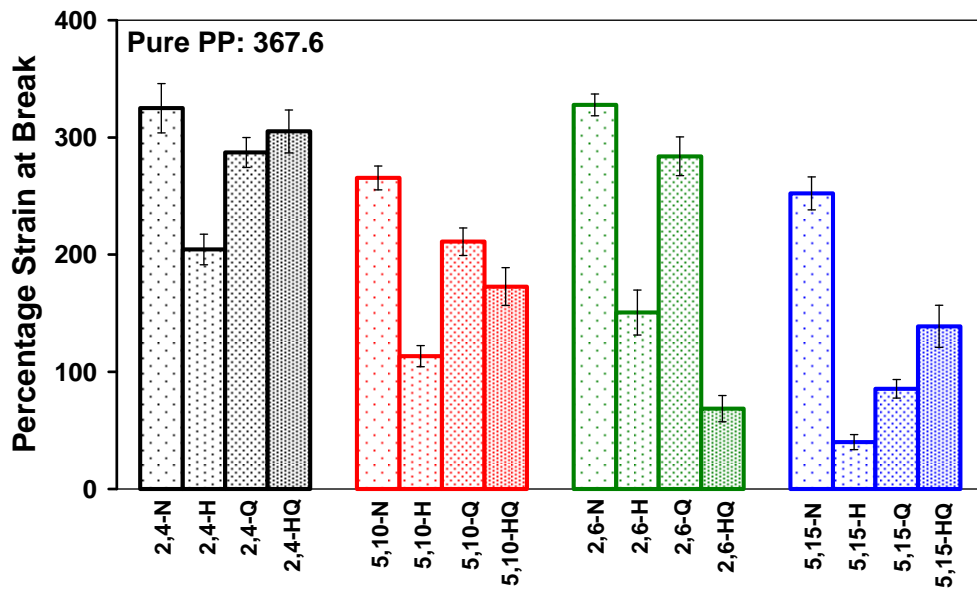


Figure 3.18 Percentage strain at break for group 2 compositions

3.6 Thermal Behavior and Crystallinity of the Matrices

DSC was employed to determine the melting temperatures and the percent crystallinity of all studied systems. Table 3.3 shows the DSC results for group 1 compositions. Pure PP exhibited a single and sharp endotherm at 167.0°C belonging to the α -phase which is the most common crystal form of isotactic-PP. Independent of processing conditions and treatments the upward shift of 1-3°C in the melting temperatures was observed for all filled systems in comparison to PP. 2-250-SH showed maximum increase with a T_m of 170.3°C. The onset melting temperatures of PP/serpentine composites are lower than of PP with the following exceptions 20-190-S, 2-250-SH, 2-250,2-SH and 5-250,2-SH. The minimum is seen in 5-250-S formulation at 152.3°C. Evidently, these changes show increased melting range (from onset to melting temperatures) for filled samples. The answer for the question why such an increase occurs in melting temperatures for the composites could be the disappearance of the crystal structure at higher temperatures than pure PP due to stabilization which may be induced by the enhanced filler-matrix interaction. Another possible explanation can be the increase in the lamellar thickness of the PP crystals leading to high melting temperatures.

The percent crystallinity of the compositions was calculated according to the following equations:

ΔH = Melting enthalpy from the thermogram (J/g)/ PP ratio

$$\% \text{ Crystallinity} = (\Delta H / \Delta H_{100}) * 100$$

where ΔH_{100} is 209 J/g [91] representing the heat of fusion for a 100% crystalline PP.

Table 3.3 DSC data for group 1 compositions

Composition	T_m onset (°C)	T_m peak (°C)	% Crystallinity
Pure PP	156.4	167.0	29.76
2-190	154.6	168.1	30.31
5-190	154.3	170.1	28.87
10-190	154.3	169.6	35.73
20-190	153.9	167.9	36.02
2-190-H	155.2	169.6	30.72
5-190-H	154.6	169.3	36.17
10-190-H	153.8	168.6	34.75
20-190-H	153.9	167.7	37.89
2-190-S	154.7	170.2	34.32
5-190-S	155.0	168.1	35.59
10-190-S	154.3	169.7	26.12
20-190-S	156.9	168.5	31.18
2-190-SH	154.5	168.3	37.80
5-190-SH	154.4	168.3	36.82
10-190-SH	154.9	168.0	33.82
20-190-SH	153.1	168.2	31.39
2-250-S	156.0	169.8	33.48
5-250-S	152.3	169.1	39.72
2-250,2-S	154.6	170.1	32.62
5-250,2-S	153.8	169.8	29.90
2-250-SH	160.3	170.3	29.68
5-250-SH	154.4	168.3	30.09
2-250,2-SH	156.8	168.7	37.40
5-250,2-SH	157.7	170.1	29.59

As in the case of melting temperatures, the change in percent crystallinity of composites was not affected by the processing conditions and treatments. The general trend seems to be a slight increase in crystallinity with few exceptions. The reason for that may be attributed to the role of filler as a nucleating agent leading to heterogeneous nucleation and increase in percent crystallinity.

Table 3.4 DSC data for group 2 compositions

Composition	T_m onset (°C)	T_m peak(°C)	% Crystallinity
2,4-N	154.1	166.9	29.12
2,4-H	156.7	166.4	25.80
2,4-Q	154.6	166.4	31.27
2,4-HQ	150.7	166.6	36.89
5,10-N	157.2	168.7	29.11
5,10-H	153.2	166.6	32.91
5,10-Q	153.9	165.7	33.88
5,10-HQ	150.6	167.9	32.33
2,6-N	153.9	166.5	27.75
2,6-H	152.4	166.7	30.82
2,6-Q	157.2	166.3	32.71
2,6-HQ	153.9	166.3	35.73
5,15-N	153.9	165.6	33.96
5,15-H	153.1	166.0	35.42
5,15-Q	152.5	165.5	33.49
5,15-HQ	152.0	167.6	35.18

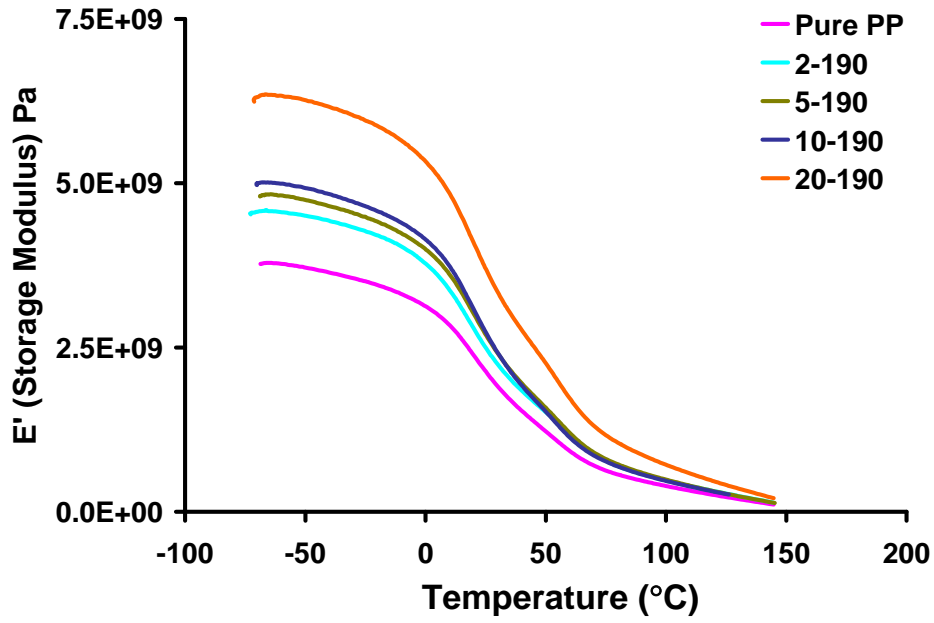
The DSC results of group 2 compositions are presented in Table 3.4. Although maleated polymers usually exhibit a shoulder on their melting endotherms, this is not very clear for PP-g-MA (see Appendix E). However in filled compositions, it becomes more evident, especially in those containing high amount of PP-g-MA compatibilizer. The explanation may be that the crystallites formed due to the graft functional groups have different stability than pure PP. PP-g-MA showed higher melting range with T_m onset of 134.5°C and T_m peak of 152.8°C and low melting enthalpy with respect to PP. Besides, the shape of the melting endotherm reveals that PP-g-MA does not have uniform crystal formation. This situation can be expected since the presence of graft functional groups may deteriorate the crystalline sizes of PP. Generally the melting point of the filled compositions experienced a decrease which is maximum for 5,15-Q (1.51°C) caused by the compatibilizer. To see the effect of compatibilizer both on melting and onset melting temperatures the compositions with the same filler but different compatibilizer content can be compared namely pairs of 2,4-N; 2,6-N and 5,10-N; 5,15-N. Examination of the data for those shows that the reduction in temperatures

is more in the case of compositions with high content of compatibilizer. It seems that PP-g-MA has no influence on the crystallinity of group 2 compositions.

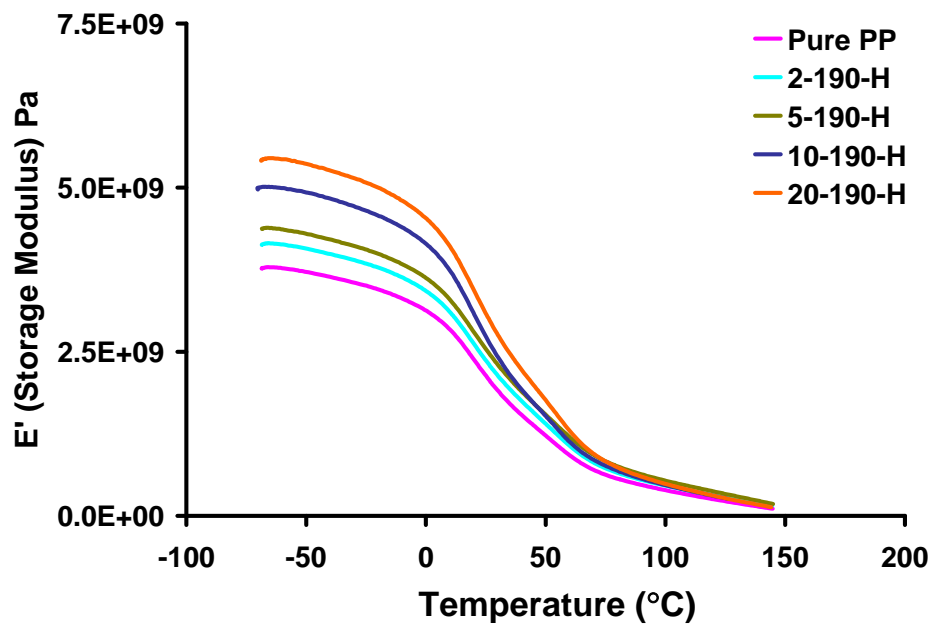
3.7 DMA

To study the performance of all compositions under loading and temperature, DMA was conducted and the results are given in terms of storage and loss moduli versus temperature through the Figures 3.19-3.24. Young's modulus of the material is somewhat different than storage and loss modulus in that the ability to store and lose energy is measured by the former and the latter, respectively. With the addition of a rigid, inorganic filler, the effect on the bulk properties e.g. modulus of the material can be followed by DMA. Referring to the figures, higher storage modulus was demonstrated in the case of filled PP compared to pure PP over the entire temperature range. Alpha (α) transition of PP (or T_g) can be seen in storage modulus-temperature scans. The reduction of modulus up to T_g is slight with temperature. However after T_g rapid decline of the values can be seen as a result of a change from glassy to rubbery state as expected. It can be generally observed that at lower temperatures the difference between the modulus values of the composites is higher, while as the temperature increased the modulus values came close to each other. Storage modulus values of N and H compositions are near to each other except 20-190 which had a pronounced increase even at higher temperatures. Although there is an increase in the case of SH composites, samples of S showed the highest moduli. It is obvious that SCA increased the stiffness as it did in Young's modulus.

Additionally, the rubbery plateau region gives us information about the crystallinity of the material [94]. PP places below the other composites indicative of low crystallinity in comparison to filled grades. A little upward shift of the plateau of the composites shows the higher crystallinity well agreed with the DSC results.

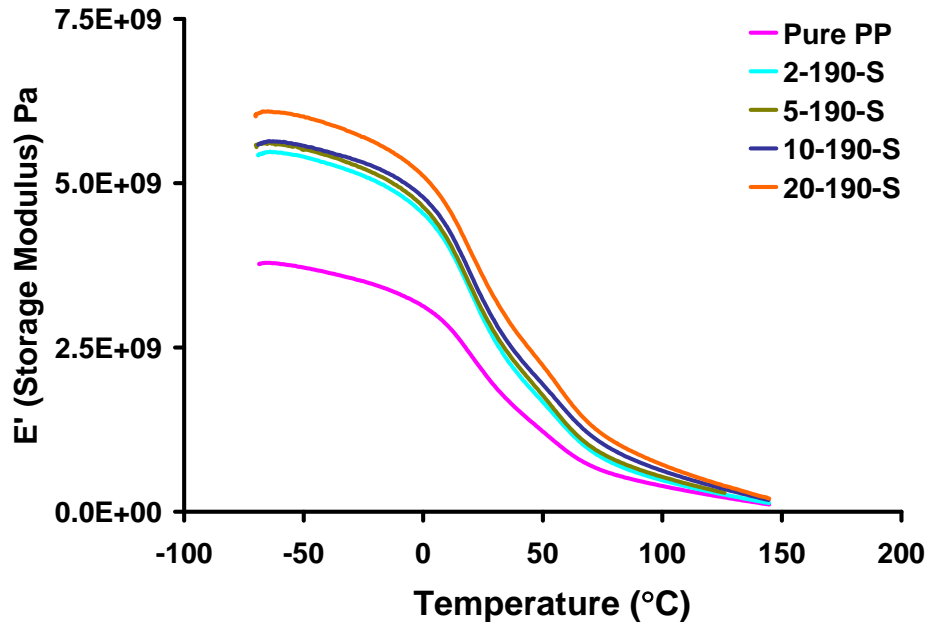


(a)

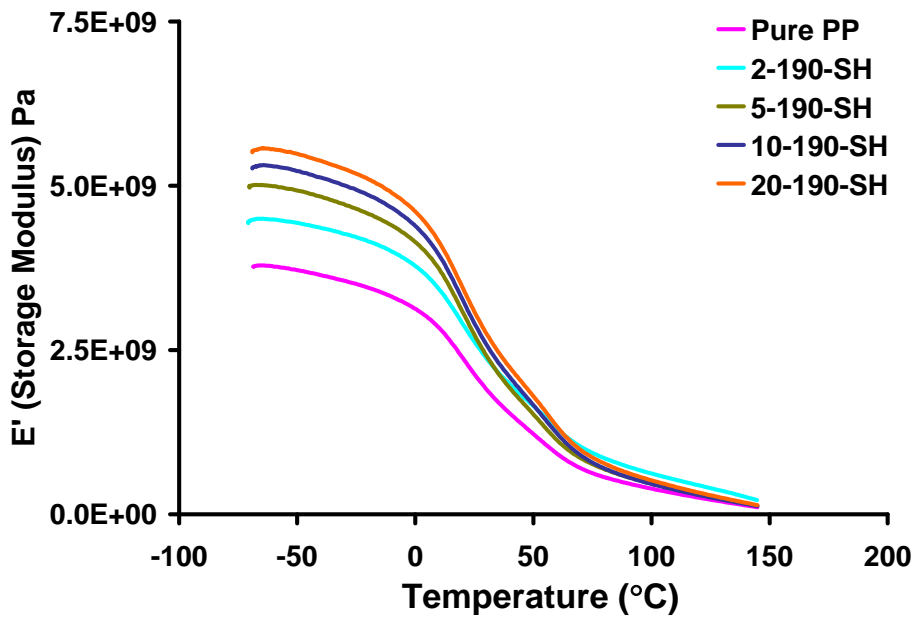


(b)

Figure 3.19 Storage modulus versus temperature scan for (a) N, (b) H compositions

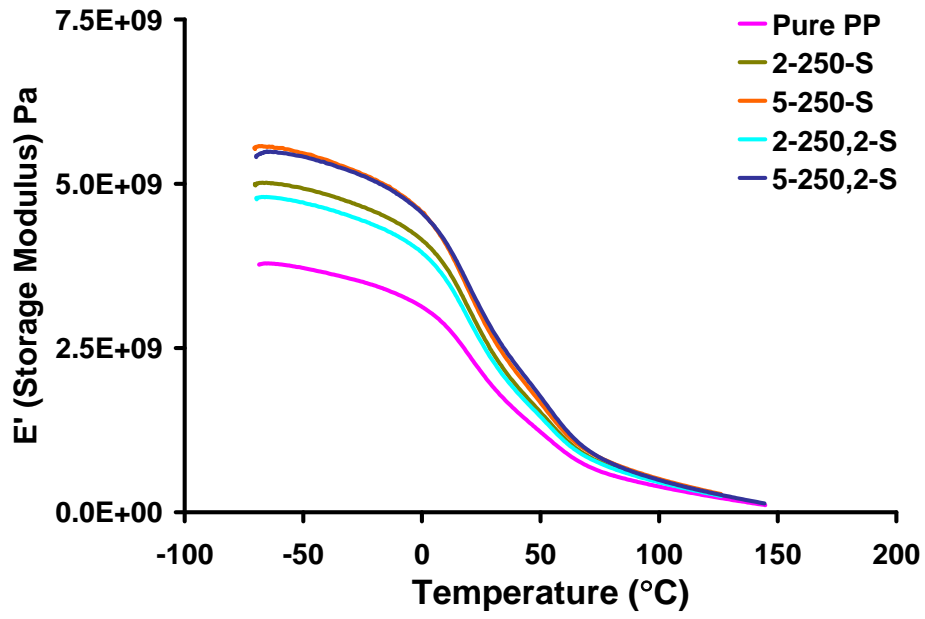


(a)

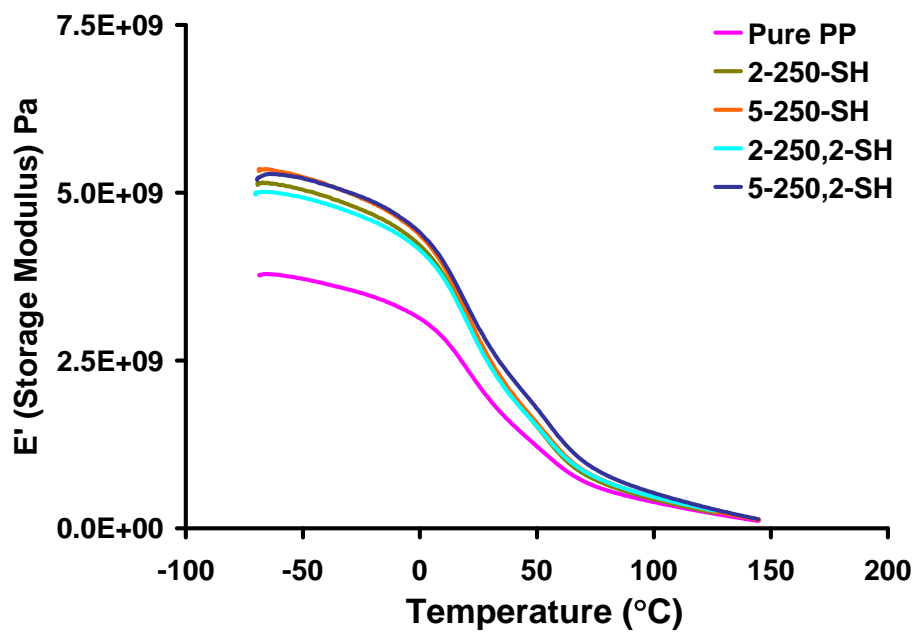


(b)

Figure 3.20 Storage modulus versus temperature scan for (a) S, (b) SH compositions

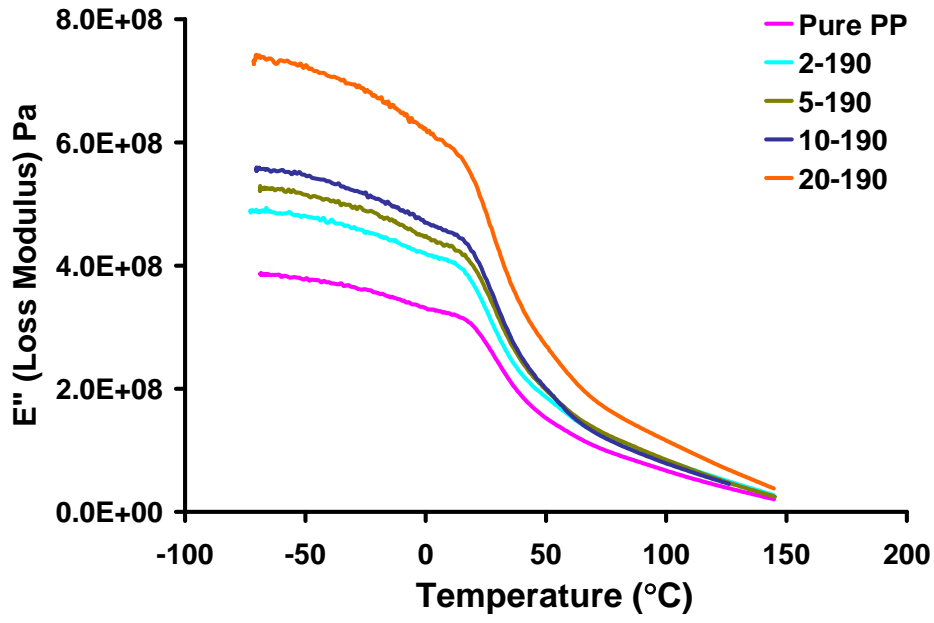


(a)

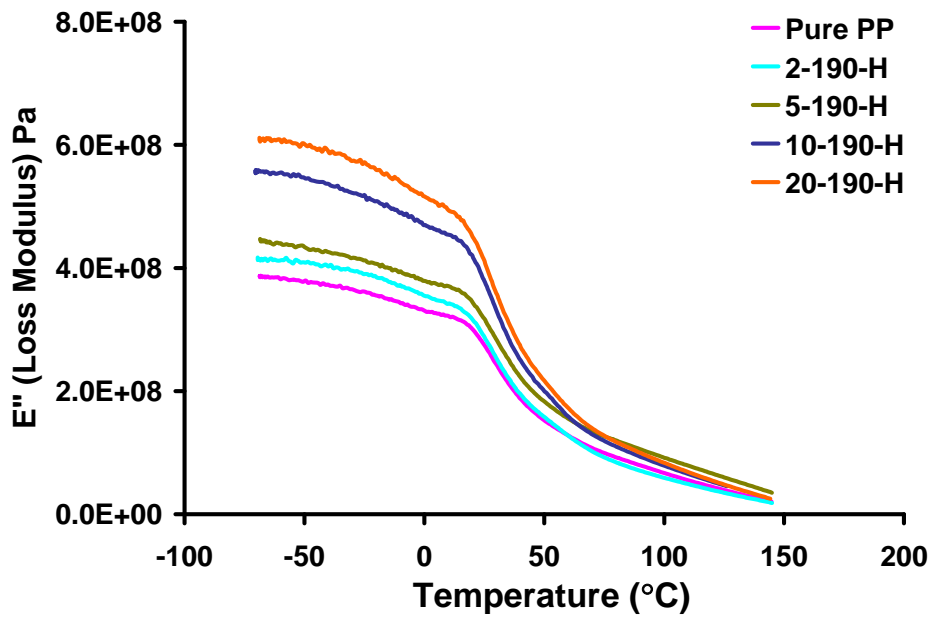


(b)

Figure 3.21 Storage modulus versus temperature scan for (a) S,250, (b) SH,250 compositions

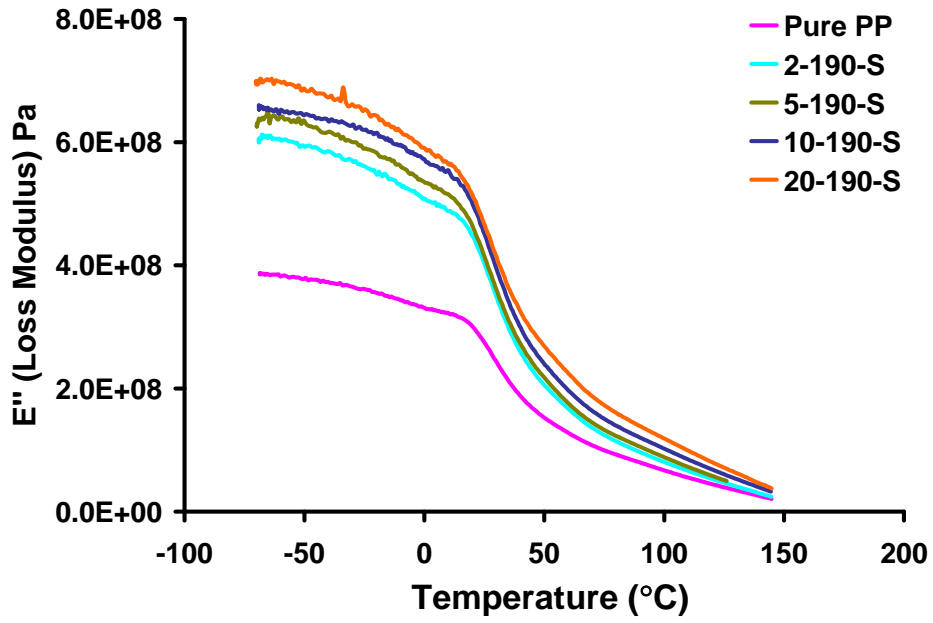


(a)

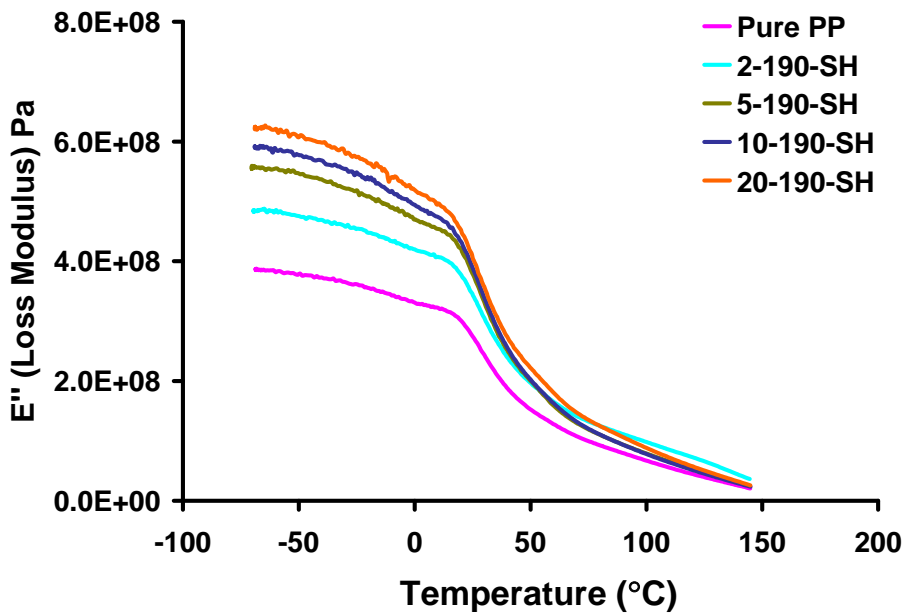


(b)

Figure 3.22 Loss modulus versus temperature scan for (a) N, (b) H compositions

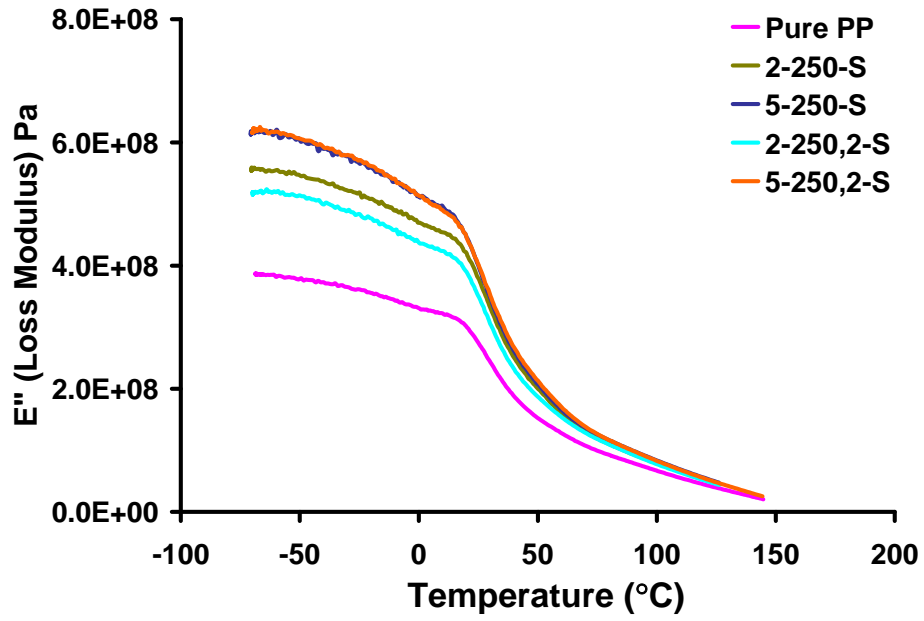


(a)

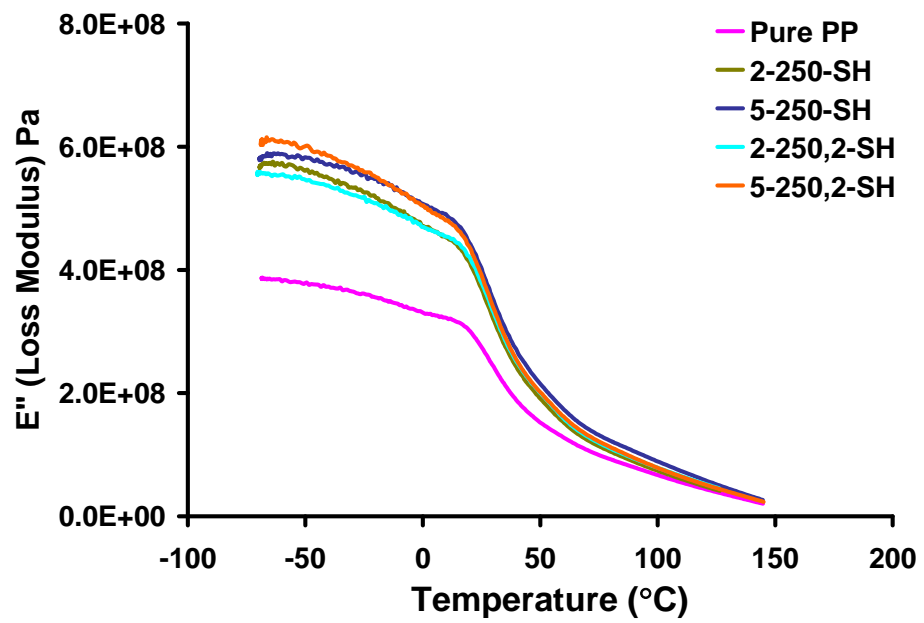


(b)

Figure 3.23 Loss modulus versus temperature scan for (a) S, (b) SH compositions



(a)



(b)

Figure 3.24 Loss modulus versus temperature scan for (a) S,250, (b) SH,250 compositions

Apparently, the loss moduli of composites are significantly higher than that of pure PP. Note that, the same trend can be seen for loss moduli as in storage moduli. Here, the α transition is more clearly shown with a relatively sharp turning point from which T_g of the composites can be determined.

There are at least five ways of assigning T_g from the storage modulus, loss modulus and $\tan \delta$ data of DMA [94]. In this study, the T_g of all compositions were found from the $\tan \delta$ temperature scans (see Appendix F) as the peak value between 0 and 50°C. Accordingly, the T_g of the composites were determined and tabulated in Table 3.5.

Table 3.5 T_g data of group 1 compositions obtained from $\tan \delta$

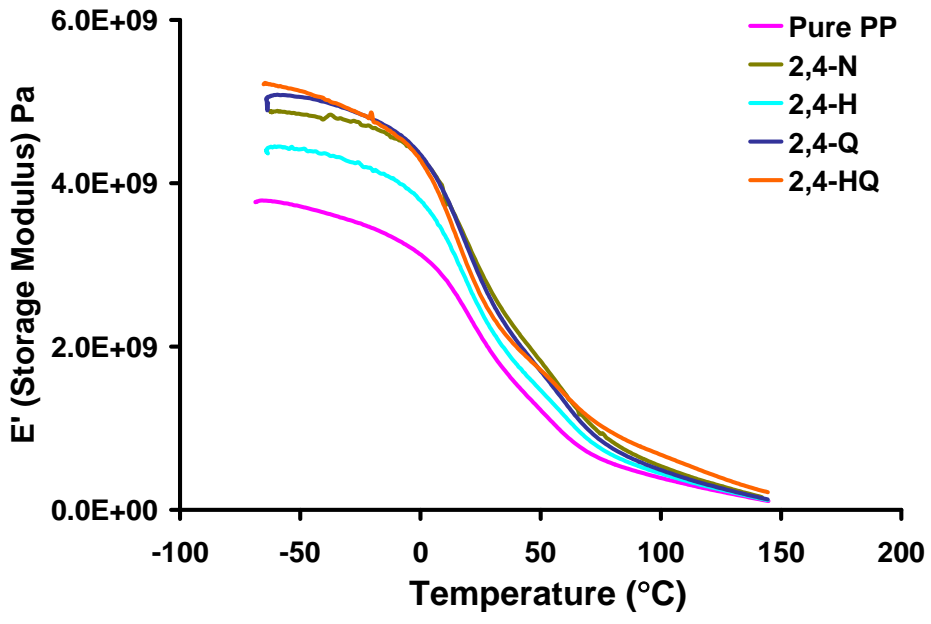
N	T_g	H	T_g
2-190	26.1	2-190-H	27.1
5-190	25.8	5-190-H	25.3
10-190	22.2	10-190-H	25.0
20-190	21.2	20-190-H	24.9
S	T_g	SH	T_g
2-190-S	24.2	2-190-SH	24.5
5-190-S	22.6	5-190-SH	24.2
10-190-S	22.6	10-190-SH	23.0
20-190-S	21.4	20-190-SH	21.6
S,250	T_g	SH,250	T_g
2-250-S	24.4	2-250-SH	24.5
5-250-S	23.4	5-250-SH	22.6
2-250,2-S	25.6	2-250,2-SH	25.3
5-250,2-S	24.3	5-250,2-SH	22.5

The T_g of pure PP which is 27.4°C is comparable to that of filled PP. The reduction in T_g of the matrix in composites is noticeable. Such a reduction was found by Hambir et al. [64] in a study involving polypropylene/clay

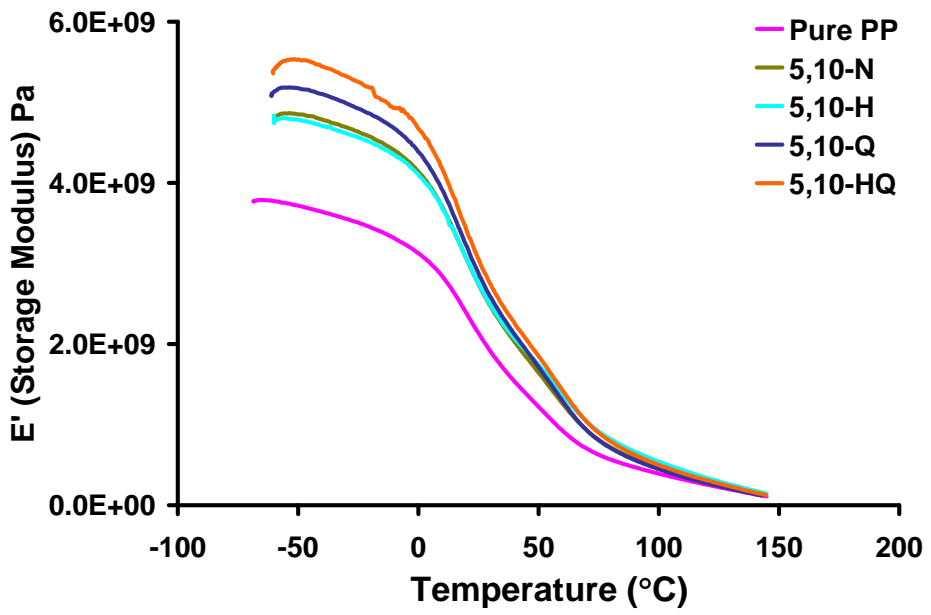
nanocomposites. They related the observed phenomena with the presence of constrained fraction in PP/clay nanocomposites and restricted cooperative motion of the polymer chains. For PP/serpentine composites, the similar comment could be made, because the reinforcing effect of serpentine filler is evident from storage and loss moduli data of DMA and tensile testing experiments.

The storage and loss moduli of group 2 compositions as a function of temperature are displayed through the Figures 3.25-3.28. All samples of the group exhibited higher storage and loss moduli compared to pure PP over the whole temperature range of study. As a general trend, similar to group 1 compositions, the moduli values are apart from each other at low temperatures. As temperature increased, the differences between the values reduced for both kinds of moduli plots. In order to interpret the results more clearly the storage modulus data are presented for representative temperatures in Table 3.6. Here, since storage and loss moduli exhibited similar trend, the former was selected for comparison.

Owing to the PP-g-MA contained in all compositions of group 2, the increase of compatibilization between PP and serpentine was expected. Along with that, PP-g-MA may react with the hydroxyl groups of serpentine causing covalent bonds to form which add to the compatibilization of the matrix and the filler. Although all compositions have higher moduli than pure PP, the increment is not much for neat samples with respect to their Young's moduli increment when PP-g-MA was introduced into the matrix. To achieve organophilization of the filler and get intercalation and/or exfoliation of the filler layers QAS treatment was employed. Except for 5,15-Q, QAS treated compositions showed higher moduli than their untreated counterparts leading us to think that the formation of dispersed layers throughout the matrix is responsible for the increase.

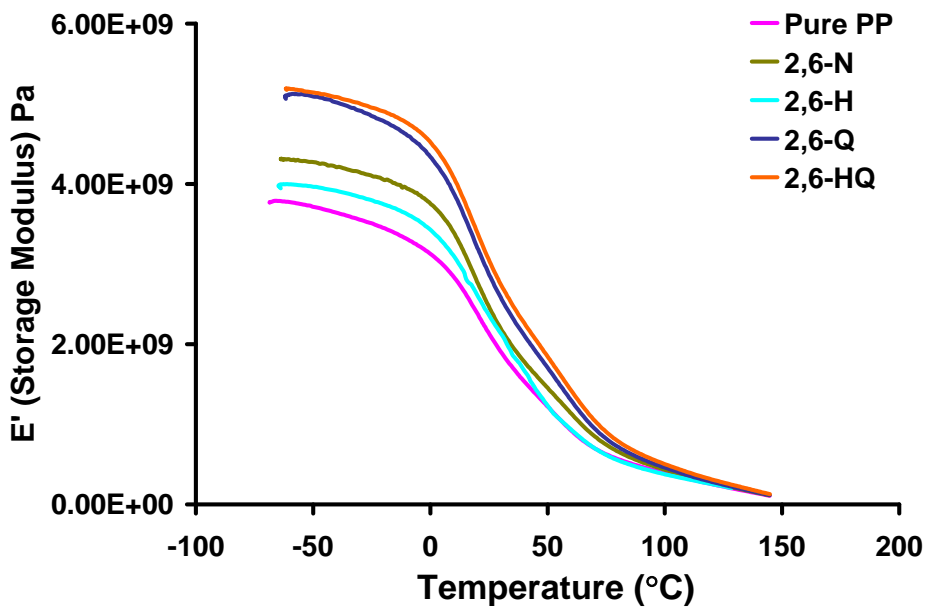


(a)

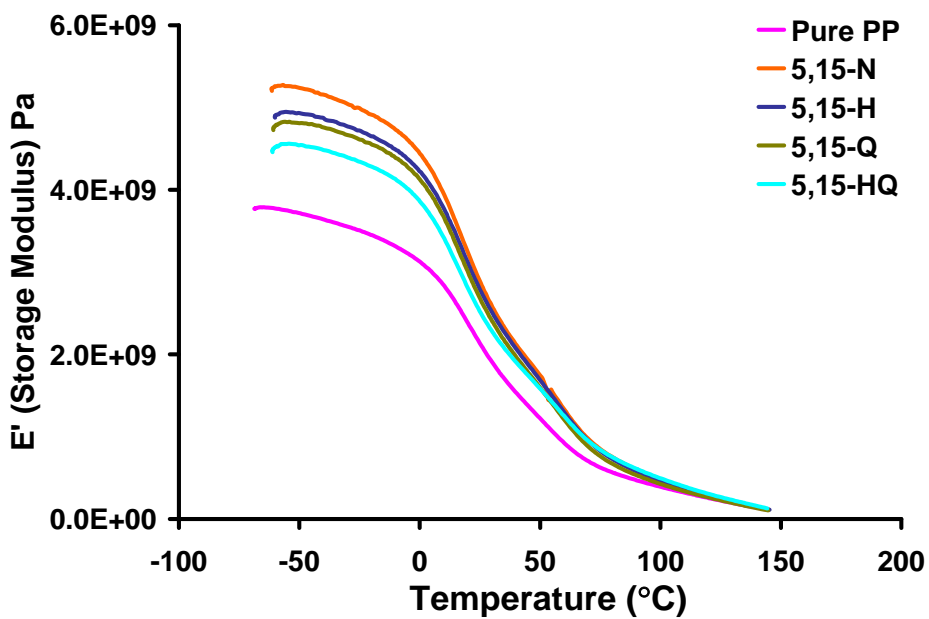


(b)

Figure 3.25 Storage modulus versus temperature scan for (a) 2,4, (b) 5,10 compositions

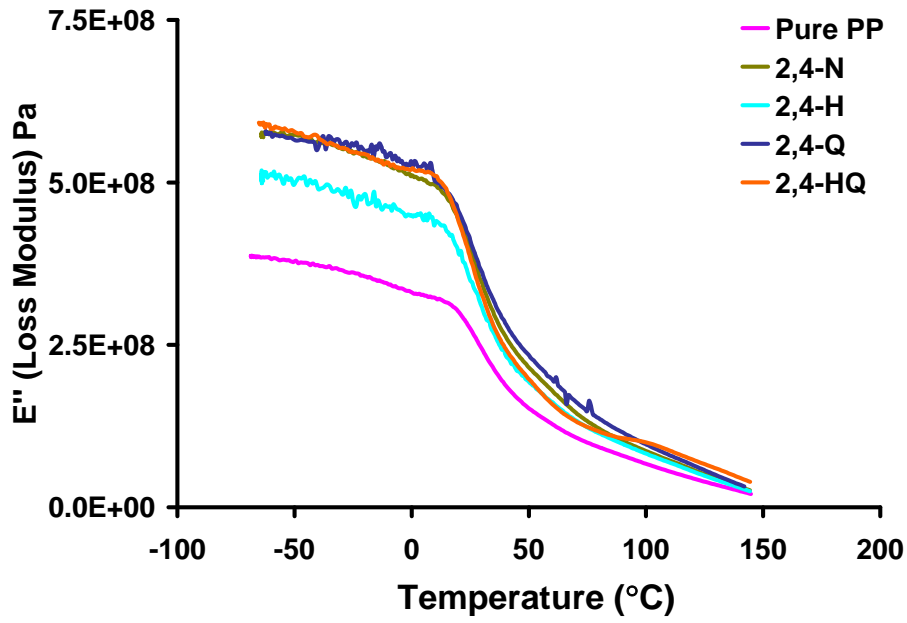


(a)

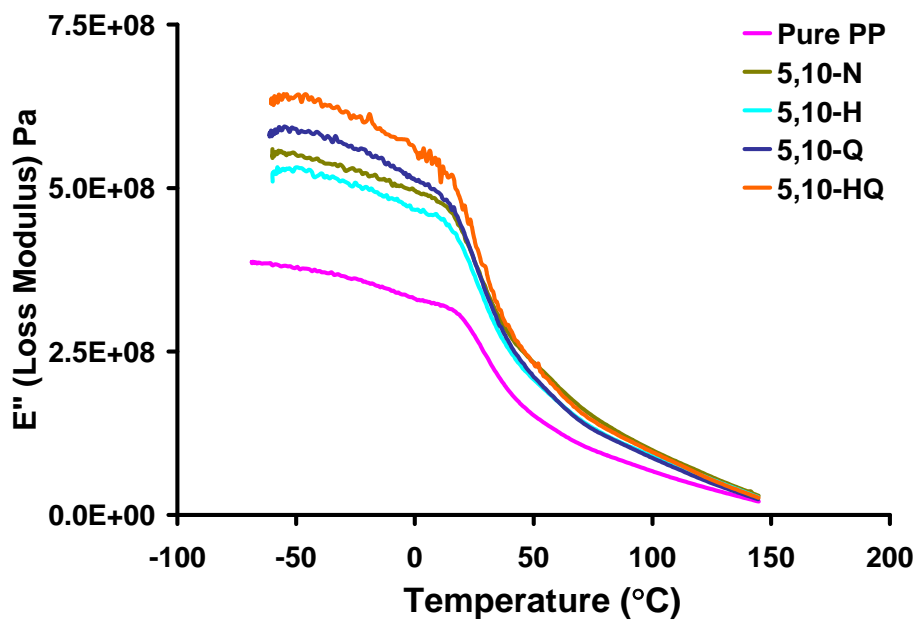


(b)

Figure 3.26 Storage modulus versus temperature scan for (a) 2,6, (b) 5,15 compositions

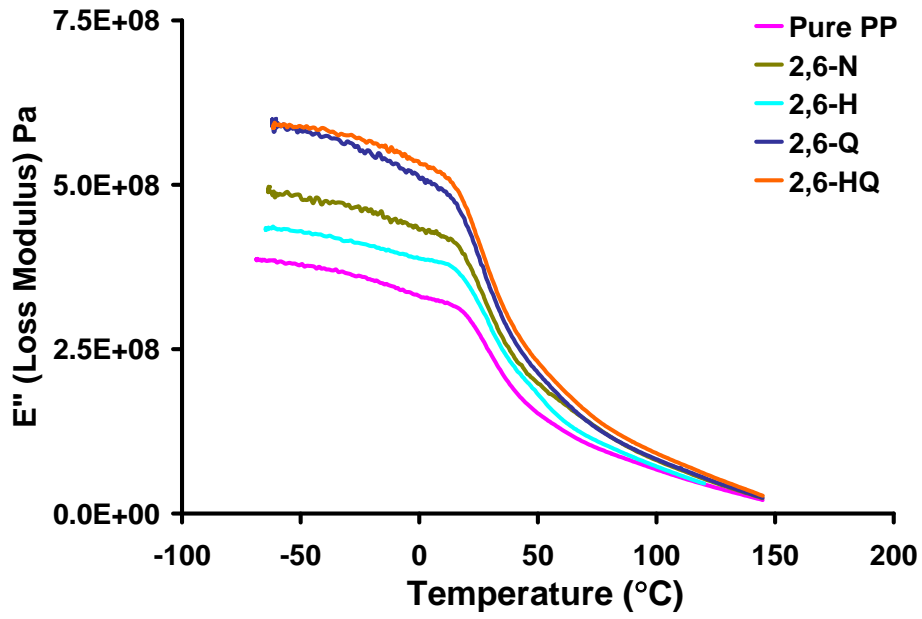


(a)

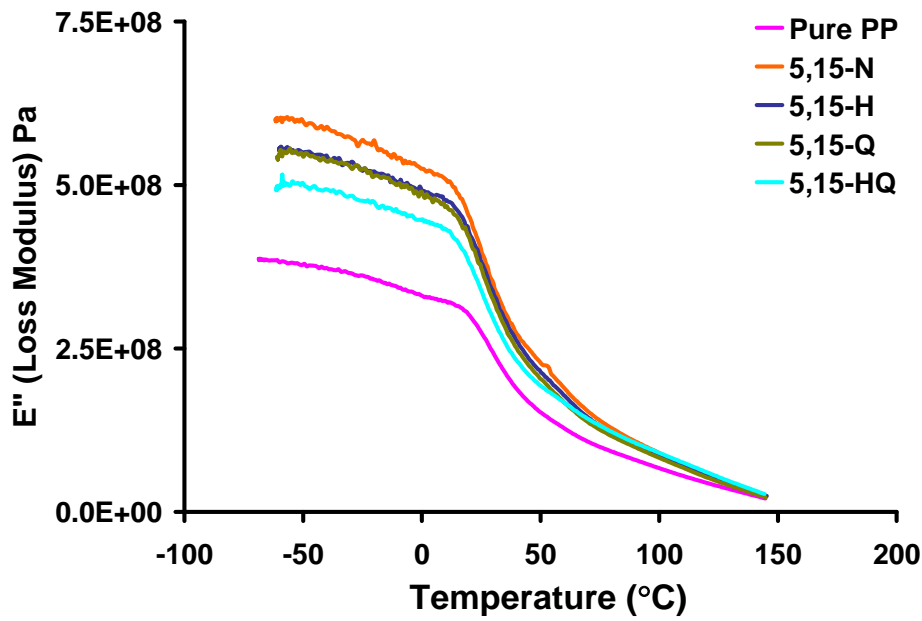


(b)

Figure 3.27 Loss modulus versus temperature scan for (a) 2,4, (b) 5,10 compositions



(a)



(b)

Figure 3.28 Loss modulus versus temperature scan for (a) 2,6, (b) 5,15 compositions

In order to see the effect of acid treatment, as in the case of group 1 compositions, samples with and without QAS were HCl treated. It is observed that, acid treatment led to lower moduli for all acid treated compositions than neat samples. The reason for the reduction in moduli for acid treated samples can be attributed to a possible layer formation during the hydrolysis which may not let the compatibilized PP interact with the filler. Interestingly, it can be inferred from the modulus data that 2,4-HQ, 2,6-HQ and 5,10-HQ exhibited the highest moduli excluding 5,15 compositions. Since all samples of group 2 contain SCA, the effect of it is also important remembering that in the case of SH compositions the Young's modulus are lower than S. For HQ treated samples the effect of SCA may be lower than in the case of H compositions due the presence of QAS.

Table 3.6 Storage modulus and T_g data of group 2 compositions

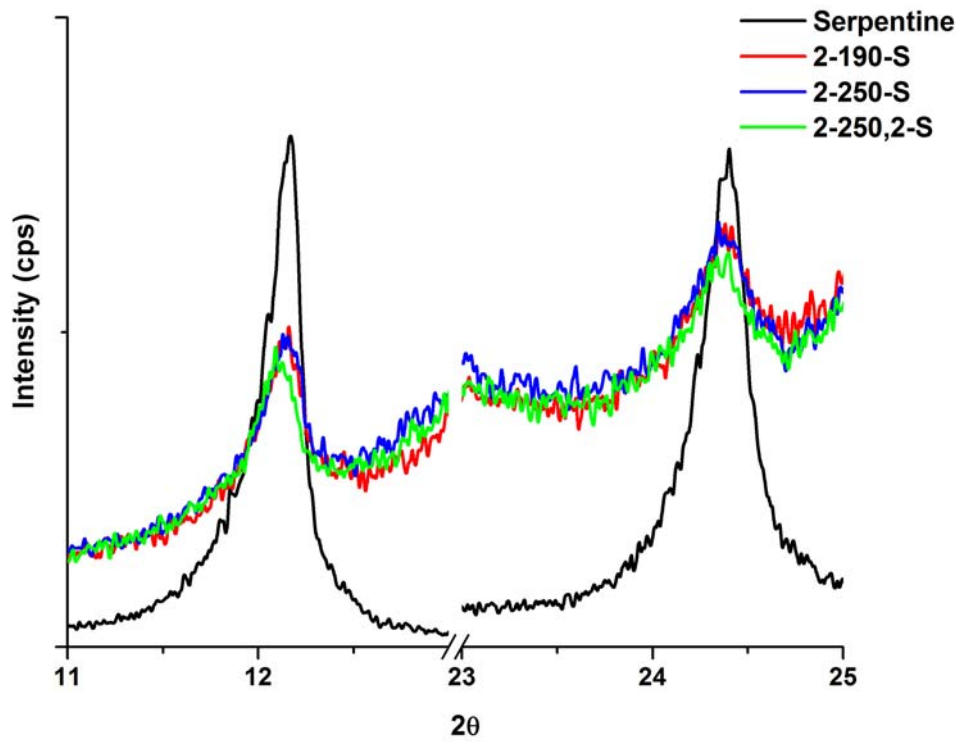
Composition	Storage Modulus (GPa)					T_g
	-40°C	0°C	40°C	80°C	120°C	
<i>2,4-N</i>	4.8	4.3	2.2	0.8	0.3	23.64
<i>2,4-H</i>	4.4	3.8	1.8	0.7	0.3	22.01
<i>2,4-Q</i>	5.0	4.4	2.1	0.7	0.3	21.02
<i>2,4-HQ</i>	5.0	4.3	2.0	0.9	0.4	20.78
<i>2,6-N</i>	4.2	3.8	1.8	0.7	0.3	24.54
<i>2,6-H</i>	3.9	3.4	1.7	0.6	0.3	23.78
<i>2,6-Q</i>	5.0	4.4	2.1	0.7	0.3	22.05
<i>2,6-HQ</i>	5.1	4.5	2.3	0.8	0.3	20.18
<i>5,10-N</i>	4.8	4.1	2.0	0.7	0.3	22.72
<i>5-10-H</i>	4.7	4.1	2.1	0.8	0.3	23.00
<i>5-10-Q</i>	5.1	4.4	2.1	0.7	0.3	20.36
<i>5,10-HQ</i>	5.4	4.7	2.3	0.8	0.3	21.74
<i>5,15-N</i>	5.2	4.4	2.1	0.8	0.3	23.11
<i>5,15-H</i>	4.9	4.2	2.1	0.7	0.3	24.09
<i>5,15-Q</i>	4.8	4.1	2.0	0.7	0.3	23.78
<i>5,15-HQ</i>	4.5	3.9	1.9	0.8	0.3	20.93

It is important to note that the dynamic modulus properties of 5,15 compositions showed close resemblance to Young's modulus as well as other tensile properties. In contrast to other compositions of group 2, all 5,15 samples behaved in a different manner. While 5,15-N exhibited the highest moduli 5,15-Q and 5,15-HQ showed relatively lower modulus. It can be thought that there should be compositions with a certain PP-g-MA/serpentine ratio which give the optimum combination of physical and mechanical properties.

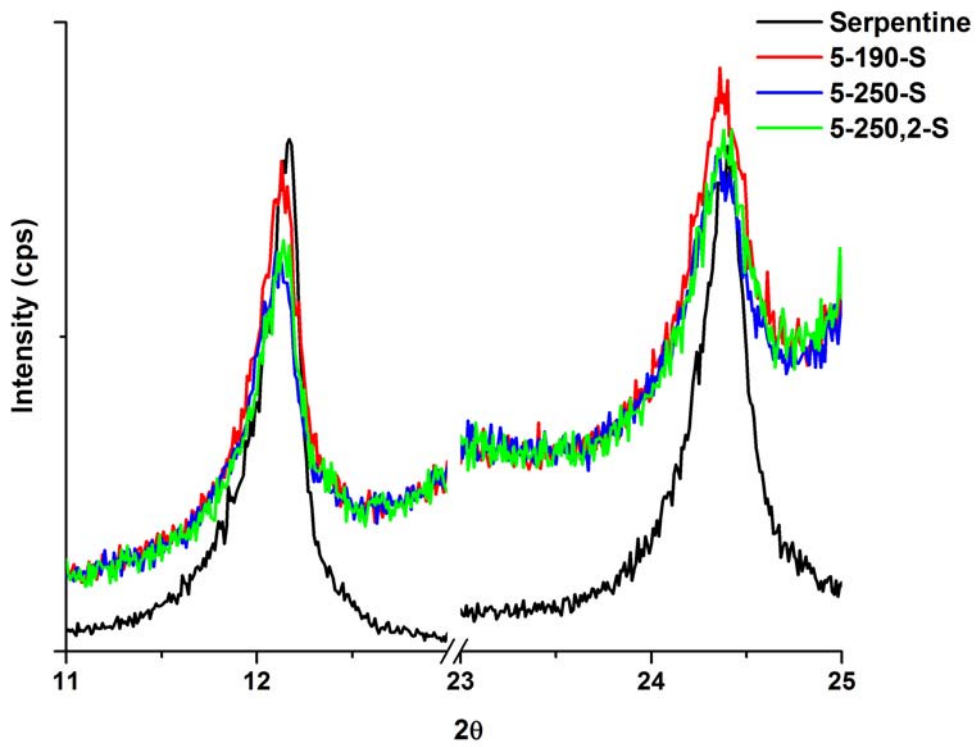
Table 3.6 also presents the T_g of group 2 compositions which are lower in magnitude compared to 27.4°C of pure PP. The situation can be explained in a manner similar to the reasoning explained before for group 1 compositions.

3.8 X-Ray Analysis

The structures of all 2 and 5% filler loaded and SCA treated composites of group 1 were characterized by XRD analysis. There are two reasons of choosing these compositions. The composites with the same filler content with group 2 were studied to see the effect of compatibilization of PP and organophilization of serpentine on the structure. In SCA treated compositions with low filler content, layer intercalation or exfoliation, if there is any, was also aimed to study. The XRD patterns of the compositions are given in Figures 3.29-3.30 and the corresponding d-spacing data are displayed in Table 3.7. As seen from the figures, only two serpentine peaks were drawn excluding the peaks coming from PP to evaluate the possible shift of the peaks more clearly. Although serpentine exhibits two intense peaks at 2θ values of 12.17 and 24.4°, d-spacing data of composites were calculated according to the former. Both figures indicate that there is no remarkable increase in the basal spacing of the composites. This can be attributed to the dependency of filler dispersion through the matrix to the modification of the filler and the compatibilization of the matrix which were absent in the case of group 1 composites.

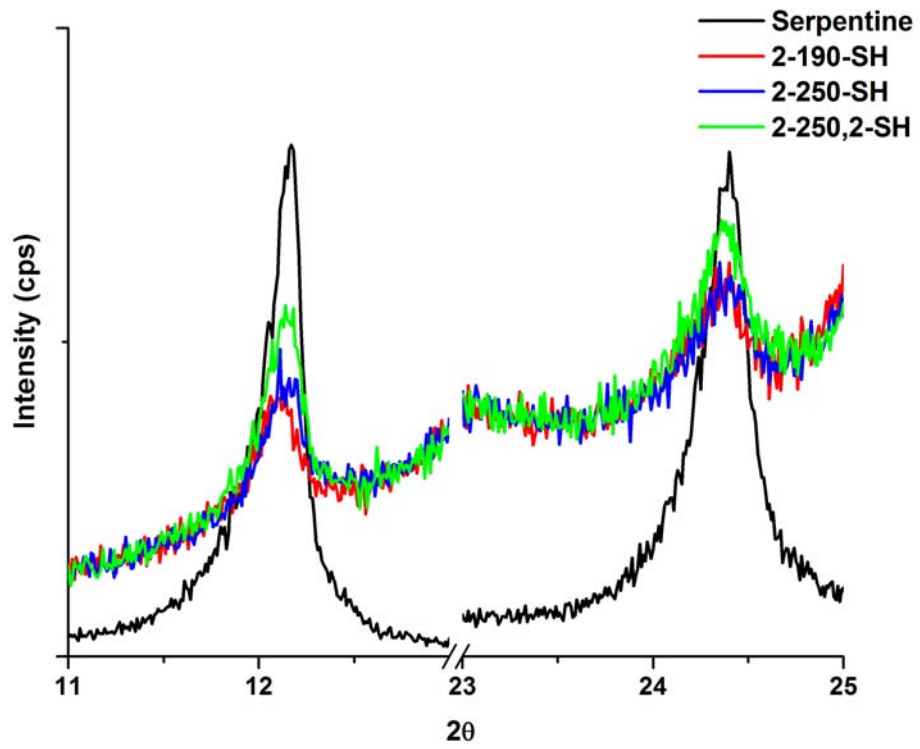


(a)

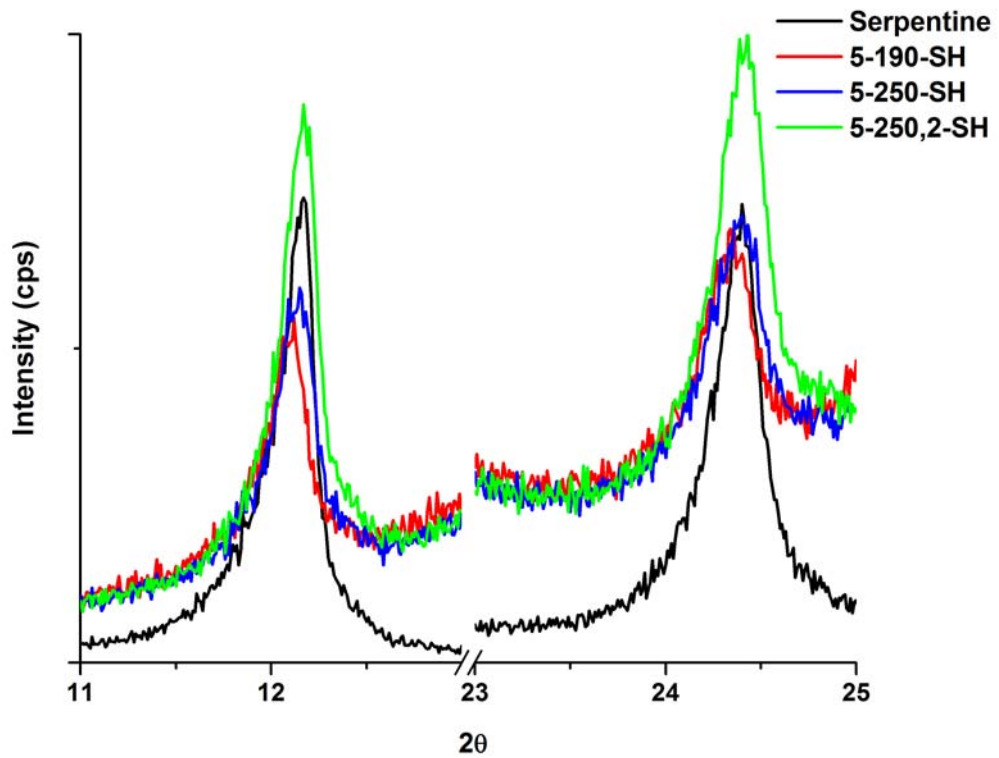


(b)

Figure 3.29 X-ray diffraction patterns for (a) 2%, (b) 5% SCA treated normal compositions of group 1



(a)



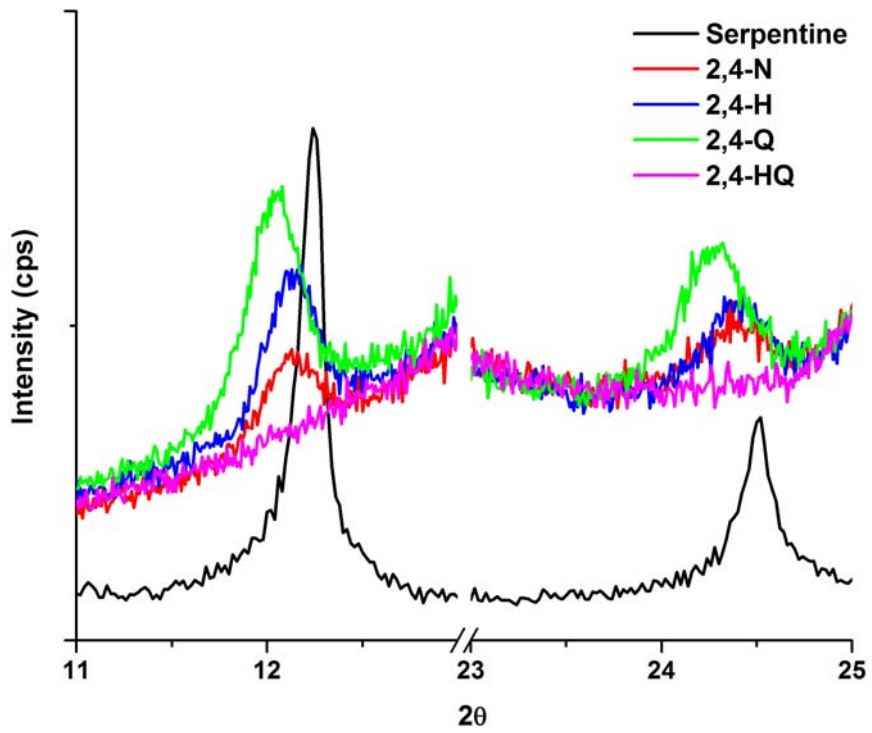
(b)

Figure 3.30 X-ray diffraction patterns for (a) 2%, (b) 5% SCA and HCl treated compositions of group 1

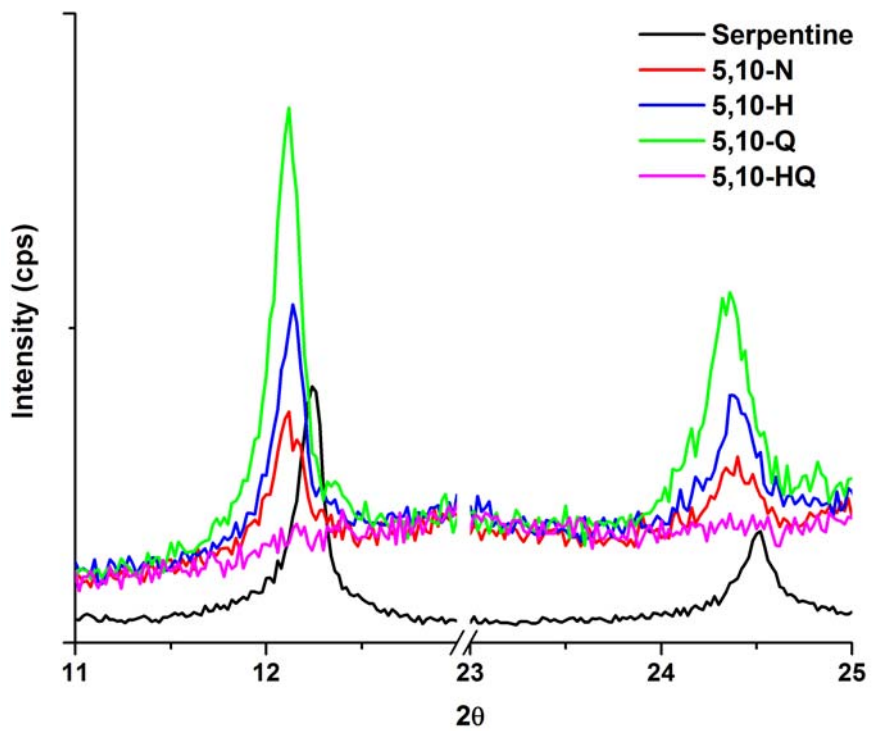
Table 3.7 Diffraction angle and d-spacing data for all 2 and 5% filler loaded SCA treated compositions of group 1

Composition	Diffraction angle (2θ)	d-spacing (Å)
Serpentine	12.17	7.26
2-190-S	12.16	7.27
2-250-S	12.13	7.28
2-250,2-S	12.10	7.31
5-190-S	12.13	7.28
5-250-S	12.10	7.31
5-250,2-S	12.14	7.28
2-190-SH	12.06	7.33
2-250-SH	12.11	7.30
2-250,2-SH	12.14	7.28
5-190-SH	12.12	7.29
5-250-SH	12.15	7.28
5-250,2-SH	12.17	7.26

As Figure 3.31 and 3.32 show the diffraction patterns for group 2 compositions, Table 3.8 gives the tabulated data for them. Here, a different diffractometer was employed to obtain the spectra as pointed out in the experimental part. In group 2, the peak employed in calculating the d-spacing of the composites of group 1 is seen at 2θ of 12.24° . The shifts in d-spacing need to be evaluated according to the diffraction angle of that peak. Therefore the amount of the shifts can be comparable with the results obtained for group 1 composites. It can be inferred from the diffractograms that, although the increase in d-spacing of the composites isn't significant, the highest values were attained for QAS treated samples in which 2,4-Q showed the maximum decrease in 2θ by 0.22° compared to serpentine. Intercalation of those should be confirmed, if any, by TEM studies. In the case of composites having acid treatment followed by QAS modification of serpentine, peaks disappeared which may indicate exfoliation of the layers which should be further studied by TEM.

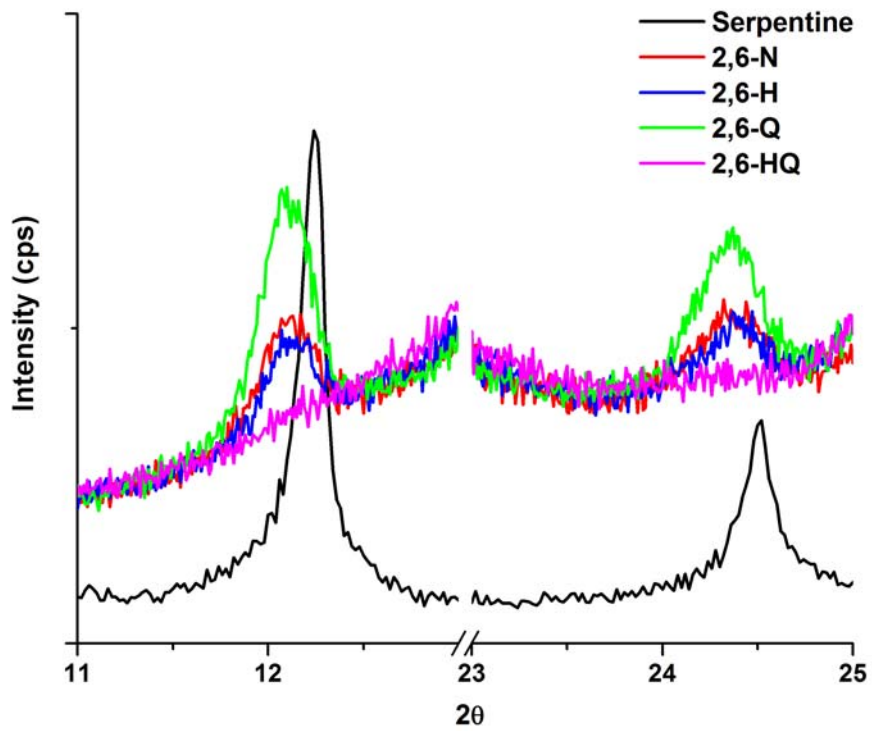


(a)

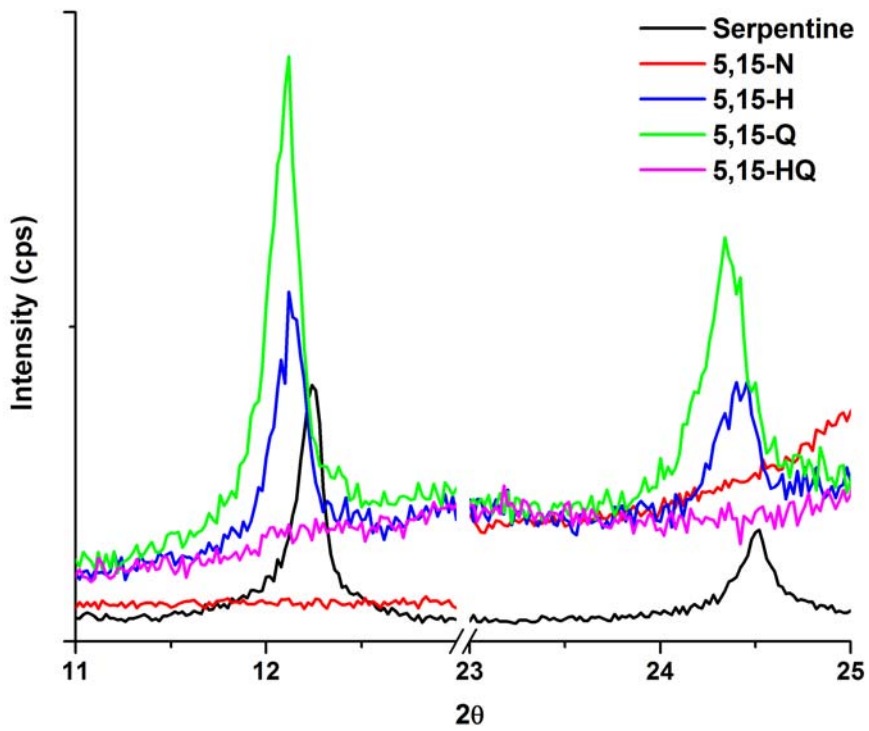


(b)

Figure 3.31 X-ray diffraction patterns for (a) 2,4, (b) 5,10 compositions of group 2



(a)



(b)

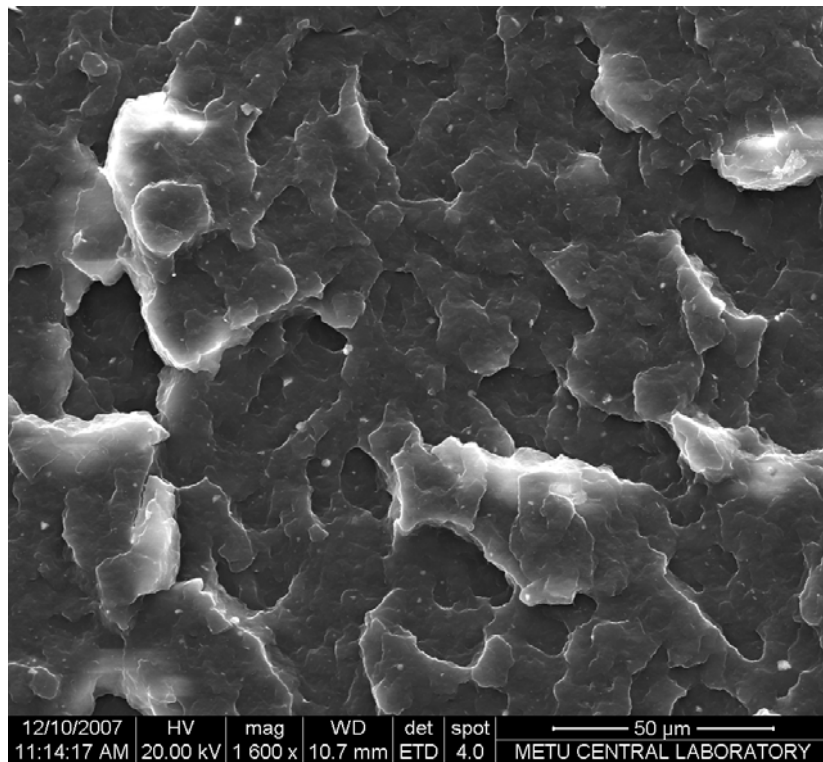
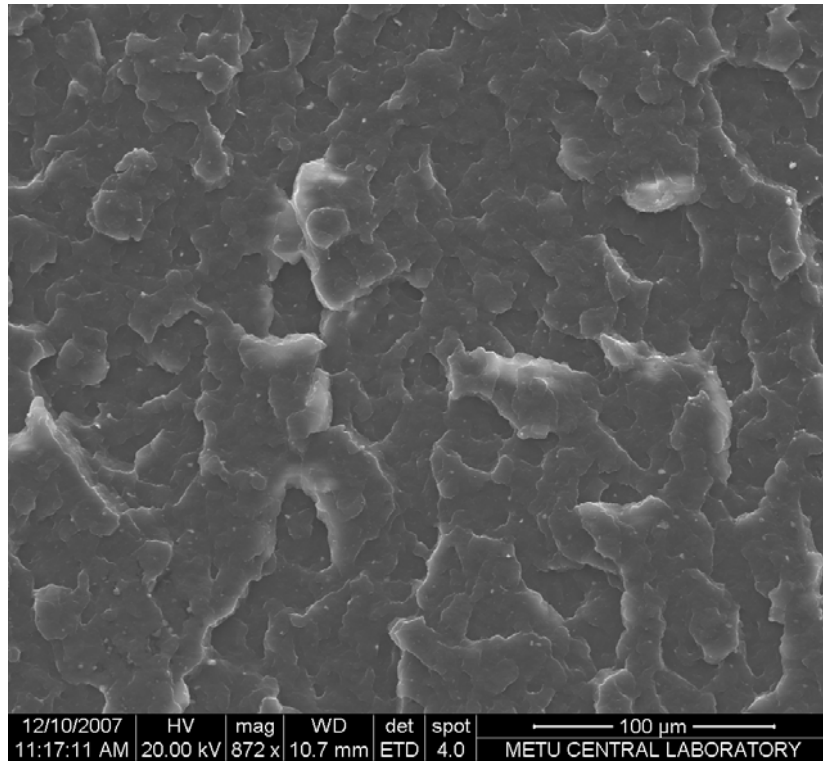
Figure 3.32 X-ray diffraction patterns for (a) 2,6, (b) 5,15 compositions of group 2

Table 3.8 Diffraction angle and d-spacing data for group 2 compositions

Composition	Diffraction angle (2θ)	d-spacing (Å)
Serpentine	12.24	7.22
2,4-N	12.13	7.28
2,4-H	12.18	7.26
2,4-Q	12.02	7.35
2,4-HQ	No peak	
5,10-N	12.12	7.29
5,10-H	12.14	7.28
5,10-Q	12.11	7.30
5,10-HQ	No peak	
2,6-N	12.12	7.29
2,6-H	12.10	7.31
2,6-Q	12.09	7.32
2,6-HQ	No peak	
5,15-N	12.12	7.29
5,15-H	12.13	7.28
5,15-Q	12.11	7.30
5,15-HQ	No peak	

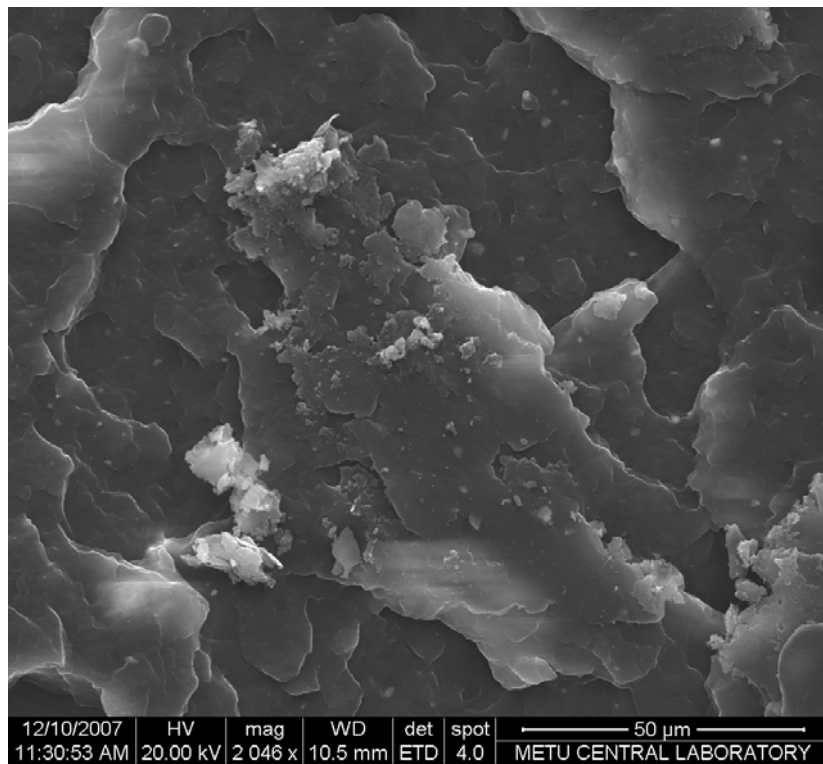
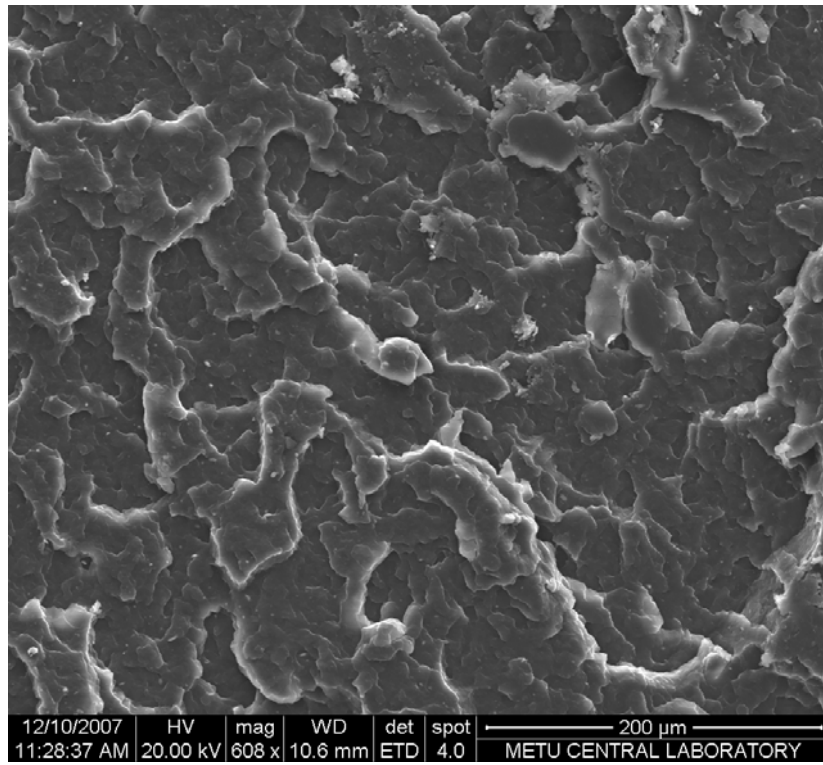
3.9 Morphology of the Composites

To understand the variations in composite properties and to follow the morphology SEM analysis was employed. SEM micrographs of impact fractured surfaces for 2-190, 2-190-H, 2-190-S and 2-190-SH are given in Figure 3.33. Overview of the images shows that serpentine did not alter the surface morphology of PP. Homogeneous distribution of the filler can be observed in the case of 2-190 and 2-190-S compositions. Along with the well-dispersed particles, aggregates of filler appeared on SEM images of samples of 2-190-H and 2-190-SH. This indicates the dependency of the filler distribution on the treatment type. Although SCA treatment didn't result in any agglomeration of the filler, acid treatment did even at low filler contents. In all of the images especially with aggregation of the filler, serpentine can be easily seen as in the form of platelets.



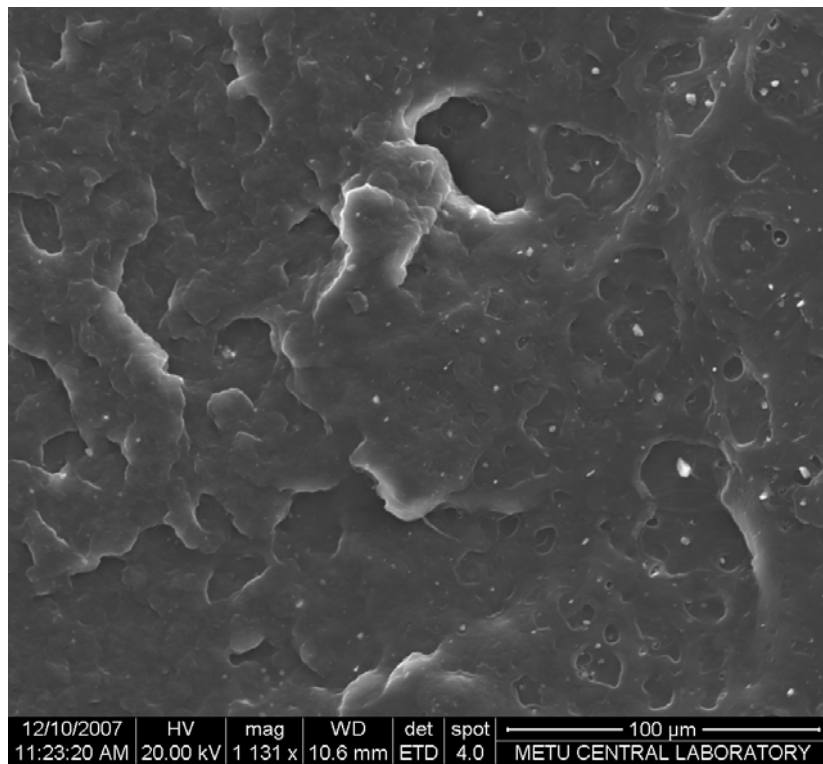
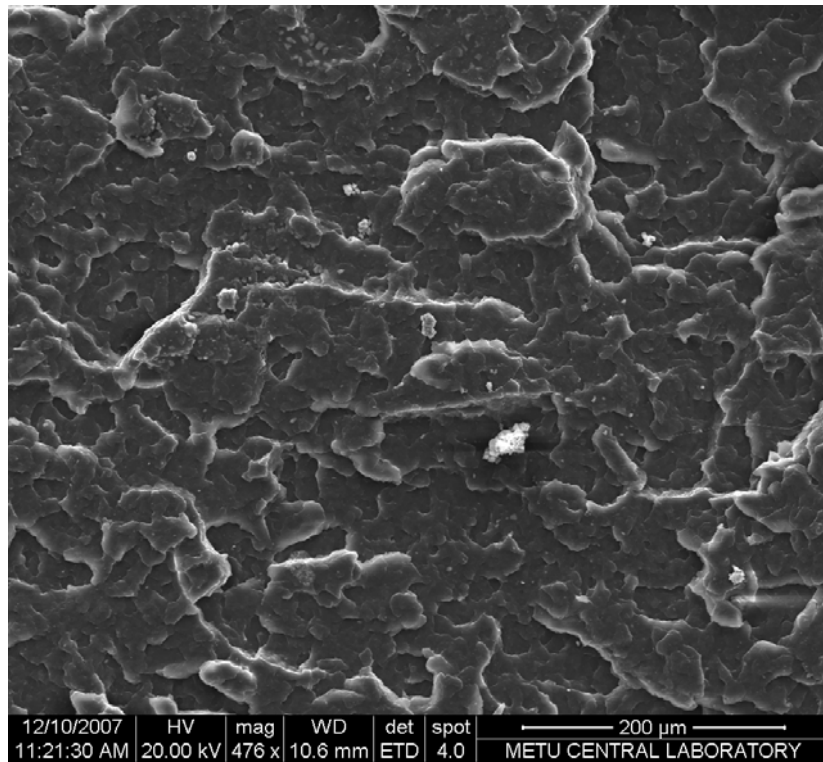
(a)

Figure 3.33 SEM images of impact fractured surfaces of (a) 2-190, (b) 2-190-H, (c) 2-190-S, (d) 2-190-SH



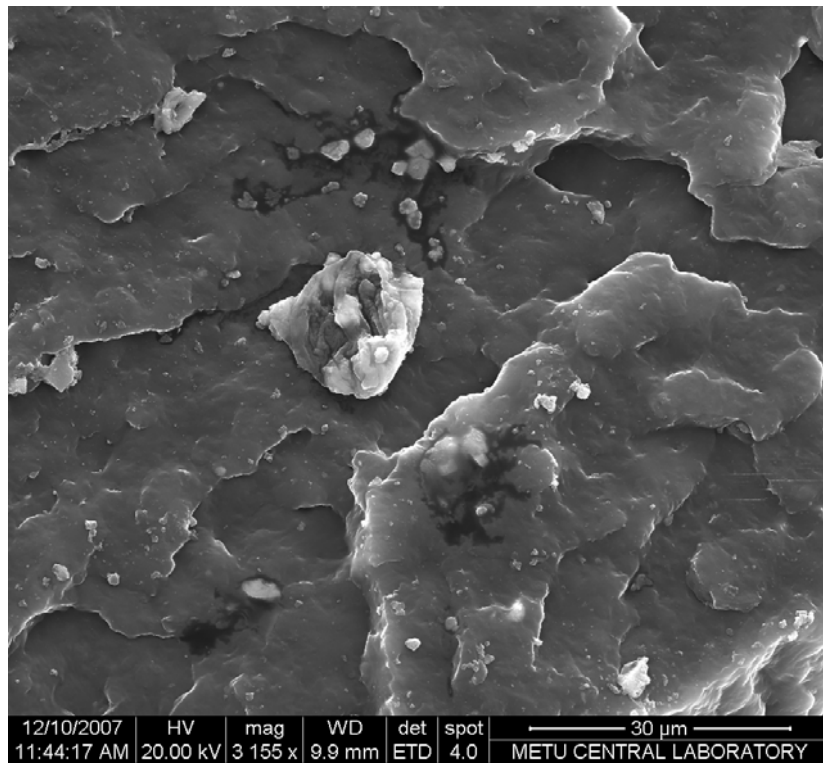
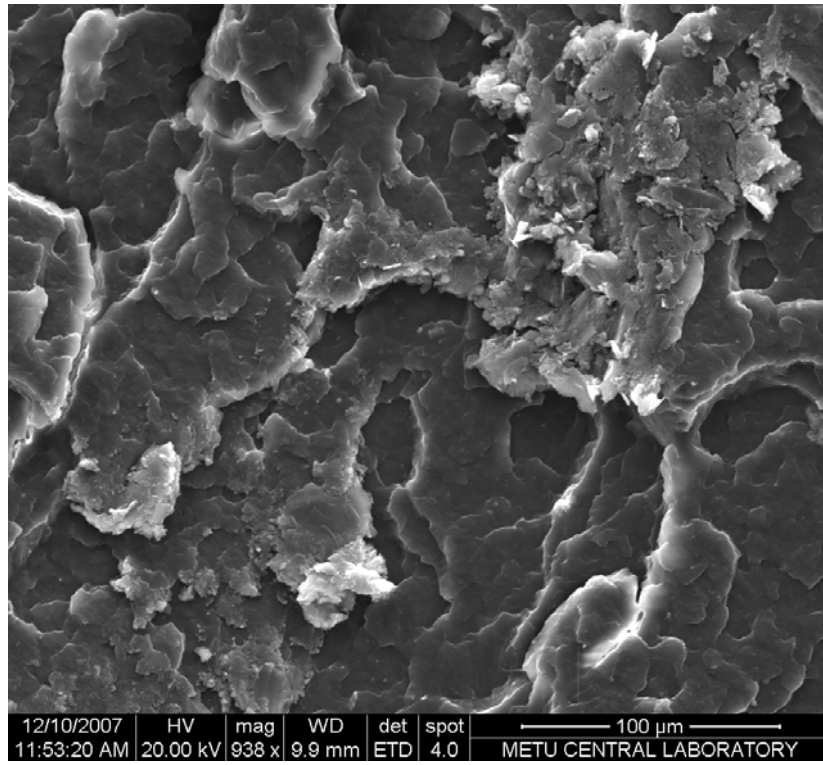
(b)

Figure 3.33 (cont'd)



(c)

Figure 3.33 (cont'd)

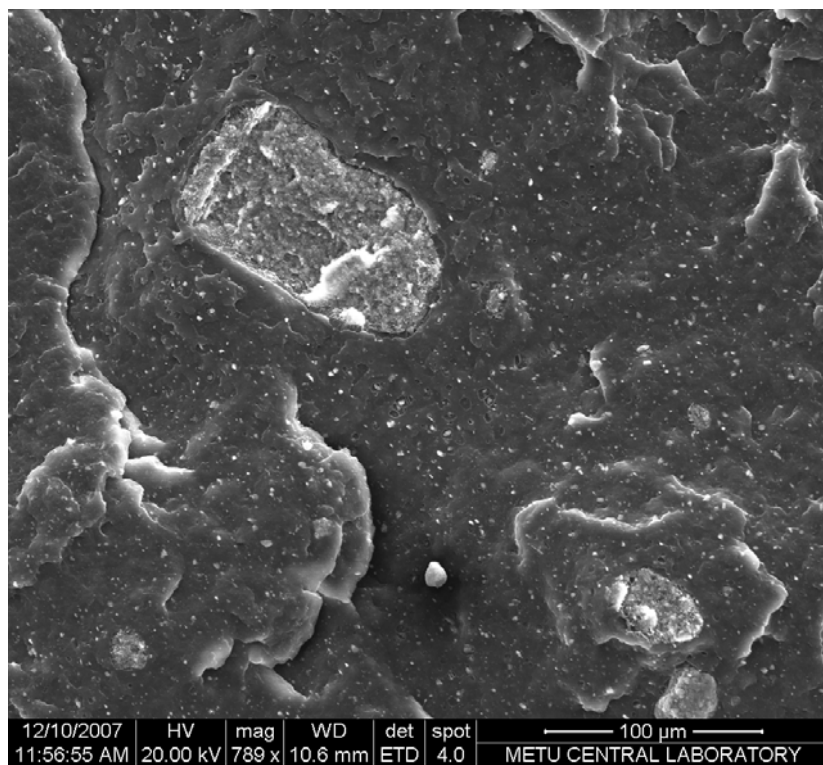
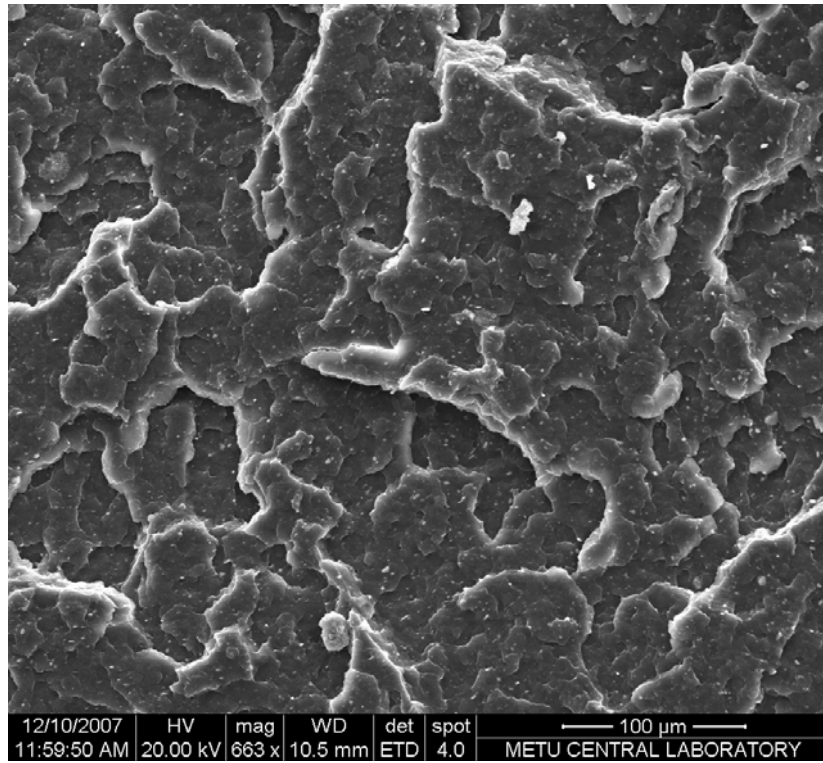


(d)

Figure 3.33 (cont'd)

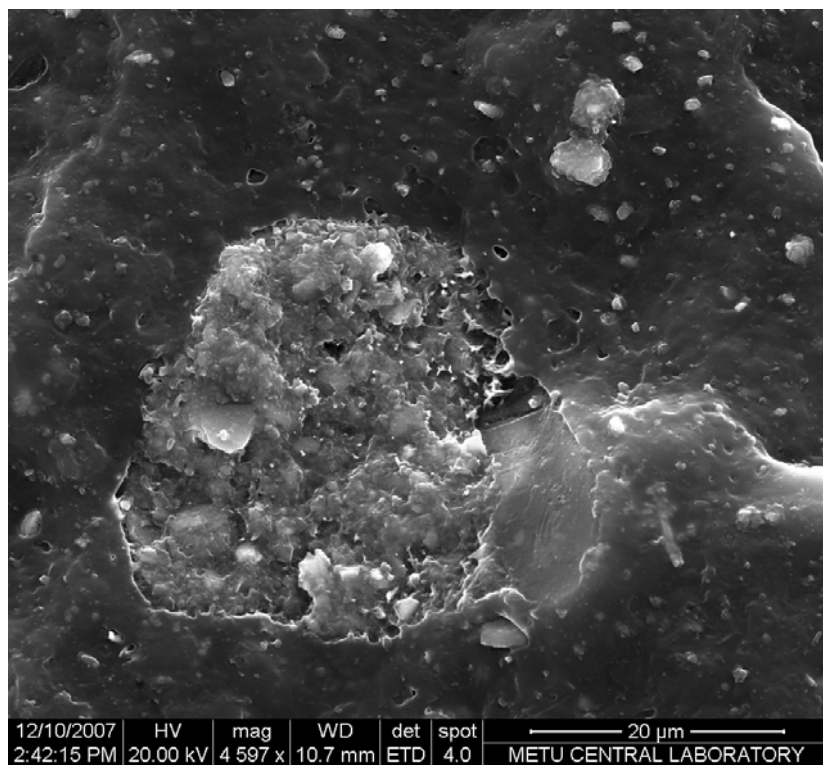
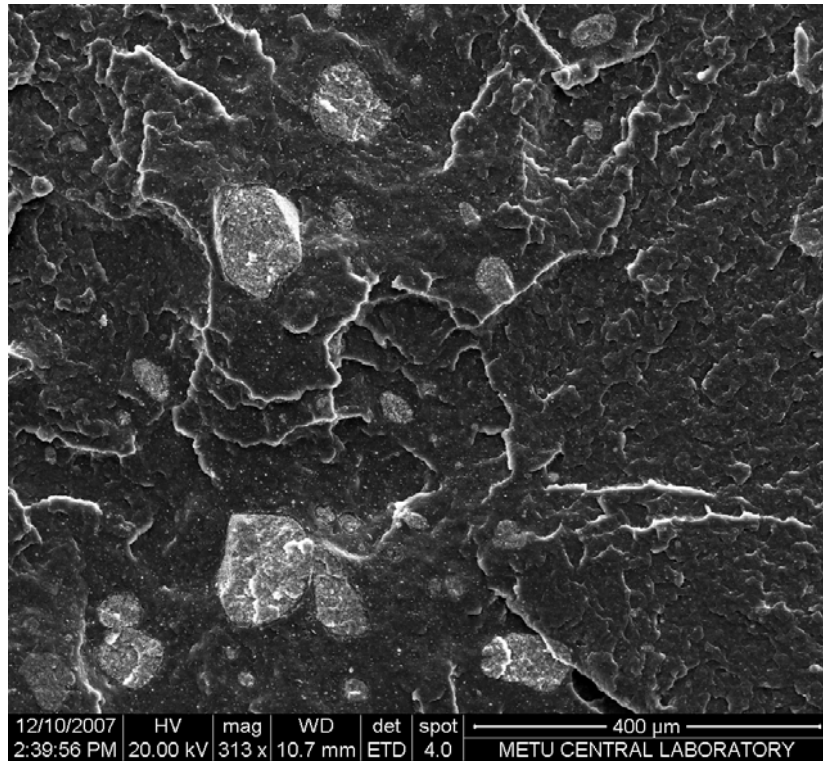
To observe the situation at high filler contents, the SEM images of 10% filler loaded compositions namely, 10-190, 10-190-H, 10-190-S and 10-190-SH are presented in Figure 3.34. Similar to 2% filled composites, homogeneous distribution of the filler particles is seen even in the presence of aggregated filler. The amount of aggregation increased with increasing filler content, but it was pronounced mostly for 10-190-H and 10-190-SH compositions. There are weak adhesion and tear at polymer filler interphase illustrated at high magnification of Figure 3.34 (b), upper right and lower left of aggregated filler portion. 10-190-SH showed strong adhesion with fibrillation all around the aggregated filler (see Figure 3.34 (d) at high magnification). In spite of having agglomerated particles, 10-190-S didn't show such a behavior. This can be seen as an evidence of strong interaction in the presence of SCA. By considering these effects, it can be possible to make some correlations to mechanical properties of the composites. SCA treated compositions exhibited enhanced tensile e.g. Young's modulus and yield stress and dynamic mechanical e.g. storage modulus properties.

Figure 3.35 (a) and (b) show micrographs of fractured surfaces of 2-250,2-S and 2-250,2-SH composites, respectively. Layered silicate structure of serpentine is clearly illustrated in the case of 2-250,2-S. Agglomerated particles can be seen in a cavity with adhesion to the matrix through SCA since the interactions of serpentine with the matrix are evident, seen in the bottom figure. The cavity formation may show pronounced separation at the interphase causing inferior mechanical properties in comparison to other group 1 composites. On the same figure, a microfibril was originated at the beginning of the cavity from the matrix. The same is valid for the SEM images of the composite that were not presented here. The occurrence of fibrillar extension of PP may change according to the compositions and the processing conditions.



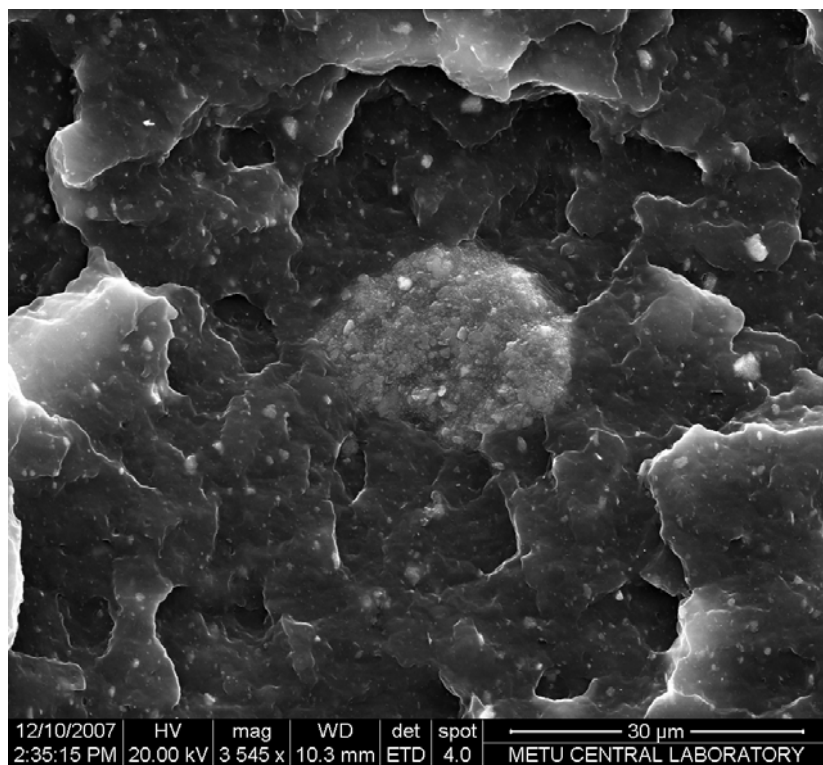
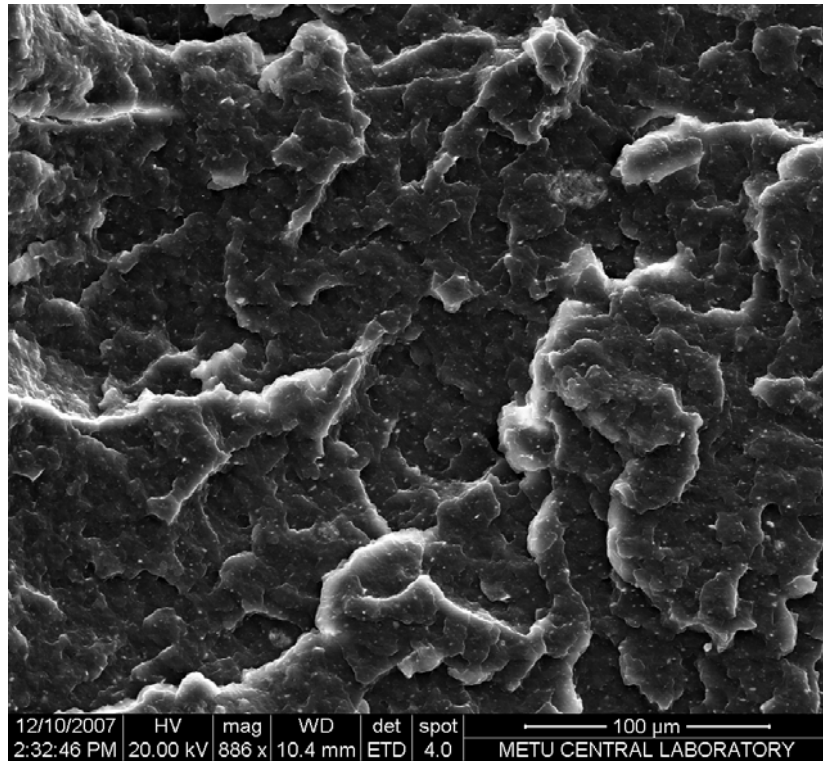
(a)

Figure 3.34 SEM images of impact fractured surfaces of (a) 10-190, (b) 10-190-H, (c) 10-190-S, (d) 10-190-SH



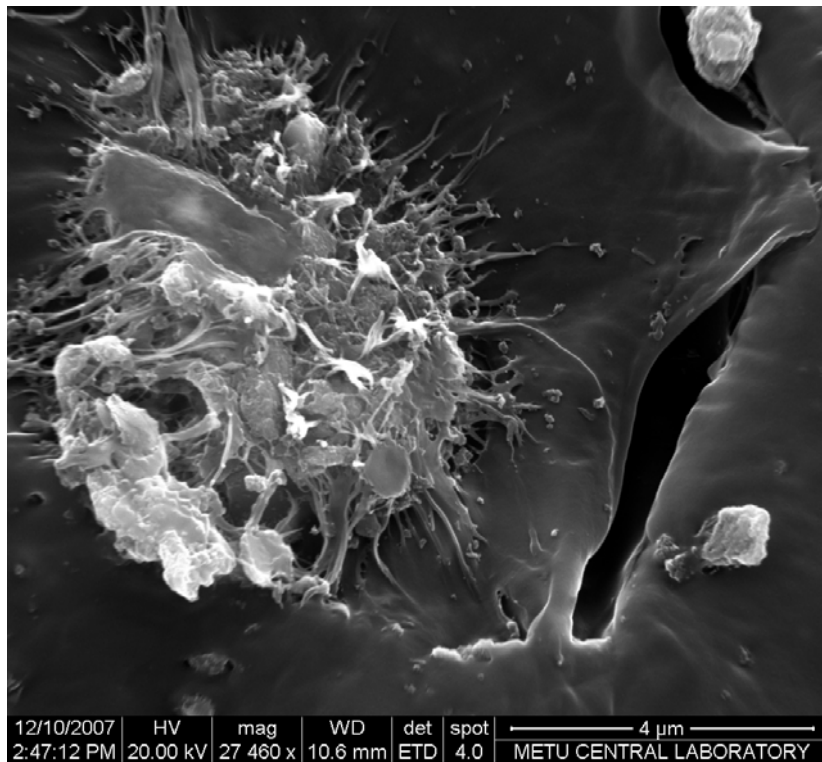
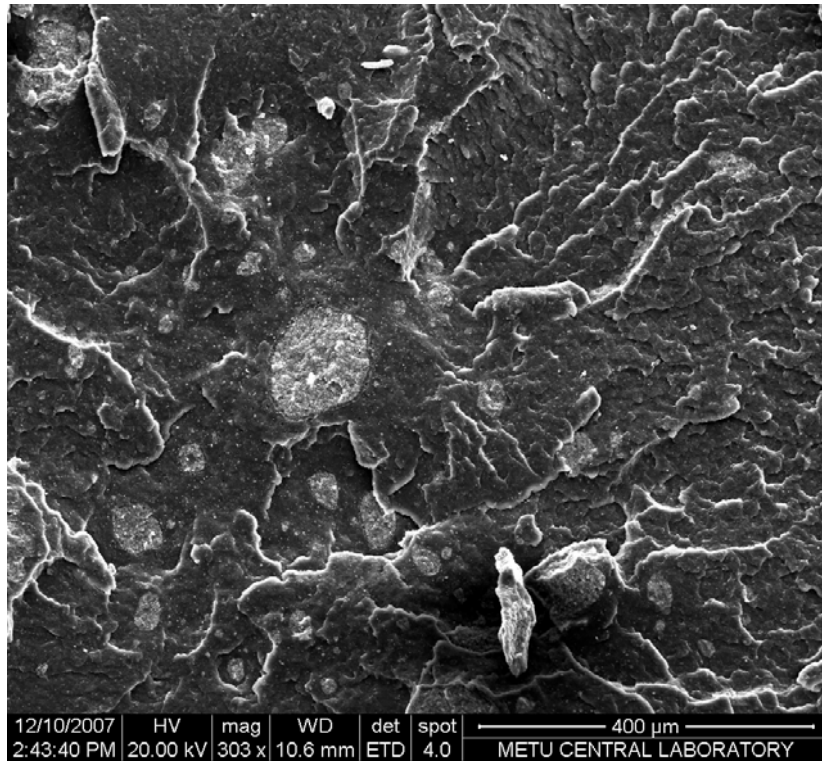
(b)

Figure 3.34 (cont'd)



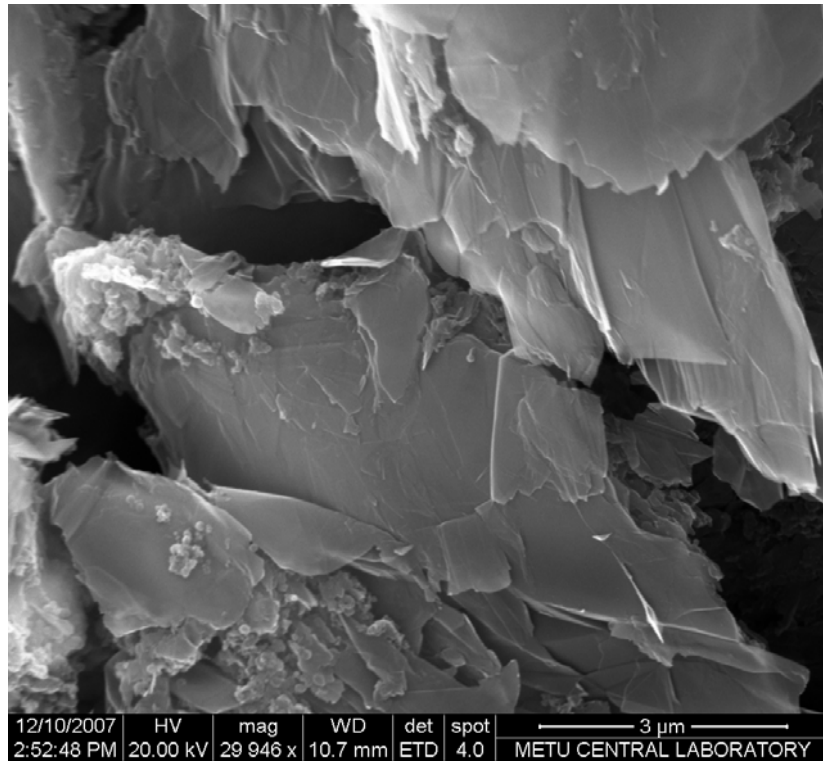
(c)

Figure 3.34 (cont'd)

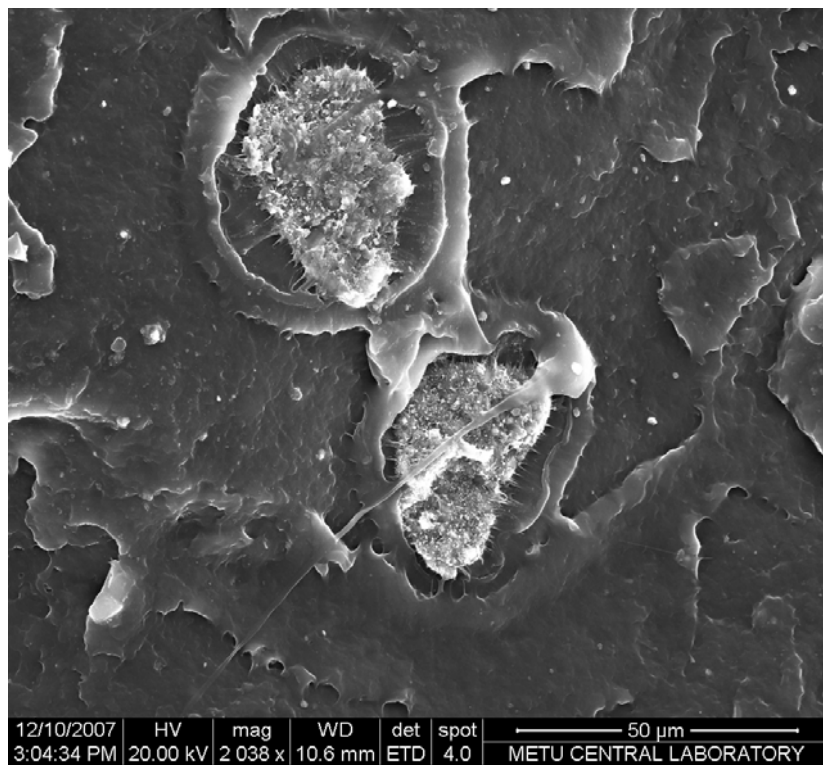


(d)

Figure 3.34 (cont'd)



(a)

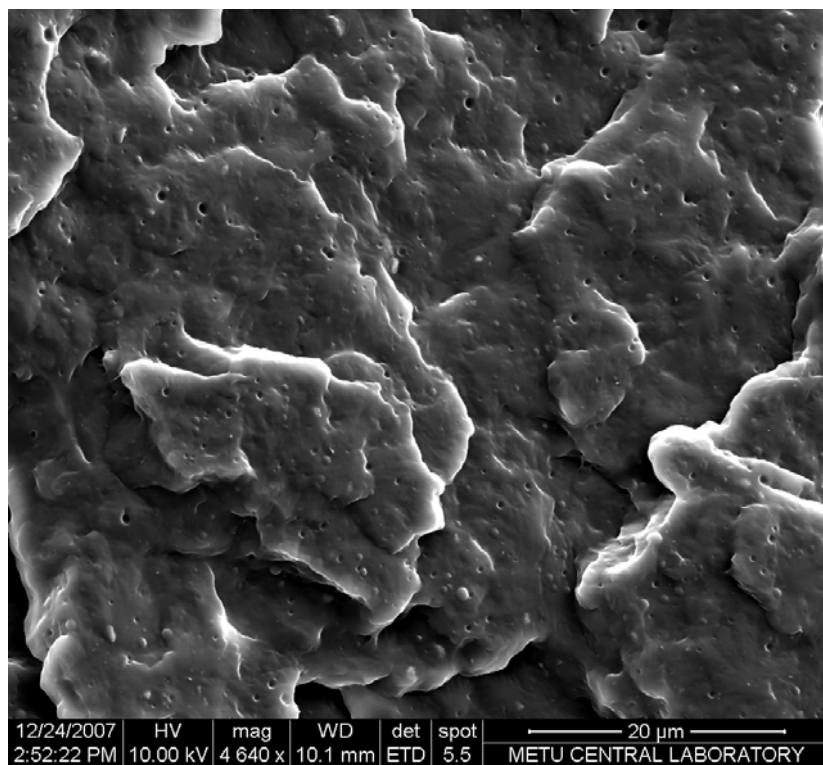
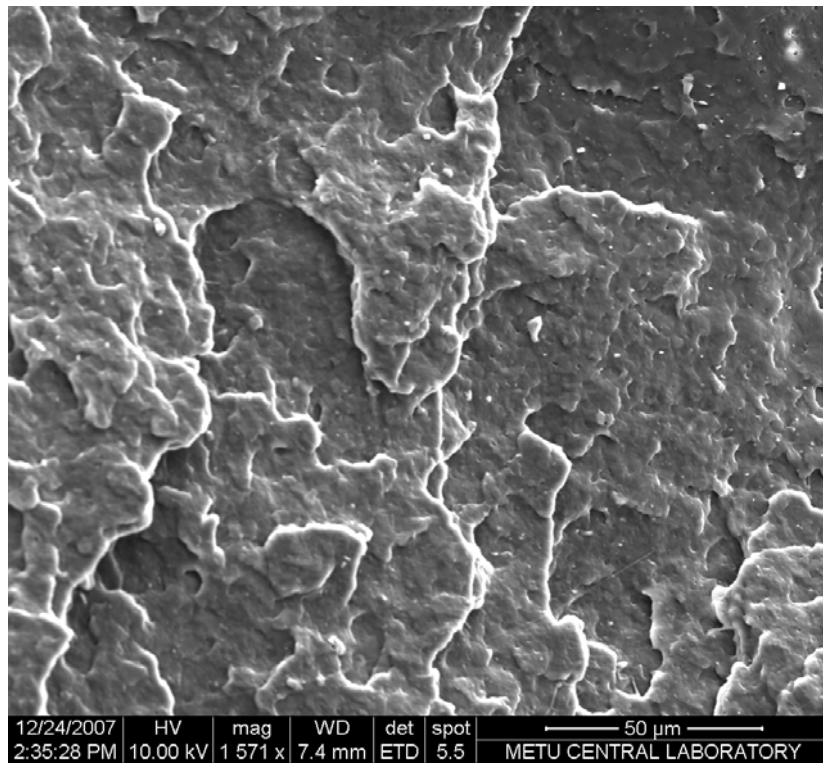


(b)

Figure 3.35 SEM images of impact fractured surfaces of (a) 2-250,2-S, (b) 2-250,2-SH

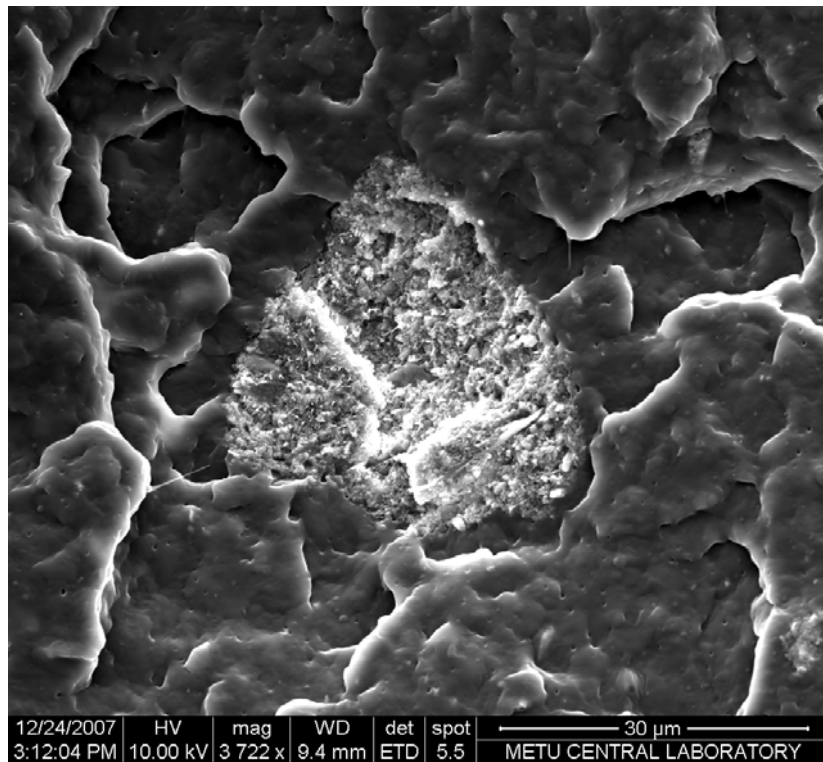
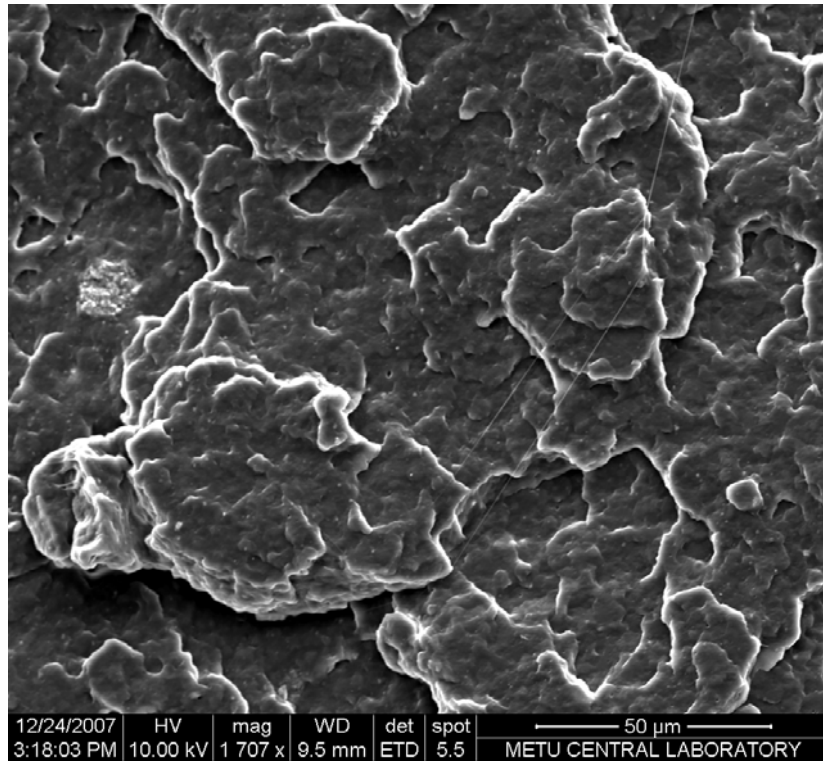
The morphology of group 2 composites were examined in terms of all 2,4 compositions and presented in Figure 3.36. Small aggregates of serpentine can be seen for H and HQ samples in common with H and SH treated samples of group 1. It can be concluded that whenever there was an acid treatment in PP/serpentine composites, alone or with other treatments, it resulted in aggregation of serpentine even at low filler contents. However, aggregated portion of the filler wasn't contained in a cavity as in 2-250,2-SH. This may be attributed to the enhanced compatibility of the matrix through PP-g-MA and modification of the filler leading to strong interaction at the interphase. On the other hand, there is no visible agglomeration instead well-dispersed filler particles for 2,4-N and 2,4-Q compositions. Microfibril formations similar to 2-250,2-SH composite are evident more or less for these composites. For example, the fractograph of 2,4-Q at high magnification shows large number of microfibrillar extensions of the matrix.

SEM images of 5% filled compositions, namely 5,10 and 5,15 are presented in Figures 3.37-3.38. Filler aggregation is observed for all of these compositions. As seen from the (c)'s of both figures, the compatibilizer is shown with rounded and well distributed structure, high in amount for 5,15 compositions. Although it exists in all compositions, it can be observed more clearly for 5,10-Q and 5,15-Q. Similar to 2,4 compositions, there was no phase separation due to the compatibility of serpentine and PP in the presence of PP-g-MA. However, every agglomerated portion of 5,15-HQ was contained in a cavity like 2-250,2-SH. As it was pointed out earlier for 2-250,2-SH, it wouldn't be wrong to say that presence of such deteriorations in the structure affects the properties badly.



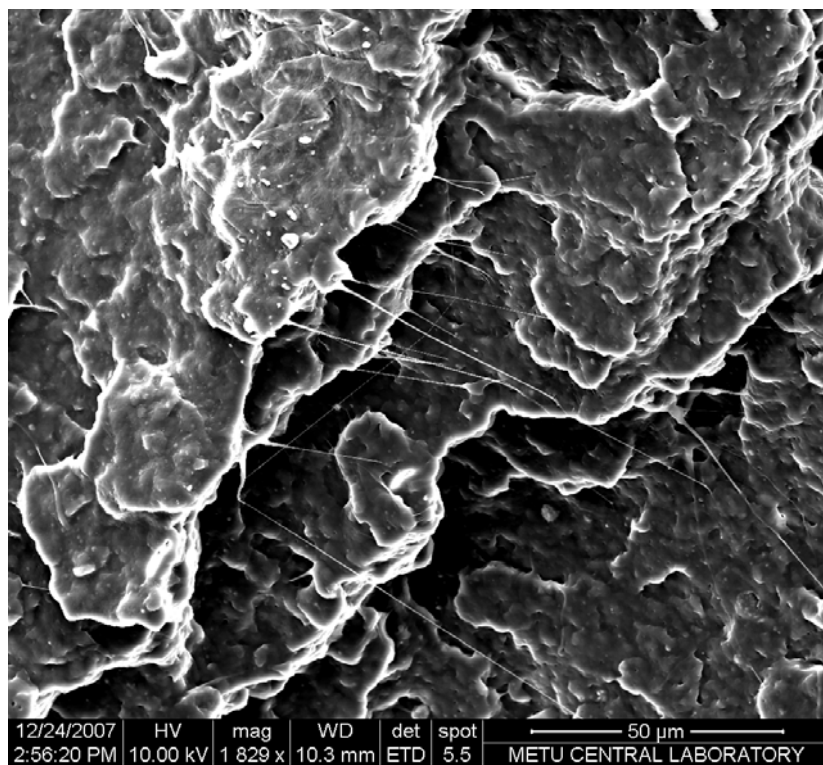
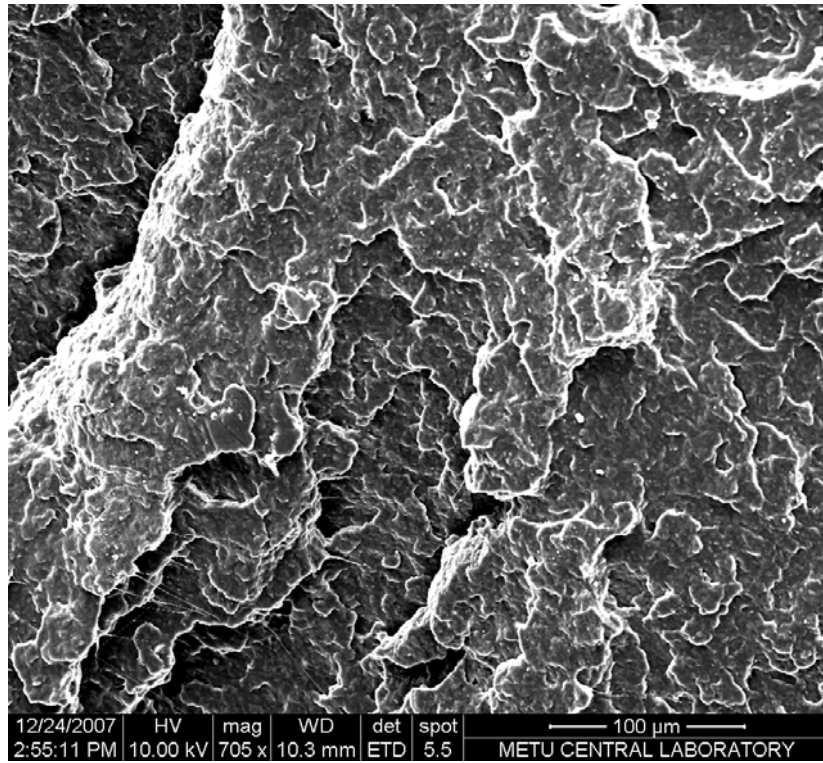
(a)

Figure 3.36 SEM images of impact fractured surfaces of (a) 2,4-N, (b) 2,4-H, (c) 2,4-Q, (d) 2,4-HQ



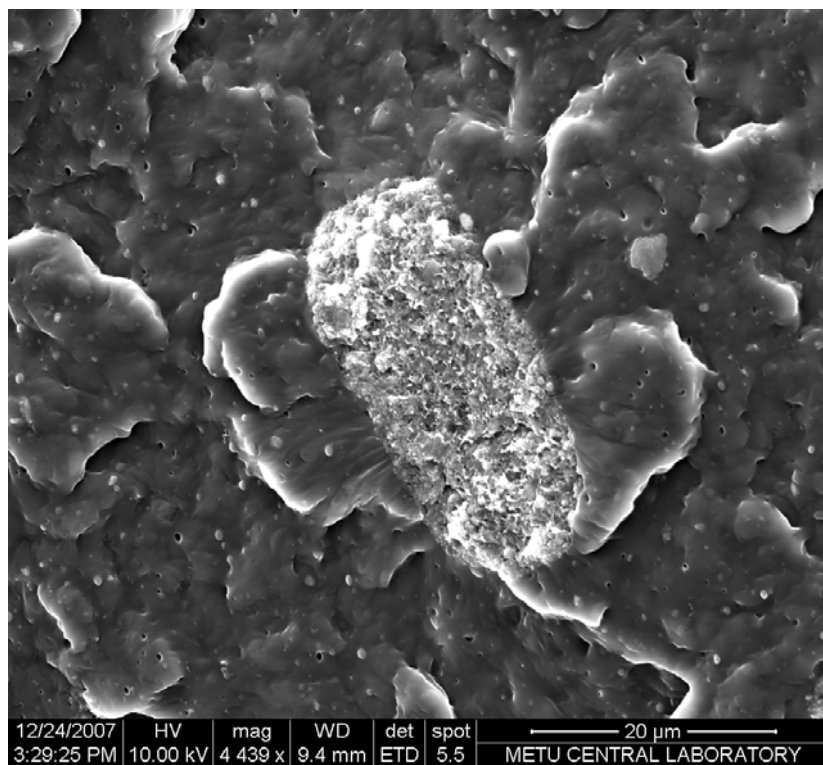
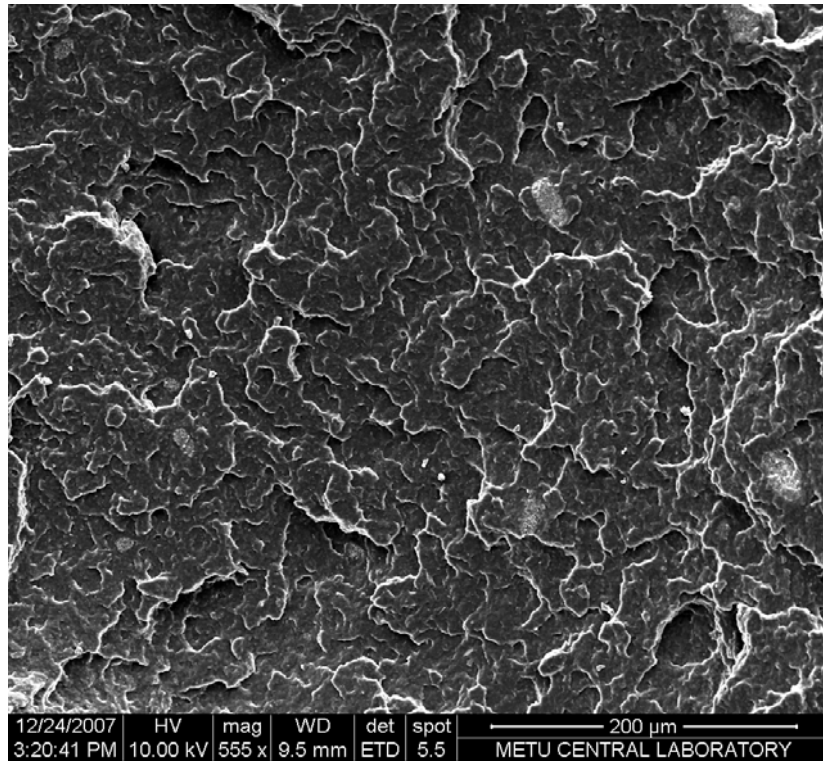
(b)

Figure 3.36 (cont'd)



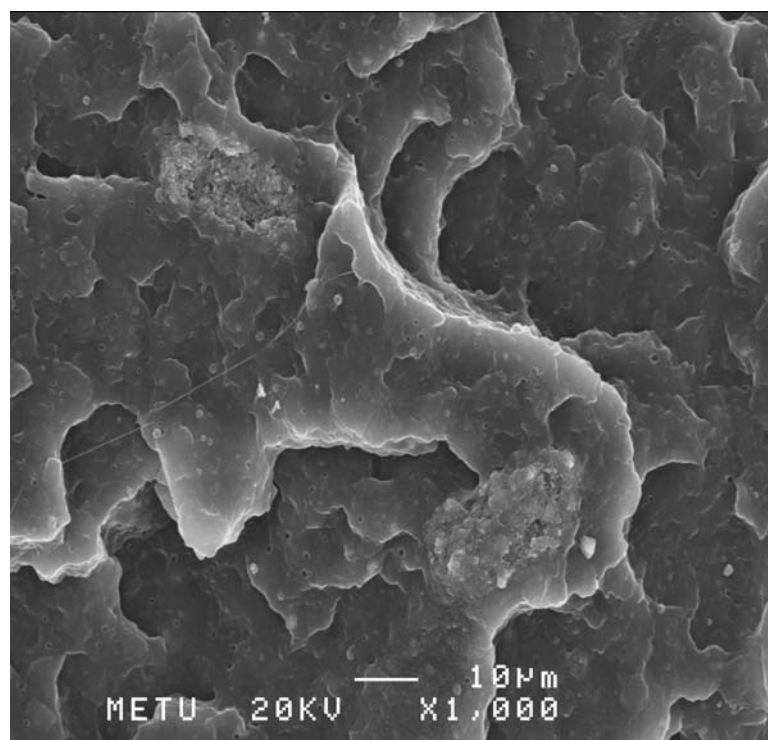
(c)

Figure 3.36 (cont'd)

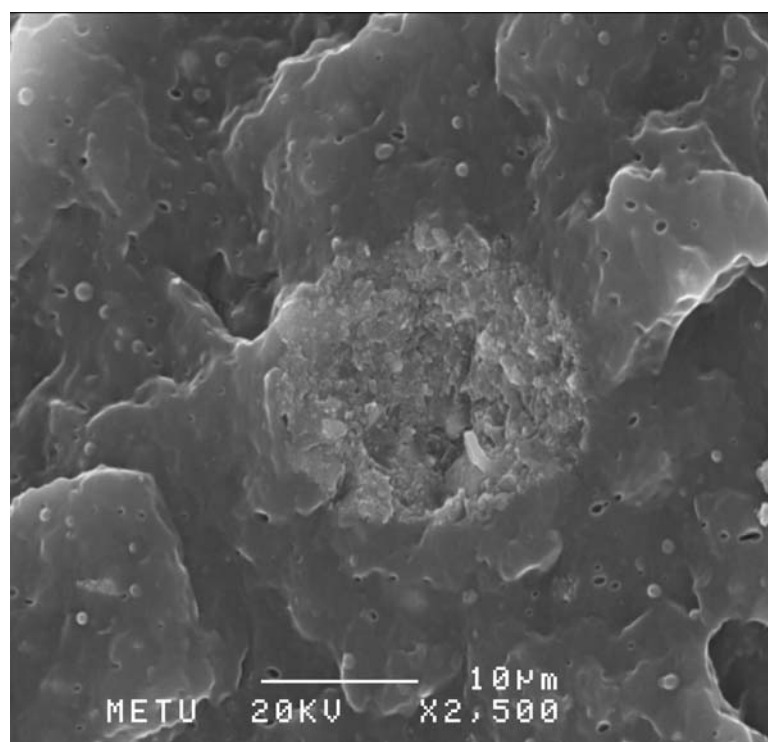


(d)

Figure 3.36 (cont'd)

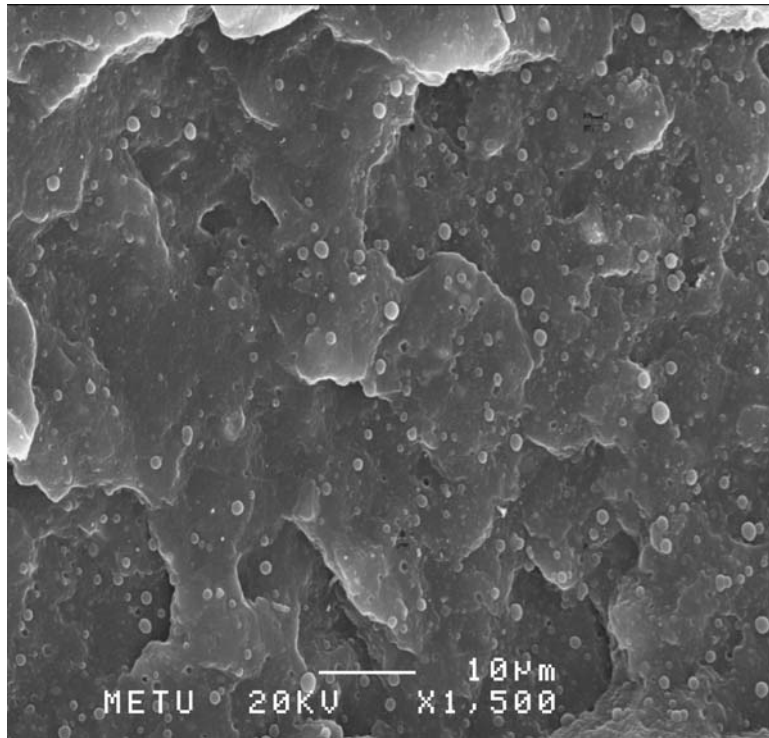


(a)

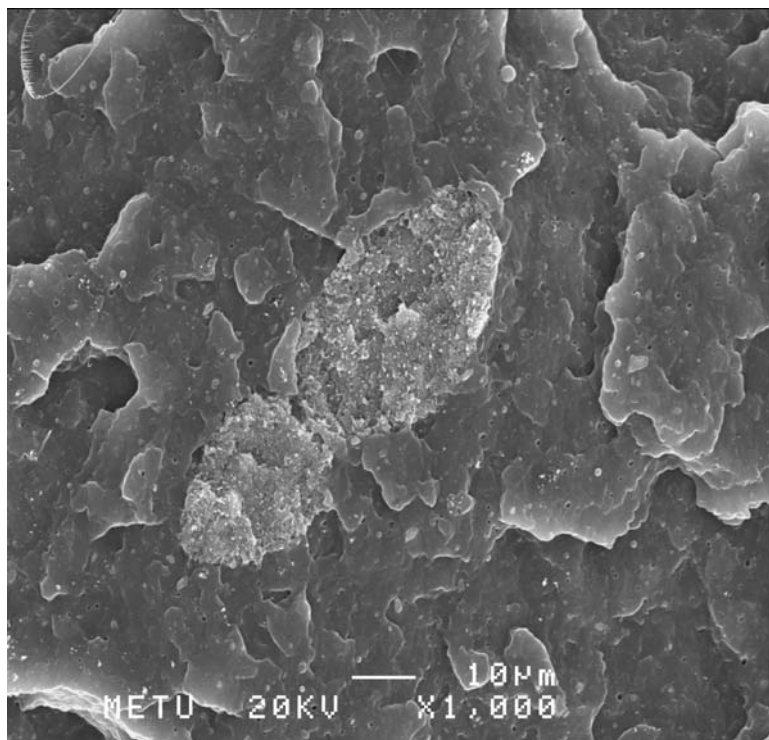


(b)

Figure 3.37 SEM images of impact fractured surfaces of (a) 5,10-N, (b) 5,10-H, (c) 5,10-Q, (d) 5,10-HQ

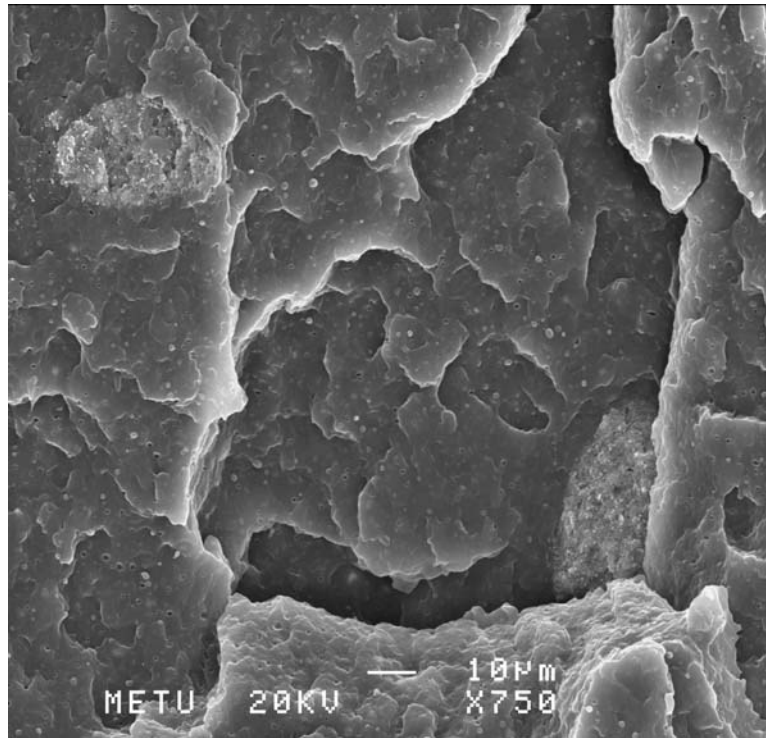


(c)

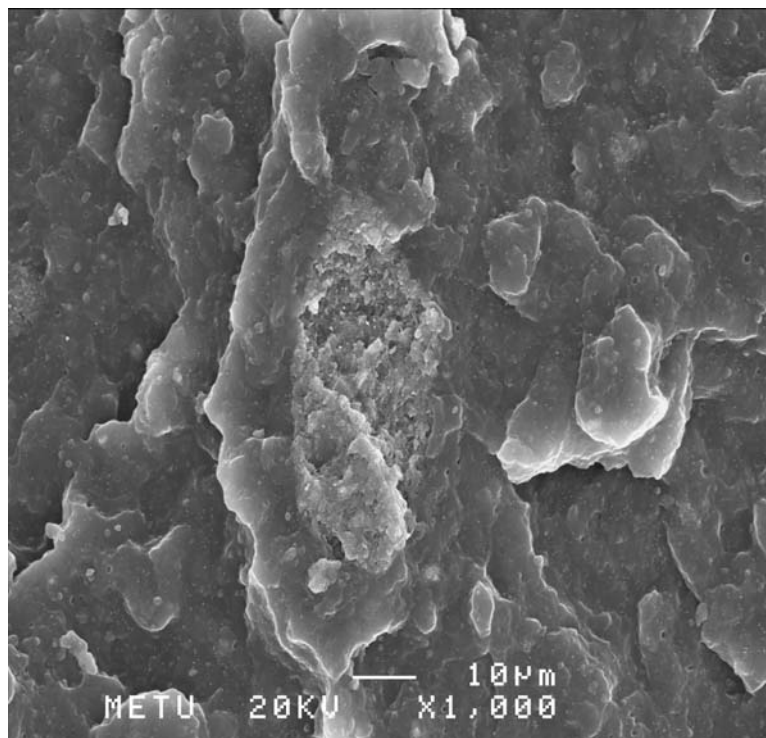


(d)

Figure 3.37 (cont'd)

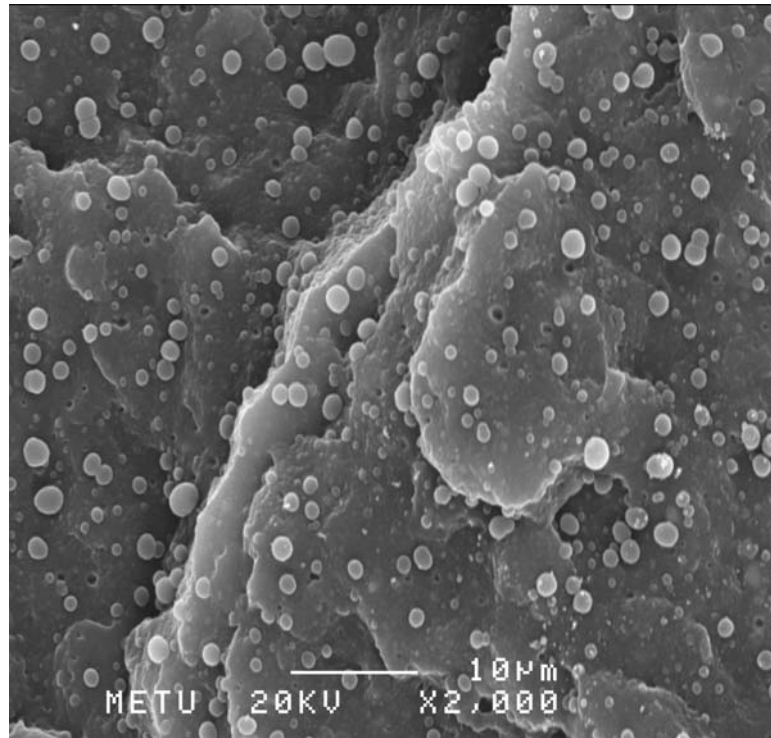


(a)

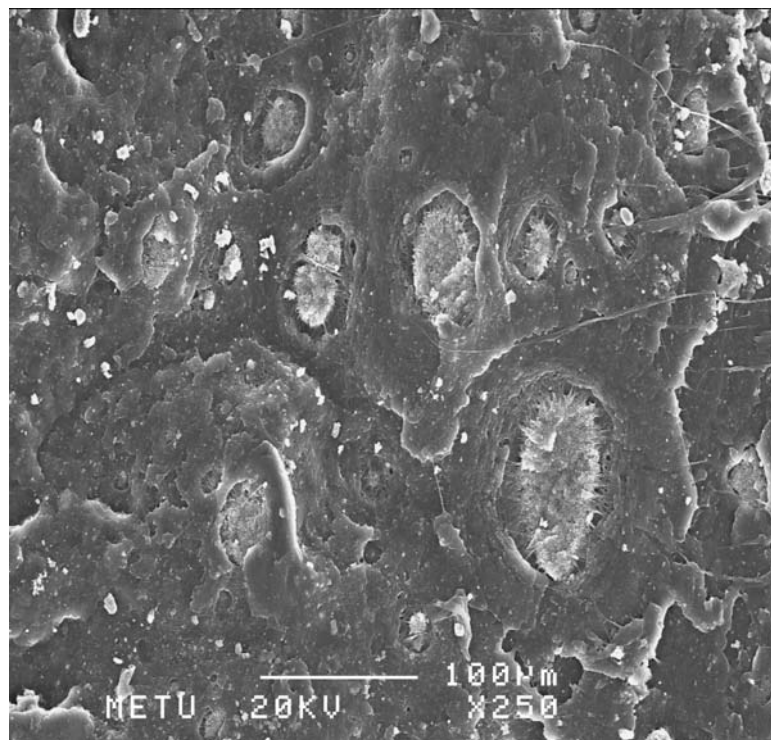


(b)

Figure 3.38 SEM images of impact fractured surfaces of (a) 5,15-N, (b) 5,15-H (c) 5,15-Q, (d) 5,15-HQ



(c)



(d)

Figure 3.38 (cont'd)

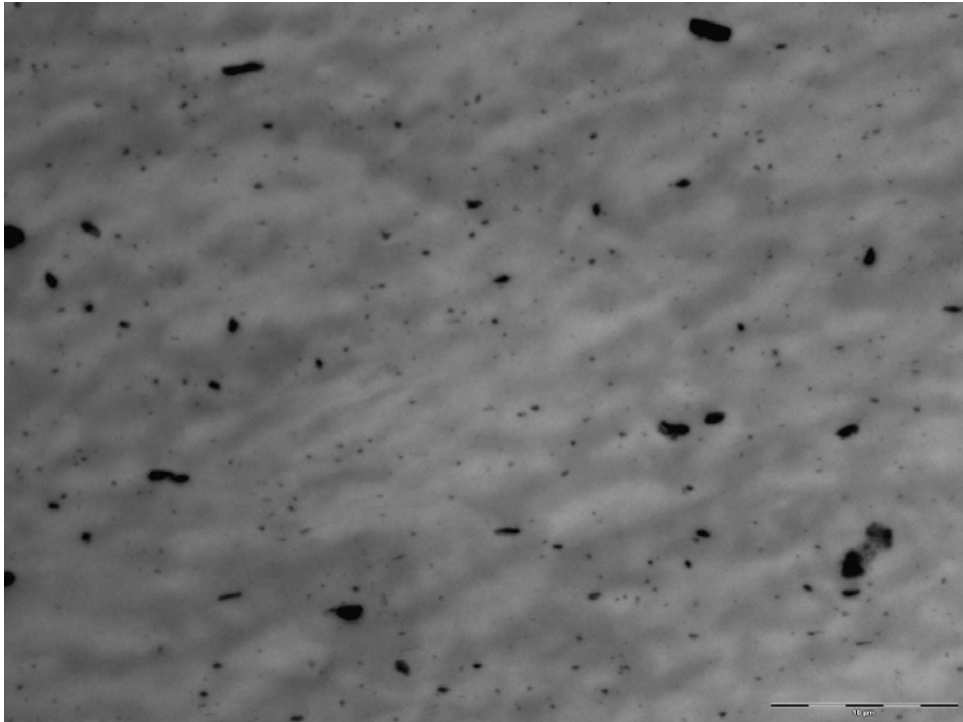
3.10 TEM Study of QAS Treated Compositions

The compositions of group 2 with only QAS treated and both QAS and HCl treated 2,4, 2,6 and 5,10 were analyzed with TEM. Through the Figures 3.39-3.44 TEM images are presented. While the light colored area represents the PP matrix, darker regions correspond to serpentine layers. Although for all analyzed samples homogeneous distribution was observed, small amount of aggregation is evident from low magnification TEM images. The situation is illustrated in the case of 2,4-Q in Figure 3.39 (a).

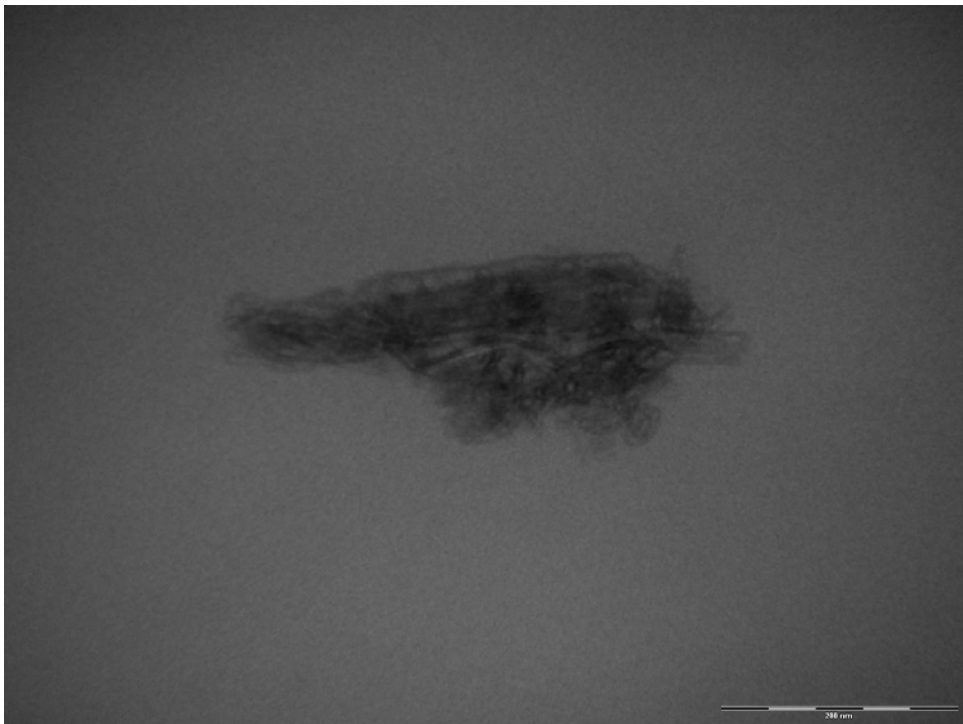
In the X-ray diffractograms of QAS and HCl treated compositions the peaks of serpentine disappeared (see Figures 3.31-3.32). This might be attributed to the total exfoliation of the filler layers. However examination of TEM images indicates that dispersion of any individual layers of the filler exfoliating in the PP matrix can not be observed.

Figure 3.39 (b) shows the TEM picture of 2,4-Q at 300K. Although darker stacked serpentine layers are seen, some individual clay layers are also evident. Similar to the TEM image of 2,4-Q, through the Figures 3.40-3.43 again stacked portions of the filler could be observed due to the clustering and aggregation of the layers. Figure 3.44 presents the TEM micrograph of 5,10-HQ X 300K on which the intercalated layers are pointed out.

There has been no study establishing the possible intercalation and/or exfoliation of serpentine layers in either any polymer or PP matrices. Besides, the interaction between nonpolar PP chains and polar serpentine layers even in the presence of PP-g-MA could be rather difficult compared to the coupling of serpentine with a polar polymer. Modification with QAS does have an effect on filler layers, since as pointed out before in the X-ray study part, composites with the same filler content did not show any peak shift. However it may be thought that compatibilizer and QAS treatment together are somewhat effective, also seen in X-ray studies and better mechanical properties.



(a)



(b)

Figure 3.39 TEM micrographs of 2,4-Q (a) X 2.5K, (b) X 150K

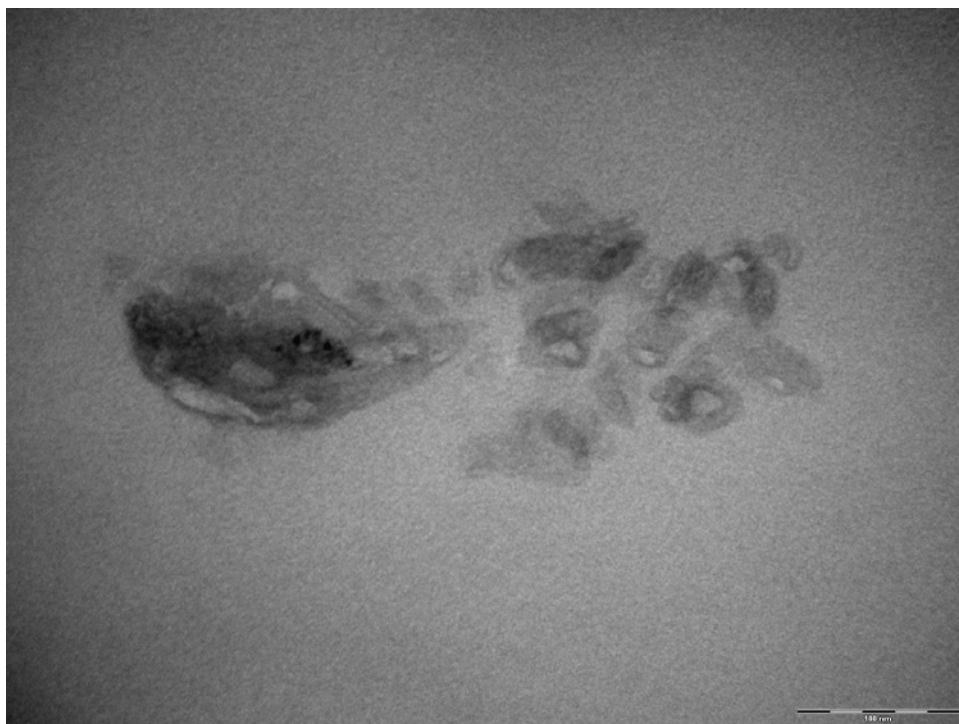


Figure 3.40 TEM micrograph of 2,4-HQ X 200K

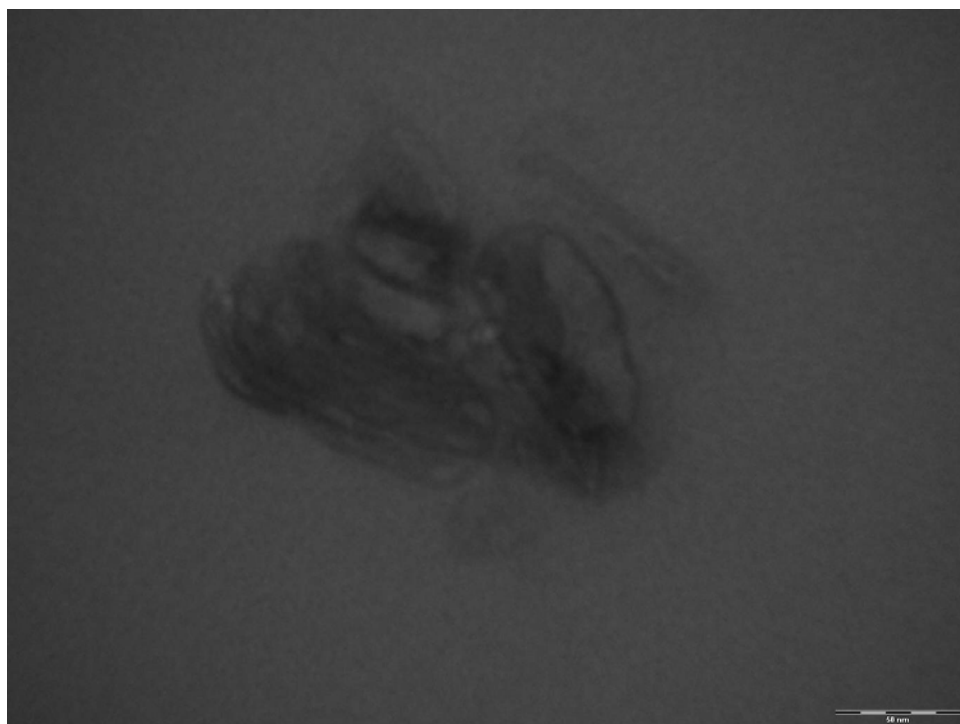


Figure 3.41 TEM micrograph of 2,6-Q X 300K

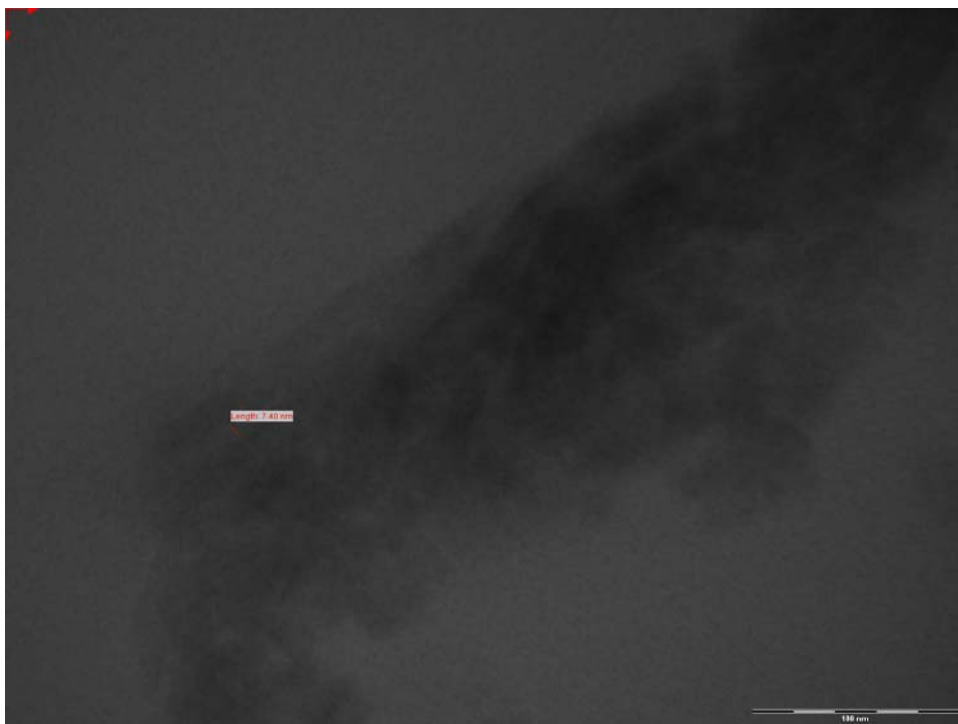


Figure 3.42 TEM micrograph of 2,6-HQ X 300K

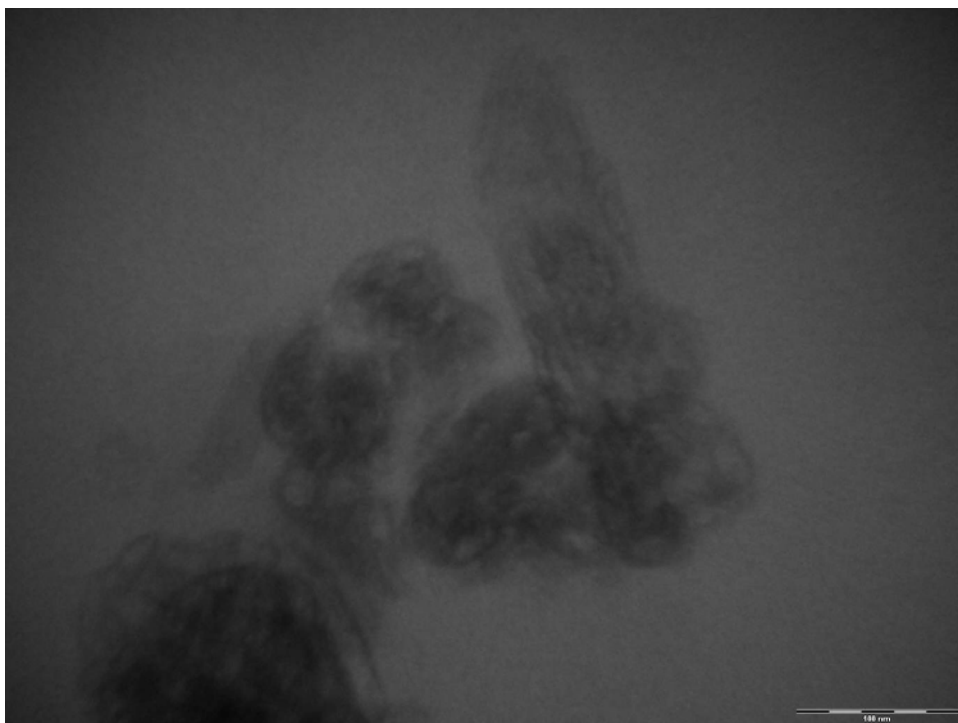


Figure 3.43 TEM micrograph of 5,10-Q X 200K

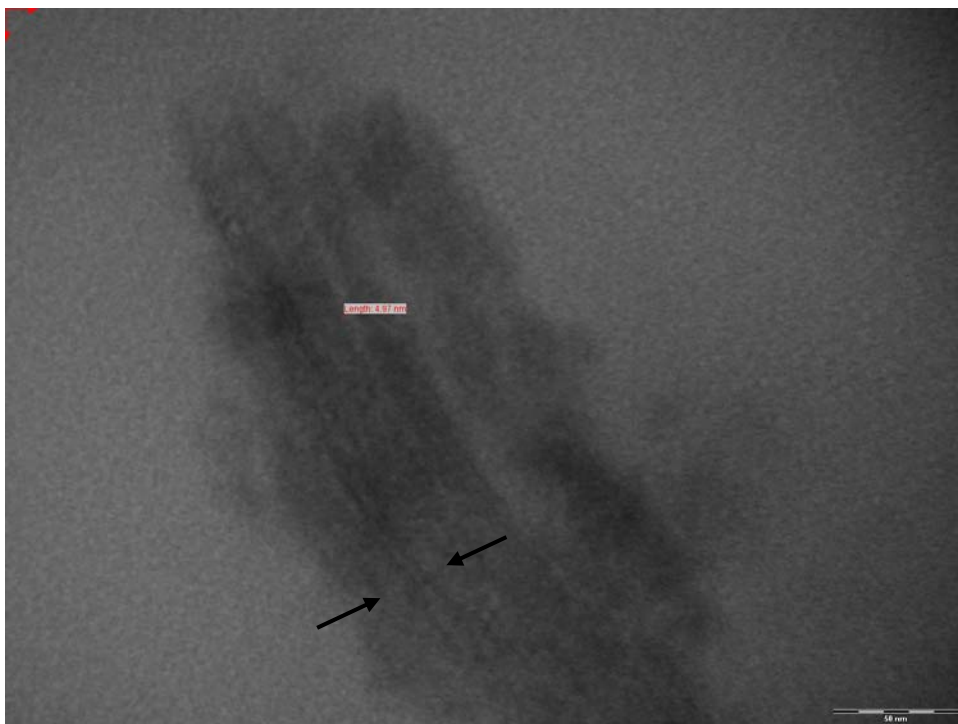


Figure 3.44 TEM micrograph of 5,10-HQ X 300K

CHAPTER 4

CONCLUSION

Normal and HCl treated composites of group 1 at filler loadings of 2 and 5 wt%, experienced nearly the same impact strength, near to that of pure PP. However at higher loadings parallel to increase in filler content impact strength decreased. The reduction was more severe for treated compositions. Upon the SCA treatment of normal composites, impact strength improved considerably due to interphase modification. In the case of acid treated and normal composites with SCA, as filler amount increased impact strength decreased; meanwhile, the reduction is high for acid treated samples. There seems to be an antagonistic effect in the presence of both SCA and HCl, especially at low filler contents. All group 2 compositions had higher impact strength due to the presence of tougher PP-g-MA in the matrix along with PP.

The MFIs of the group 1 compositions decreased as filler content increased. Apart from that, SCA treatment introduced further reduction in MFI values due to its coupling effect. In group 2 compositions, as compatibilizer content increased melt viscosity also increased due the anhydride groups of PP-g-MA.

It was observed that with the increase in the filler content, Young's modulus also increased. The increase was realized as 53% and 71% for 2-190 and 2-190-S, respectively compared to pure PP. This indicates that serpentine was very successful as a filler even at very small contents. The high yield stress and stress at break values which are well above that of pure PP for all filler contents could be seen as another indication for that. Here, the powerful effect of SCA as in the case of elastic modulus is evident. Percentage strain at break showed a decreasing trend with filler content. When these mechanical properties are concerned, serpentine is

very suitable reinforcing filler for PP even better in the presence of SCA. On the average, HCl treatment resulted in no significant changes in mechanical properties. Processing at 250 rpm and application of second extrusion didn't result in any positive effects due to the chain scission of PP under those processing conditions. In group 2 compositions, the introduction of PP-g-MA further increased the elastic modulus values. QAS treatment led to additional increase except for 5,15 compositions. The maximum improvement was achieved in the case of 2,6-Q which had 2.9 times higher elastic modulus than pure PP. This could be perceived as an indication of possible intercalation of the serpentine layers. Similar to group 1 composites, high stress at yield and stress at break values were attained. Different percentage strain at break behavior was obtained for group 2 members in that they didn't experience pronounced reduction instead they showed high elongation at break comparable to pure PP.

The melting temperatures of the group 1 composites increased 1-3°C with respect to PP. The percent crystallinity showed an increasing trend indicating the nucleating effect of serpentine in PP matrix. Generally, the melting point of group 2 compositions experienced a decrease caused by PP-g-MA.

Like elastic moduli behavior, storage and loss moduli increased with the filler content for group 1 composites. SCA treated compositions showed additional increase. The decrease in T_g of filled members of both groups could be correlated to the possible restricted mobility of PP chains. In group 2 compositions high storage and loss moduli values were attained over the whole temperature of study.

The filler addition didn't seem to cause changes on the surface morphology of the matrix. Although, in general homogeneous distribution of the filler through the matrix was observed, agglomerated portions are evident especially at high filler contents.

From the X-ray studies of QAS and HCl treated compositions of group 2 small peak shifts were obtained. Interpretation of these results with TEM analysis leads

to a conclusion that, there is partial intercalation of serpentine layers ending up with PP/serpentine nanocomposites. It is considered that, if serpentine had higher layer charge and/or unit distances like smectite clays (please refer to Figure 1.4 and Table 1.2) higher degree of exfoliation would be probable.

REFERENCES

- [1] Battey M.H., Mineralogy for Students, Hafner Press, New York, 1973.
- [2] Vanders I., Kerr P.F., Mineral Recognition, John Wiley & Sons Inc., New York, 1967.
- [3] Liebau F., Structural Chemistry of Silicates, Springer-Verlag, Berlin, 1985.
- [4] Eitel W., The Physical Chemistry of the Silicates, The University of Chicago Press, Chicago Illinois, 1954.
- [5] Wenk H.R., Bulakh A., Minerals-Their Constitution and Origin, Cambridge University Press, Cambridge, 2004.
- [6] Nesse W.D., Introduction to Mineralogy, Oxford University Press Inc., New York, 2000.
- [7] Sinkansas J., Mineralogy for Amateurs, D. Van Nostrand Company Inc., Princeton, 1964.
- [8] Putnis A., Introduction to Mineral Sciences, Cambridge University Press, Cambridge, 1992.
- [9] Kraus E.H., Hunt W.F., Ramsdell L.S., Mineralogy; An Introduction to the Study of Minerals and Crystals, McGraw-Hill Book Company, New York, 1959.

- [10] Zoltai T., Stout J.H., Mineralogy Concepts and Principles, Burgess Publishing Company, Minnesota, 1984.
- [11] Klein C., Hurlbut C.S., Manual of Mineralogy, John Wiley & Sons Inc., New York, 1993.
- [12] Bailey S.W., Hydrous Phyllosilicates: (Exclusive of Micas), Mineralogical Society of America Book Crafters Inc., Washington D.C., 1988.
- [13] Cairns-Smith A.G., Hartman H., Clay Minerals and the Origin of Life, Cambridge University Press, Cambridge, 1986.
- [14] Chamley H., Clay Sedimentology, Springer-Verlag, Berlin, 1989.
- [15] Dietrich R.V., Skinner B.J., Rocks and Rock Minerals, John Wiley & Sons Inc., New York, 1979.
- [16] Deer W.A., Howie R.A., Zussman J., Rock Forming Minerals Vol. 3: Sheet Silicates, Longmans, London, 1962.
- [17] Weaver C.E., Pollard L.D., The Chemistry of Clay Minerals, Elsevier Scientific Publishing Company, Amsterdam, 1973.
- [18] Velde B., Origin and Mineralogy of Clays, Springer-Verlag, Berlin, 1995.
- [19] Betekhtin A., A Course of Mineralogy, Peace Publishers, Moscow, 1968.
- [20] Tartaj P., Cerpa A., Garcia-Gonzalez M.T., Serna C.J., Journal of Colloid and Interface Science, Vol.231, 176-181, (2000).

- [21] Deer W.A., Howie R.A., Zussman J., An Introduction to the Rock Forming Minerals, Longman, New York, 1966.
- [22] Auzende A-L., Daniel I., Reynard B., Lemaire C., Guyot F., Phys. Chem. Minerals Vol.31, 269-277, (2004).
- [23] Azer M.K., Khalil A.E.S., Journal of African Earth Sciences, Vol.43(5), 525-536, (2005).
- [24] Simpson B., Rocks and Minerals, Pergamon Press, Oxford, 1966.
- [25] Correns C.W., Introduction to Mineralogy Crystallography and Petrology, Springer-Verlag, New York, 1969.
- [26] Zhang Q., Sugiyama K., Saito F., Hydrometallurgy, Vol.45, 323-331, (1997).
- [27] Kim D.J., Chung H.S., Particulate Science and Technology, Vol.20, 159-168, (2002).
- [28] Ernst W.G., Serpentine and Serpentinities: Mineralogy, Petrology, Geochemistry, Ecology, Geophysics, and Tectonics, Bellwhether Publishing Ltd., Columbia, 2004.
- [29] Perkins D., Mineralogy, Prentice Hall, Upper Saddle River N.J., 2002.
- [30] Rogers A.F., Introduction to the Study of Minerals, McGraw-Hill Book Company Inc., New York, 1937.
- [31] Bragg S.L., Claringbull G.F., The Crystalline State Vol. IV, Crystal Structures of Minerals, G. Bell & Sons Ltd, London, 1965.

- [32] Chisholm J.E., *Journal of Physics D-Applied Physics*, Vol.24, 199-202, (1991).
- [33] Zega T.J., Garvie L.A.J, Dodony I., Stroud R.M., Buseck P.R., *Lunar and Planetary Science XXXVI*, (2005).
- [34] Amelinckx S., Devouard B., Baronnet A., *Acta Cryst. Section A*, Vol.52, 850-878, (1996).
- [35] Hollaway L.C., Head P.R., *Advanced Polymer Composites and Polymers in the Civil Infrastructure*, Elsevier, Oxford, 2001.
- [36] Schwartz M.M., *Composite Materials, Volume I: Properties, Nondestructive Testing, and Repair*, Prentice-Hall Inc., New Jersey, 1997.
- [37] Miller T.E., *Introduction to Composites*, Composites Institute, New York, 1990.
- [38] Chung D.D.L., *Composite Materials Functional Materials for Modern Technologies*, Springer-Verlag, London, 2003.
- [39] Chawla K.K., *Composite Materials Science and Engineering*, Springer-Verlag, New York, 1987.
- [40] Frank H.P., *Polypropylene*, Gordon and Breach Science Publishers Inc., New York, 1968.
- [41] Tripathi D., *Practical Guide to Polypropylene*, Rapra Technology Ltd., Shawbury, 2002.
- [42] Rotheron R.N., *Particulate-Filled Polymer Composites*, Rapra Technology Limited, Shrewsbury, 2003.

- [43] Rothon R.N., Particulate Fillers for Polymers, Vol.12, Number 9, Rapra Review Reports, Rapra Technology Ltd., Shawbury, 2002.
- [44] Pukánszky B., Móczó J., Macromol. Symp., Vol.214, 115-134, (2004).
- [45] Kocsis J.K., Polypropylene Structure, Blends and Composites, Volume 3: Composites, Chapman & Hall, Cambridge, 1995.
- [46] Karian H.G., Handbook of Polypropylene and Polypropylene Composites, Marcel Dekker Inc., New York, 2003.
- [47] Silva A.L.N., Rocha M.C.G., Moraes M.A.R., Valente C.A.R., Countino F.M.B., Polymer Testing, Vol.21, 57-60, (2002).
- [48] Weidenfeller B., Höfer M., Schilling F.R., Composites:Part A, Vol.35, 423-429, (2004).
- [49] Leong Y.W., Abu Bakar M.B., Ishak Z.A.M., Ariffin A., Pukanszky B., Journal of Applied Polymer Science, Vol.91, 3315-3326, (2004).
- [50] Leong Y.W., Abu Bakar M.B., Ishak Z.A.M., Ariffin A., Journal of Applied Polymer Science, Vol.98, 413-426, (2005).
- [51] Felix A.H.O.,Cardozo N.S.M., Nachtigall S.M.B., Mauler R.S., Macromol. Mater. Eng., Vol.291, 418-427, (2006).
- [52] Yazdani H., Morshedian J., Khonakdar H.A., Polymer Composites, Vol.27, 491-496, (2006).
- [53] Liang J.Z., Macromol. Mater. Eng., Vol.286, 714-718, (2001).

- [54] Akın-Oktem G., Tanrisinibilir S., Tinçer T., Journal of Applied Polymer Science, Vol.81(5), 2607-2618, (2001).
- [55] Chen X.L., Yu J., Guo S.Y., Journal of Applied Polymer Science, Vol.102(5), 4943-4951, (2006).
- [56] Nachtigall S.M.B., Cerveira G.S., Rosa S.M.L., Polymer Testing, Vol.26(5), 619-628, (2007).
- [57] Zugenmaier P., Pure and Applied Chemistry, Vol.78(10), 1843-1855, (2006).
- [58] Gogotsi Y., Nanomaterials Handbook, Taylor&Francis, Boca Raton, 2006.
- [59] Ristolainen N., Vainio U., Paavola S., Torkkeli M., Journal of Polymer Science Part B: Polymer Physics, Vol.43, 1892-1903, (2005).
- [60] Utracki L.A., Clay Containing Polymeric Nanocomposites Volume 1, Rapra Technology Limited, Shawbury, 2004.
- [61] Liu J., Boo W.J., Clearfield A., Sue H.J., Materials and Manufacturing Processes, Vol.20, 143-151, (2006).
- [62] Friedrich K., Fakirov S., Zhang Z., Polymer Composites from Nano to Macro Scale, Springer, New York, 2005.
- [63] Vaia R.A., Jandt K.D., Kramer E.J., Giannelis E.P., Chem. Mater., Vol.8, 2628-2635, (1996).
- [64] Hambir S., Bulakh N., Jog J.P., Polymer Engineering and Science, Vol. 42, 1800-1807, (2002).

- [65] Yuan M., Misra R.D.K., *Polymer*, Vol.47, 4421-4433, (2006).
- [66] Koo C.M., Kim M.J., Choi M.H., Kim S.O., Chung I.J., *Journal of Applied Polymer Science*, Vol.88, 1526-1535, (2003).
- [67] Usuki A., Kawasumi Y., Kojiyama M., Fukushima Y., Okada A., Kurauchi T., Kamigaito O., *J. Mater. Res.*, Vol.8, 1179-1184, (1993).
- [68] Geckeler K.E., Rosenberg E., *Functional Nanomaterials*, American Scientific Publishers, California, 2006.
- [69] Kozak M., Domka L., *Journal of Physics and Chemistry of Solids*, Vol.65, 441-445, (2004).
- [70] Baldassari S., Komerneni S., Mariani E., Villa C., *Applied Clay Science*, Vol.31, 134-141, (2006).
- [71] Leuteritz A., Pospiech D., Kretzschmar B., Willeke M., Jehnichen D., Jentzsch U., Grundke K., Janke A., *Macromol. Symp.*, Vol.221, 53-61, (2005).
- [72] Marchant D., Jayaraman K., *Ind. Eng. Chem. Res.*, Vol.41, 6402-6408, (2002).
- [73] Shmuel Y., Cross H., *Organo-Clay Complexes and Interactions*, Marcel Dekker Inc., New York, 2002.
- [74] Ajayan P.M., Schadler L.S., Braun P.V., *Nanocomposite Science and Technology*, Wiley-VCH, Weinheim, 2003.
- [75] Okamoto M., *Polymer/Layered Silicate Nanocomposites Volume 14*, Rapra Technology Limited, Boston, 2003.

- [76] Tjong S.C., Nanocrystalline Materials: Their Synthesis-Structure-Property Relationship and Applications, Elsevier Ltd., Oxford, 2006.
- [77] Koo C.M., Kim J.H., Wang K.H., Chung I.J., Journal of Polymer Science Part B: Polymer Physics, Vol.43, 158-176, (2005).
- [78] Hambir S., Bulakh N., Kodgire P., Kalgaonkar R., Jog J.P., Journal of Polymer Science Part B: Polymer Physics, Vol.39, 446-450, (2001).
- [79] Burmistr M.V., Sukhyy K.M., Shilov V.V., Pissis P., Spanoudaki A., Sukha I.V., Tomilo V.I., Gomza Y.P., Polymer, Vol.46, 12226-12235, (2005).
- [80] López-Quintanilla M.L., Sánchez-Valdés S., Ramos de Valle L.F., Medellín-Rodríguez F.J., Journal of Applied Polymer Science, Vol.100, 4748-4756, (2006).
- [81] Kim J.H., Koo C. M., Choi Y. S., Wang K. H., Chung I. J., Polymer, Vol.45, 7719-7727, (2004).
- [82] García- López D., Picazo O., Merino J.C., Pastor J.M., European Polymer Journal, Vol.39, 945-950, (2003).
- [83] Mai Y.W., Yu Z-Z., Polymer Nanocomposites, Woodhead Publishing Limited, Cambridge, 2006.
- [84] Maiti P., Nam P.H., Okamoto M., Kotaka T., Polymer Engineering and Science, Vol.42, 1864-1871, (2002).
- [85] Nam P.H., Maiti P., Okamoto M., Kotaka T., Hasegawa N., Usiki A., Polymer, Vol.42, 9633-9640, (2001).

[86] Kawasumi M., Hasegawa N., Kato M., Usiki A., Okada A., *Macromolecules*, Vol.30, 6333-6338, (1997).

[87] Velasco J.I., Ardanuy M., Realinho V., Antunes M., Fernández A.I., González-Peña J.I., Rodríguez-Pérez M.A., de Saja J.A., *Journal of Applied Polymer Science*, Vol.102, 1213-1223, (2006).

[88] Kodgire P., Kalgaonkar R., Hambir S., Bulakh N., Jog J.P., *Journal of Applied Polymer Science*, Vol.81, 1786-1792, (2001).

[89] Modesti M., Lorenzetti A., Bon D., Besco S., *Polymer Degradation and Stability*, Vol.91, 672-680, (2006).

[90] Villaluenga J.P.G., Khayet M., López-Manchado M.A., Valentin J.L., Seoane B., Mengual J.I., *European Polymer Journal*, Vol.43, 1182-1143, (2007).

[91] Brandrup J., Immergut E.H., *Polymer Handbook*, Wiley-Interscience Publication, New York, 1989.

[92] Stricker F., Bruch M., Mülhaupt R., *Polymer*, Vol.38(21), 5347-5353, (1997).

[93] Pukanszky B., *Composites*, Vol.21, 255-262, (1990).

[94] Menard K.P., *Dynamic Mechanical Analysis: A Practical Introduction*, CRC Press, Boca Raton, 1999.

APPENDIX A

PORE SIZE DISTRIBUTION GRAPHS

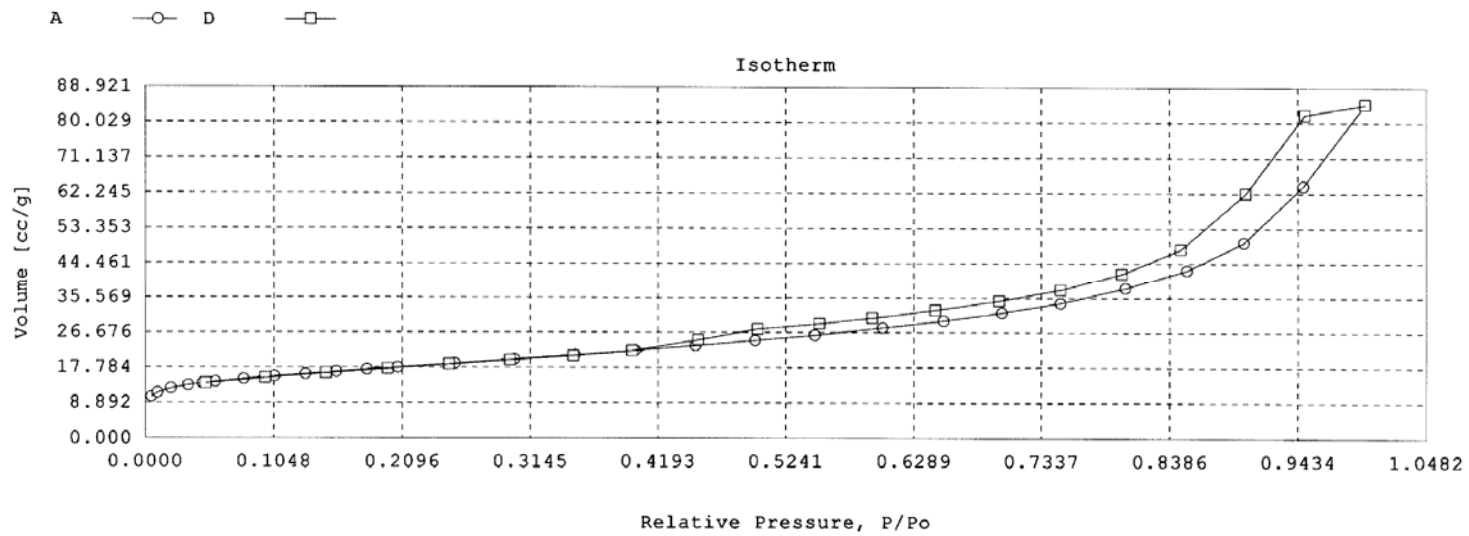


Figure A.1 Adsorption isotherm of 48 hours milled serpentine

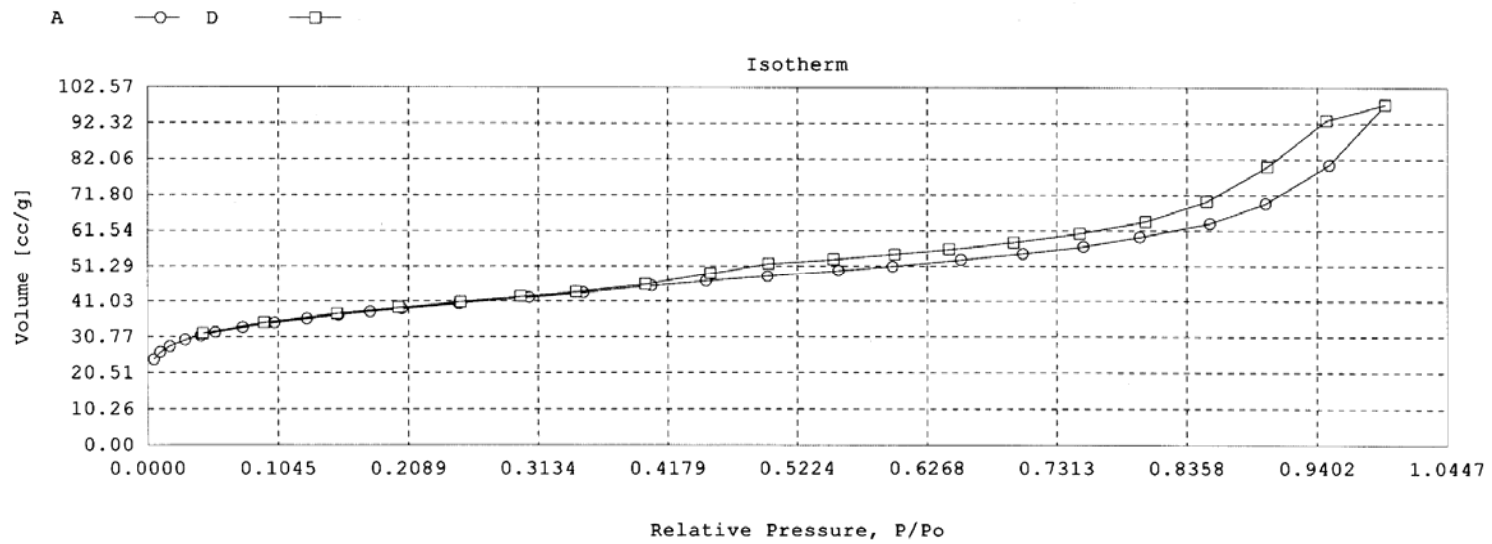


Figure A.2 Adsorption isotherm of 48 hours milled acid treated serpentine

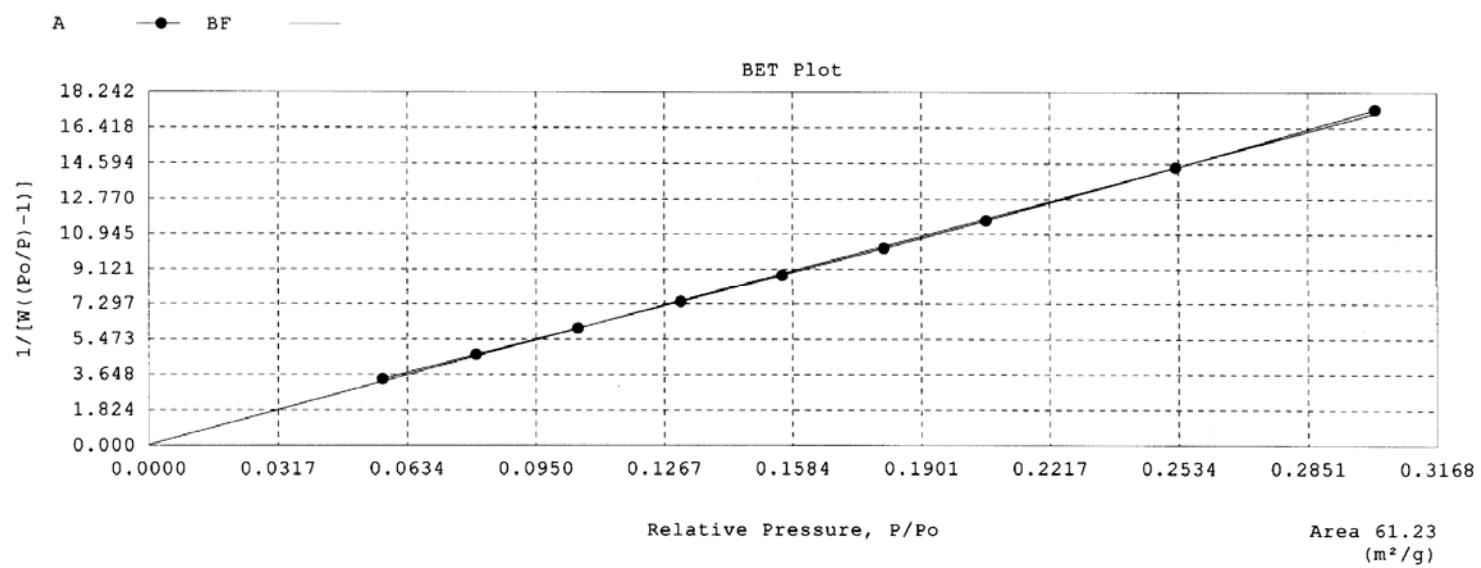


Figure A.3 BET plot of 48 hours milled serpentine

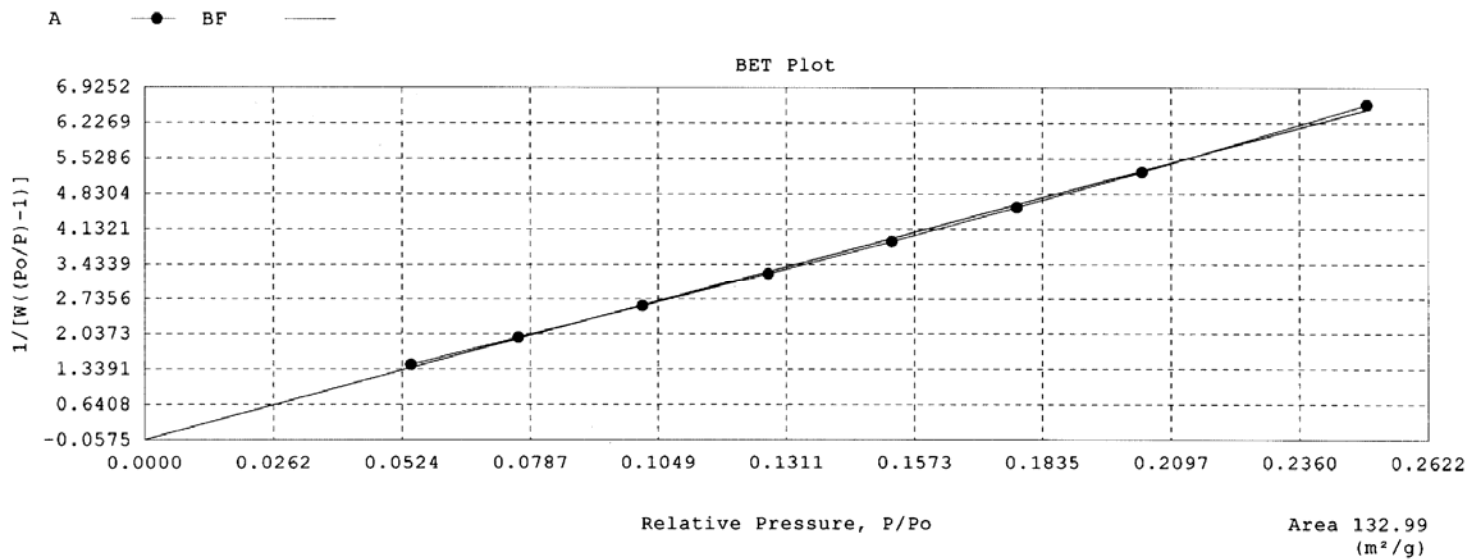


Figure A.4 BET plot of 48 hours milled acid treated serpentine

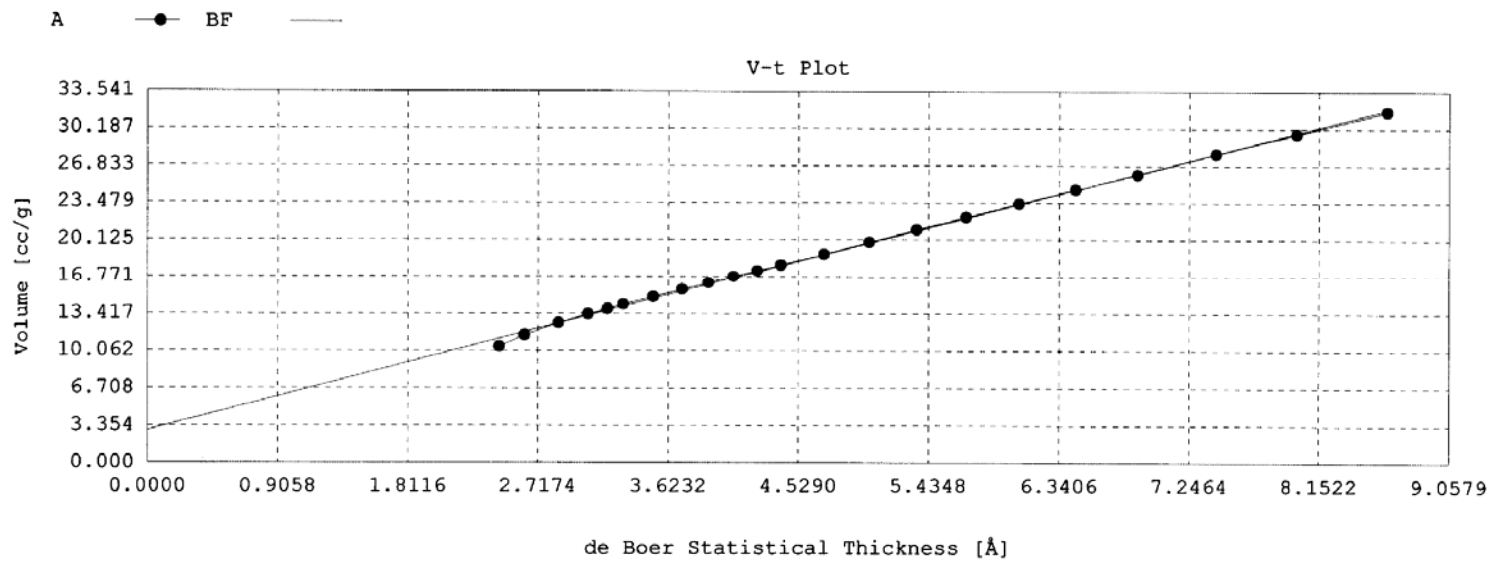


Figure A.5 V-t plot of 48 hours milled serpentine

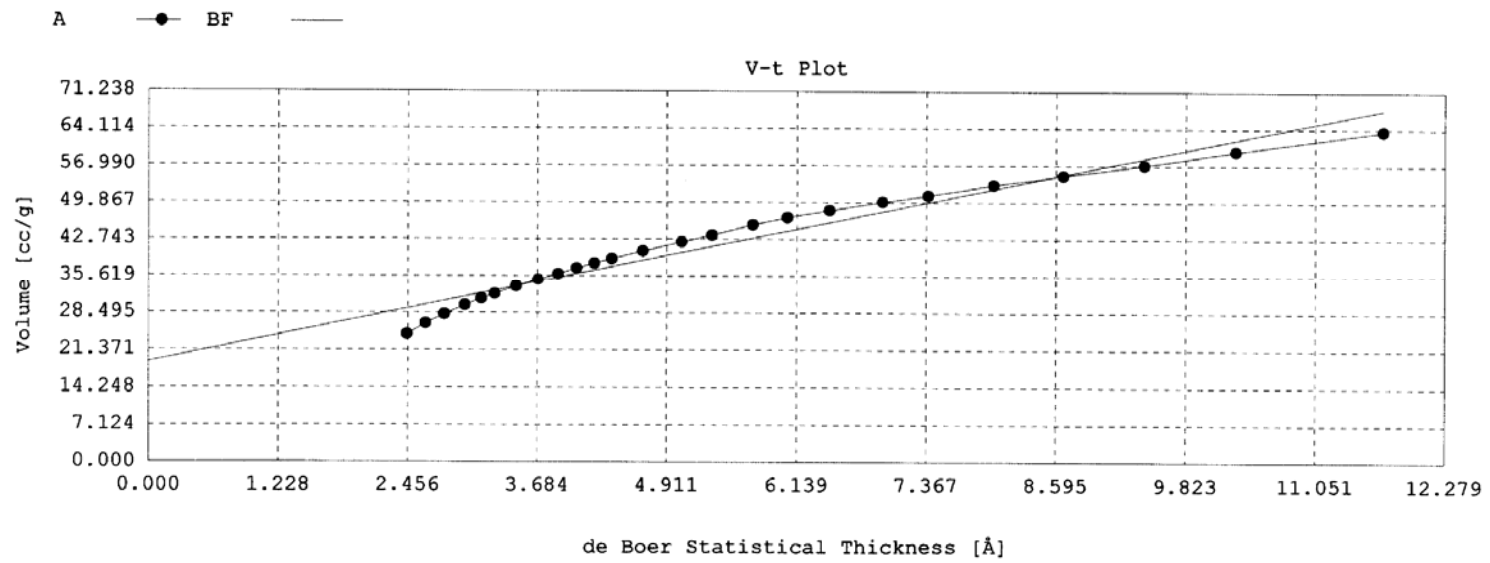


Figure A.6 V-t plot of 48 hours milled acid treated serpentine

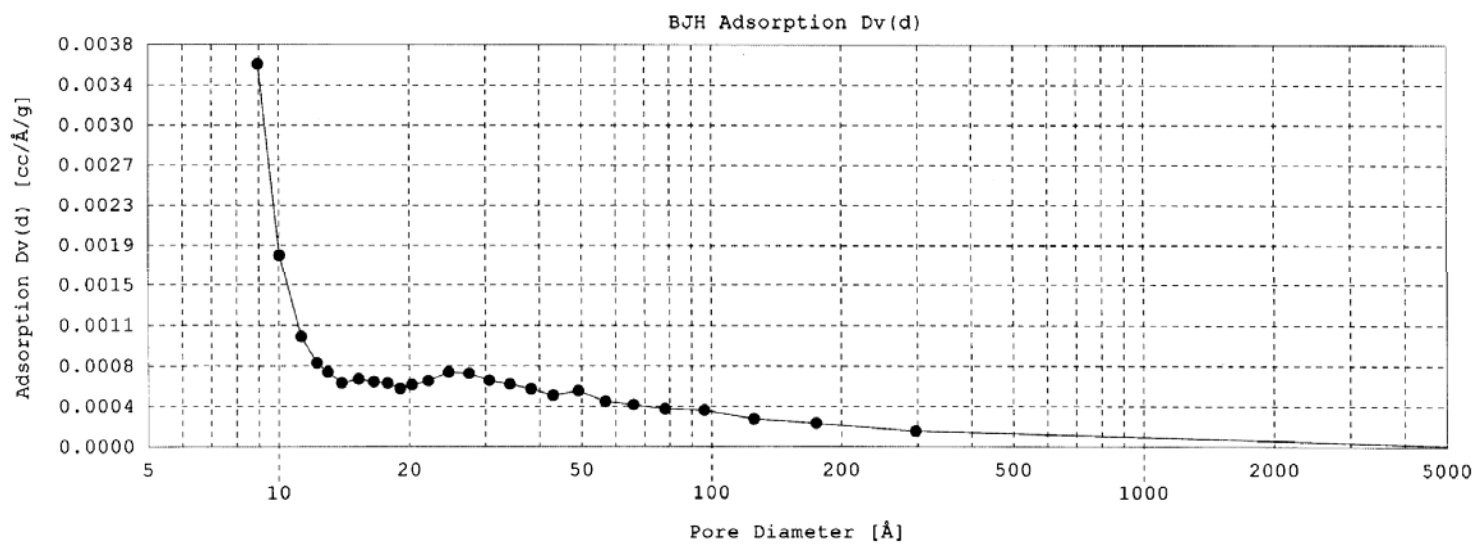


Figure A.7 BJH Adsorption plot of 48 hours milled serpentine

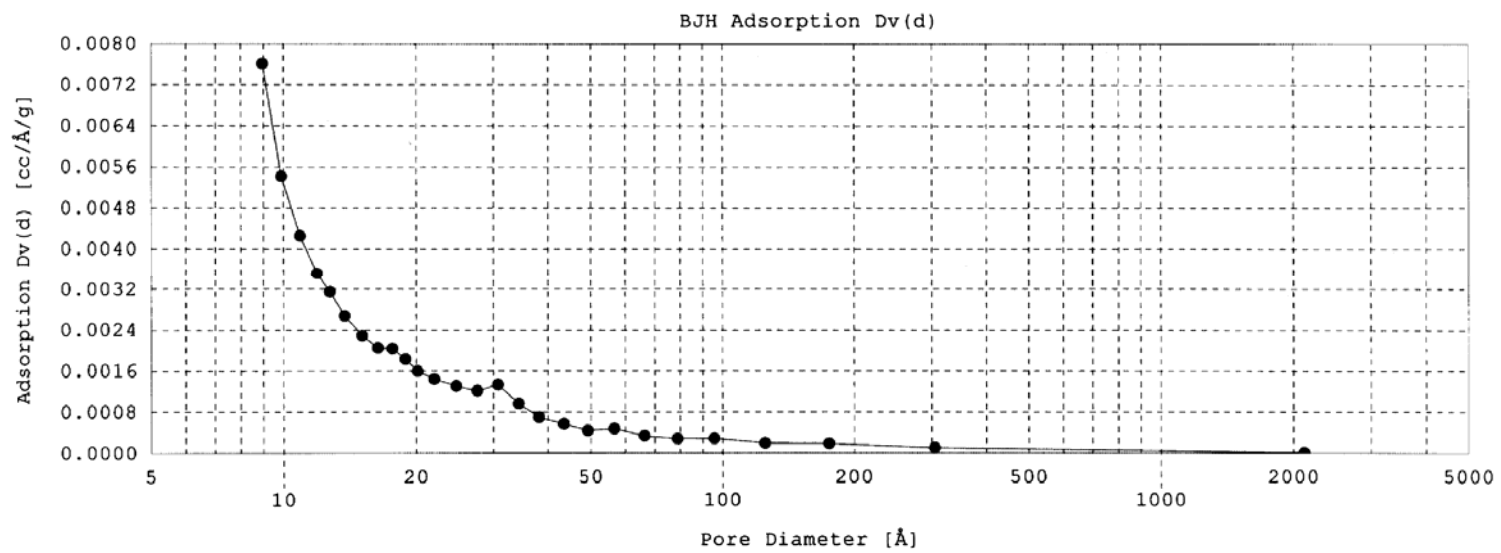


Figure A.8 BJH Adsorption plot of 48 hours milled acid treated serpentine

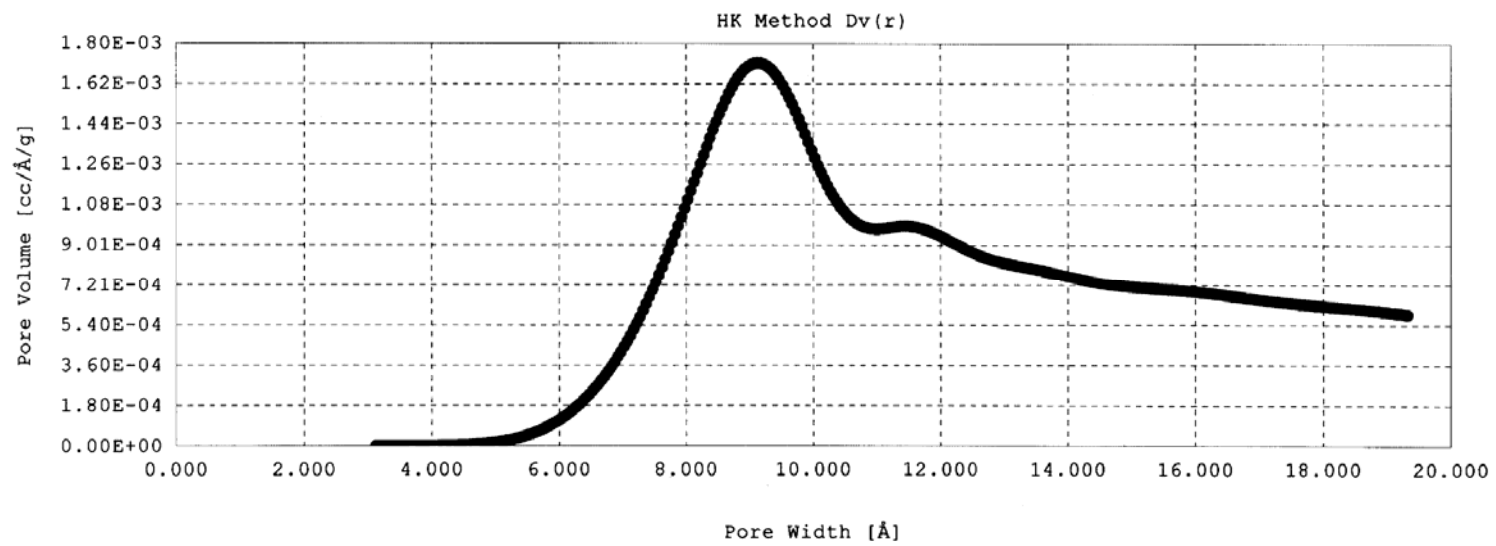


Figure A.9 HK plot of 48 hours milled serpentine

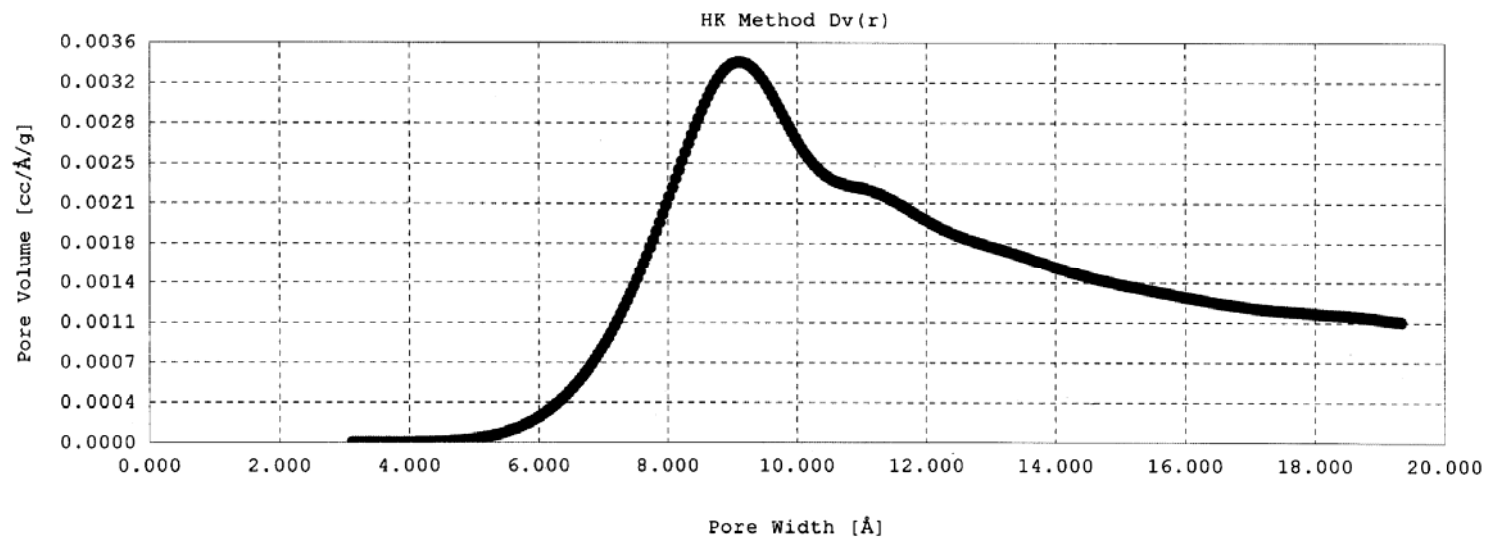


Figure A.10 HK plot of 48 hours milled acid treated serpentine

APPENDIX B

IMPACT STRENGTH DATA

Table B.1 The variation of impact strength (kJ/m^2) with respect to group 1 compositions

Pure PP 35.7±2.2			
2-190 23.1±3.5	5-190 22.8±2.3	10-190 19.1±0.5	20-190 14.2±0.8
2-190-H 25.6±1.3	5-190-H 23.9±1.9	10-190-H 14.0±1.4	20-190-H 7.9±0.3
2-190-S 27.7±2.9	5-190-S 25.0±0.8	10-190-S 17.4±0.6	20-190-S 14.5±0.9
2-190-SH 21.4±2.1	5-190-SH 17.5±1.6	10-190-SH 14.2±0.8	20-190-SH 9.2±0.3
2-250-S 25.0±1.7	5-250-S 23.1±2.4	2-250,2-S 29.0±3.3	5-250,2-S 24.0±0.5
2-250-SH 23.7±3.2	5-250-SH 16.3±1.6	2-250,2-SH 33.4±1.8	5-250,2-SH 18.1±2.1

Table B.2 The variation of impact strength (kJ/m^2) with respect to group 2 compositions

2,4-N 50.3±1.6	2,4-H 49.0±2.1	2,4-Q 50.7±3.2	2,4-HQ 50.4±1.0
5,10-N 45.3±3.8	5,10-H 41.7±1.9	5,10-Q 46.9±2.8	5,10-HQ 41.6±2.9
2,6-N 45.0±2.5	2,6-H 43.2±2.7	2,6-Q 49.1±3.3	2,6-HQ 44.9±3.4
5,15-N 48.8±2.9	5,15-H 46.5±3.0	5,15-Q 46.3±2.7	5,15-HQ 41.1±3.2

APPENDIX C

MFI DATA

Table C.1 MFI (g/10 min) for group 1 compositions

Pure PP 15.1			
2-190 17.3	5-190 15.5	10-190 14.7	20-190 12.4
2-190-H 18.1	5-190-H 16.8	10-190-H 12.7	20-190-H 10.8
2-190-S 16.1	5-190-S 13.8	10-190-S 12.5	20-190-S 10.5
2-190-SH 17.8	5-190-SH 16.4	10-190-SH 12.1	20-190-SH 10.1
2-250-S 16.4	5-250-S 15.6	2-250,2-S 18.8	5-250,2-S 16.5
2-250-SH 17.7	5-250-SH 14.1	2-250,2-SH 19.6	5-250,2-SH 14.8

Table C.2 MFI (g/10 min) for group 2 compositions

2,4-N 16.3	2,4-H 15.3	2,4-Q 16.1	2,4-HQ 15.2
5,10-N 13.4	5,10-H 13.1	5,10-Q 13.4	5,10-HQ 12.4
2,6-N 16.2	2,6-H 14.8	2,6-Q 16.1	2,6-HQ 14.0
5,15-N 12.0	5,15-H 10.1	5,15-Q 11.9	5,15-HQ 9.8

APPENDIX D

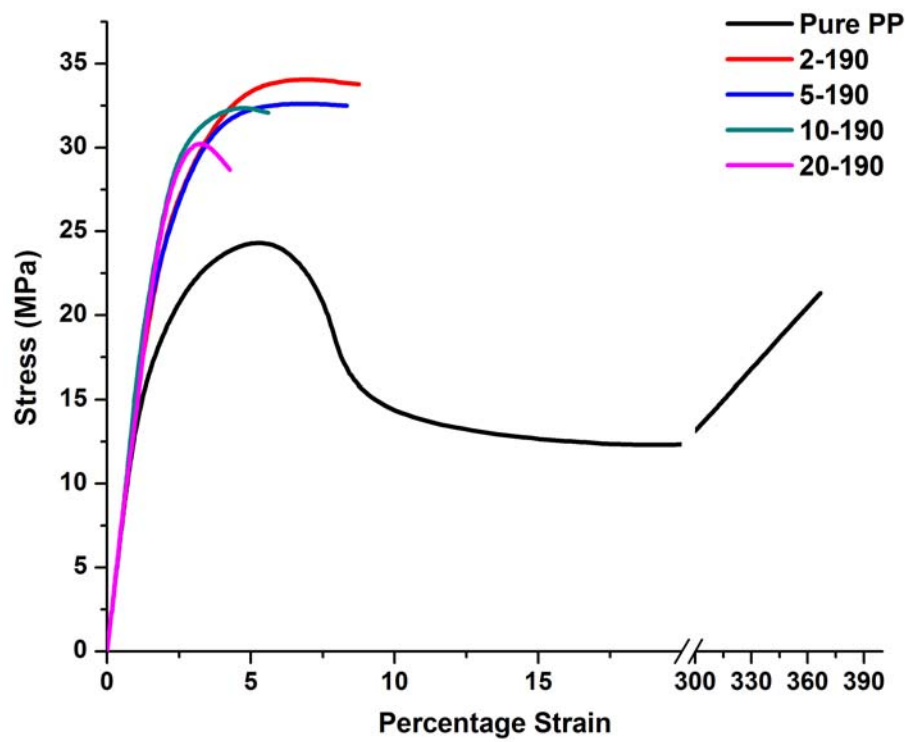
TENSILE PROPERTIES DATA

Table D.1 The tensile properties of group 1 compositions

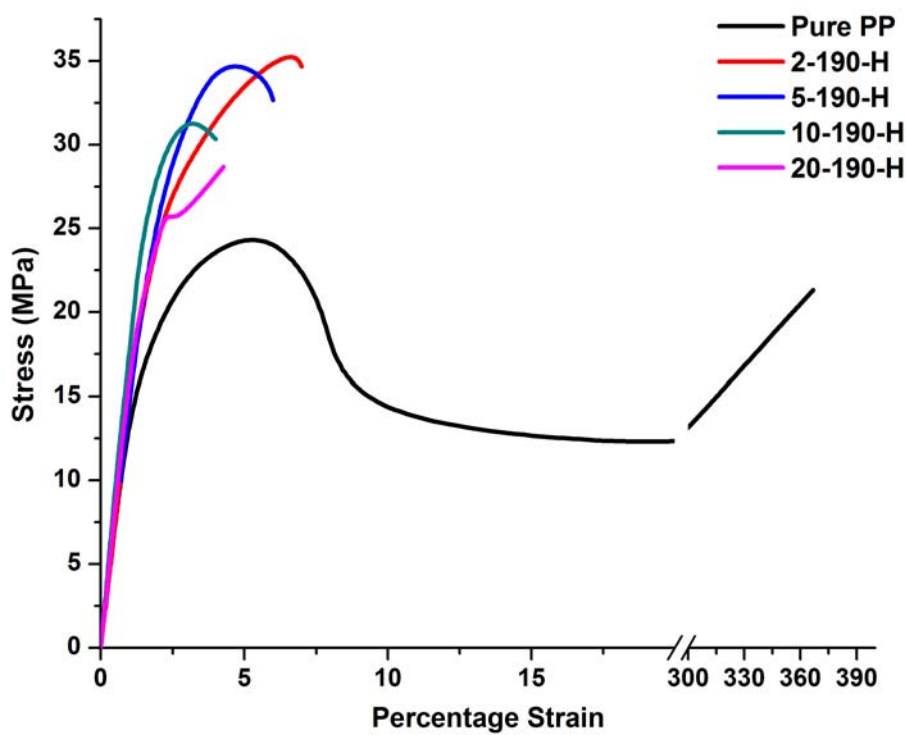
Composition	Young's Modulus (Mpa)	Stress at Yield (Mpa)	Stress at Break (Mpa)	Percentage Strain at Break
2-190	1088±37	35.2±1.7	34.5±1.2	10.0±1.4
5-190	1103±79	33.7±1.2	33.7±1.5	8.5±0.6
10-190	1151±42	33.6±0.9	32.5±1.3	6.7±1.2
20-190	1233±64	30.8±1.8	28.7±1.8	4.2±0.5
2-190-H	1067±26	34.8±1.0	33.6±1.2	6.7±0.5
5-190-H	1109±83	33.3±2.2	31.8±2.0	5.9±0.3
10-190-H	1184±35	31.5±0.5	29.7±0.7	3.8±1.0
20-190-H	1250±81	27.8±1.9	27.9±2.5	2.5±0.4
2-190-S	1218±26	38.7±1.4	37.5±0.6	6.9±0.7
5-190-S	1283±59	38.1±1.2	37.0±1.4	5.5±0.8
10-190-S	1349±50	37.3±2.1	36.2±1.0	4.5±0.4
20-190-S	1475±67	36.2±1.1	35.0±0.6	3.7±0.7
2-190-SH	1084±73	35.2±0.8	33.0±1.2	6.2±0.9
5-190-SH	1183±62	34.2±1.8	30.4±1.8	5.7±0.4
10-190-SH	1268±37	31.6±0.7	29.1±1.4	3.9±0.7
20-190-SH	1337±45	28.5±1.7	27.4±2.3	2.3±0.3

Table D.2 The tensile properties of group 2 compositions

Composition	Young's Modulus (Mpa)	Stress at Yield (Mpa)	Stress at Break (Mpa)	Percentage Strain at Break
2,4-N	1319±52	43.7±2.4	20.1±2.2	324.9±21.0
2,4-H	1681±87	44.5±0.7	22.9±1.4	204.4±13.1
2,4-Q	1488±64	48.2±0.9	30.1±1.9	287.1±12.8
2,4-HQ	1757±63	49.6±1.3	32.8±2.2	305.1±18.3
5,10-N	1338±47	35.2±1.1	18.6±2	265.5±10.2
5,10-H	1081±72	41.7±0.7	17.3±2	113.3±9.0
5,10-Q	1662±94	47.6±0.9	21.2±1.4	211.0±16.5
5,10-HQ	1433±50	50.3±2.2	34.3±1.2	172.7±16.1
2,6-N	1648±73	43.9±1.6	25.9±0.9	327.7±9.3
2,6-H	1429±59	47.6±1.2	24.0±1.0	150.6±19.2
2,6-Q	2065±77	48.8±1.7	33.4±1.1	283.8±16.5
2,6-HQ	1850±94	45.3±1.5	21.0±1.2	68.5±11.2
5,15-N	2046±144	54.4±1.2	16.1±0.8	252.2±14.1
5,15-H	1526±98	38.2±1.0	18.5±0.8	40.0±6.4
5,15-Q	1459±82	38.3±1.7	19.2±1.2	85.5±7.9
5,15-HQ	1807±105	43.2±1.0	15.4±1.4	138.8±18.0



(a)



(b)

Figure D.1 Stress-strain plots of (a) N, (b) H compositions

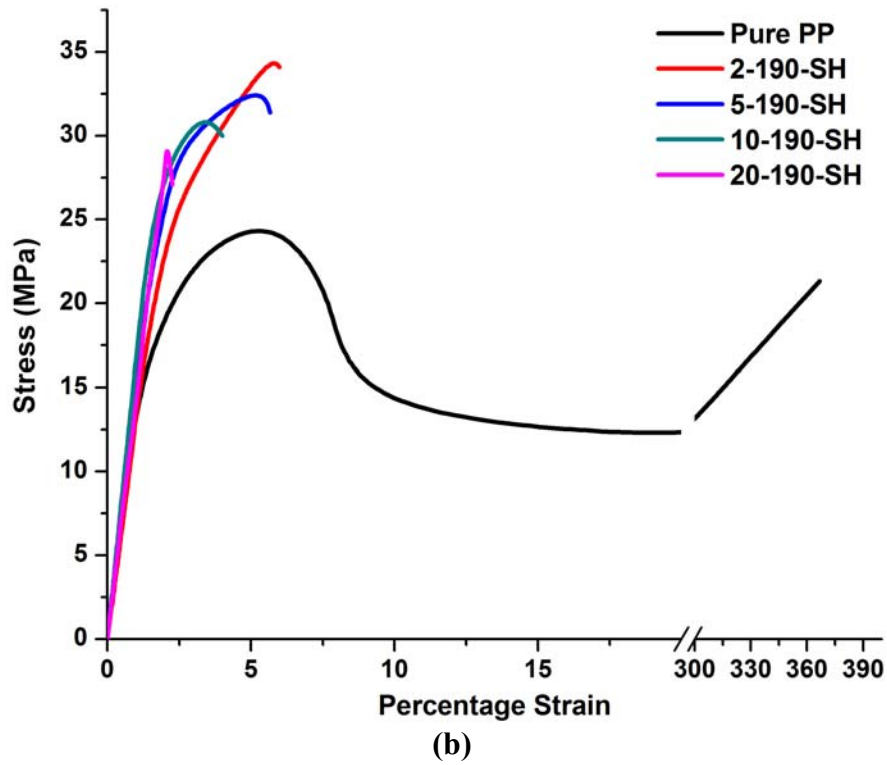
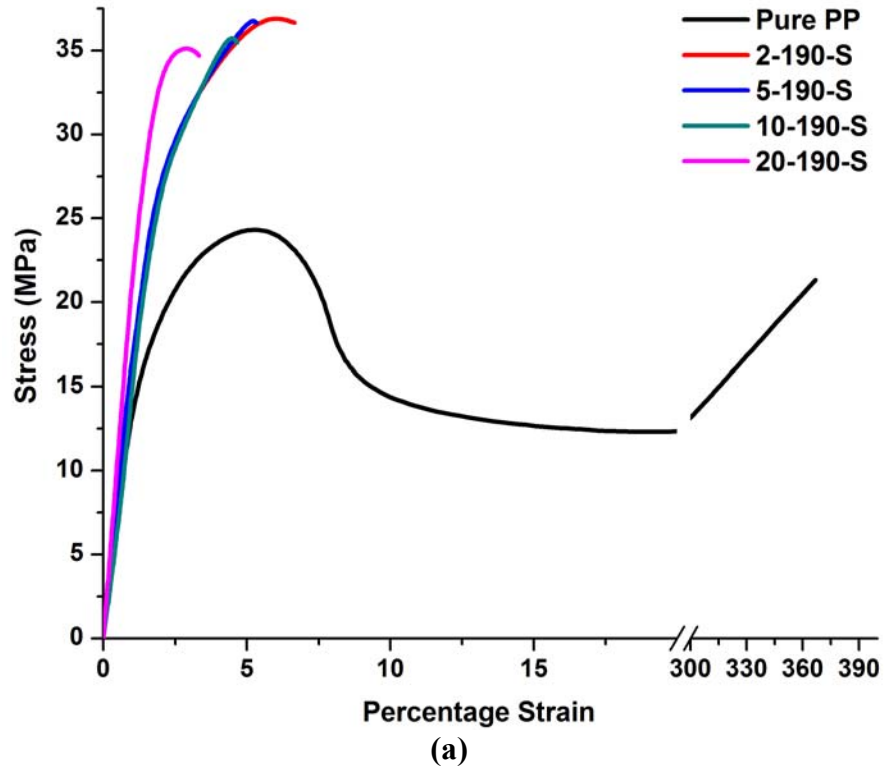
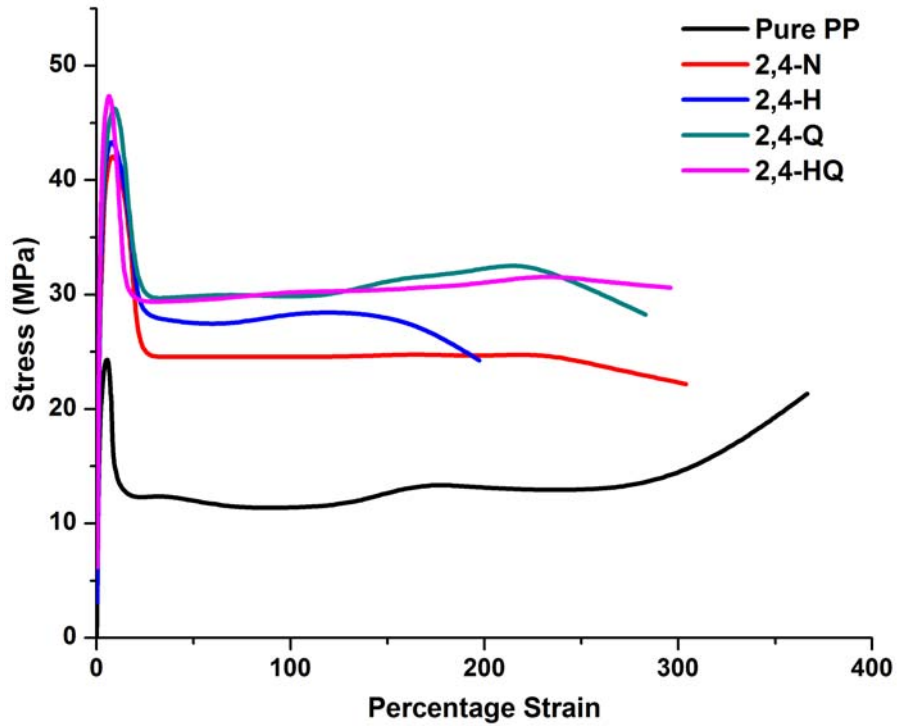
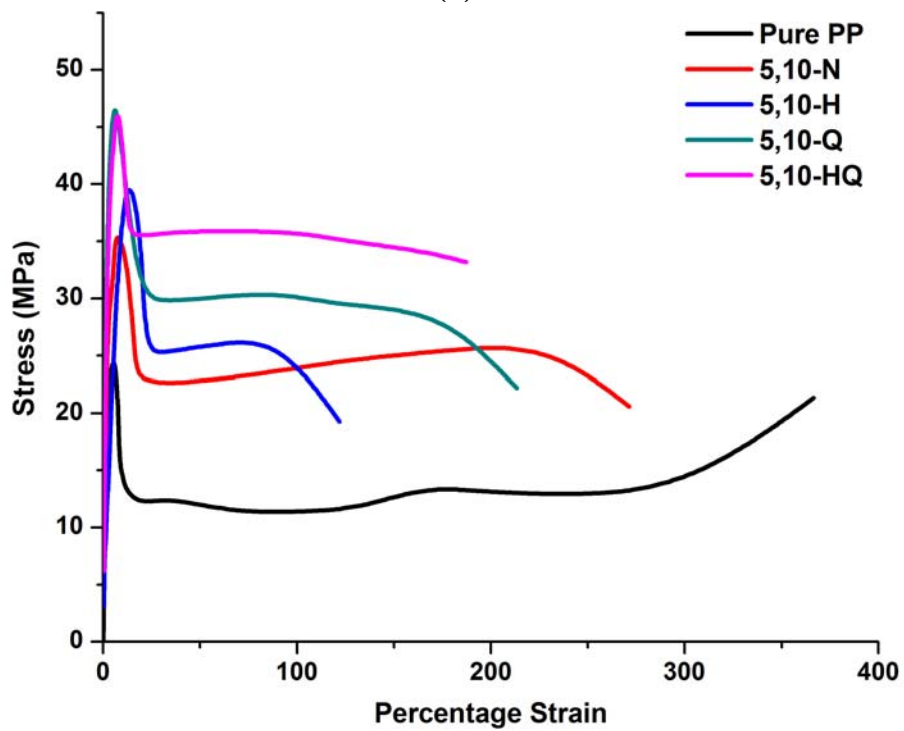


Figure D.2 Stress-strain plots of (a) S, (b) SH compositions



(a)



(b)

Figure D.3 Stress-strain plots of (a) 2,4, (b) 5,10 compositions

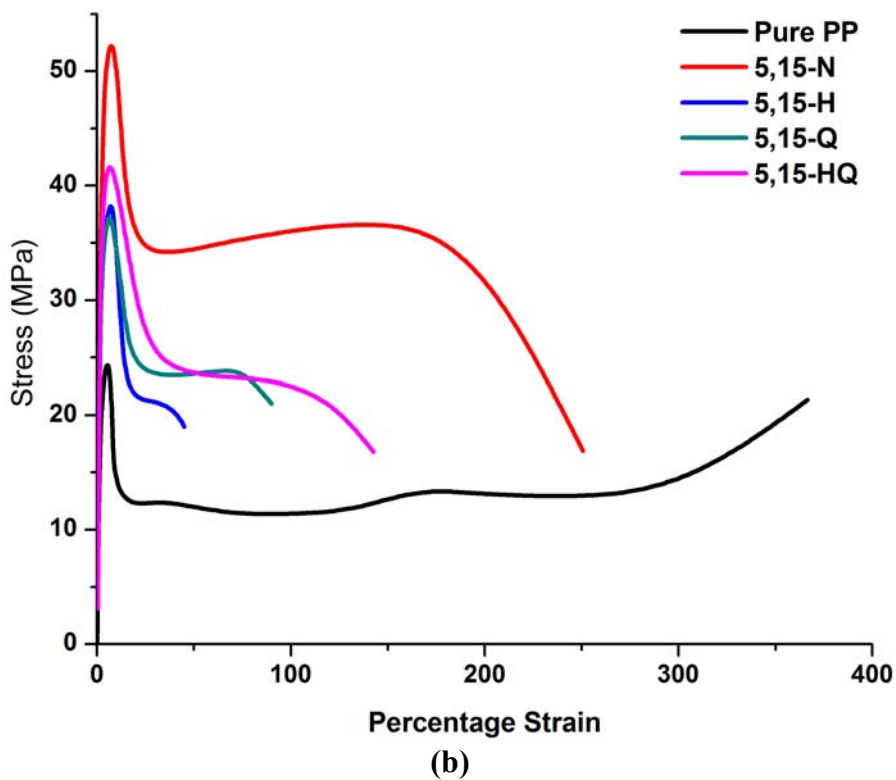
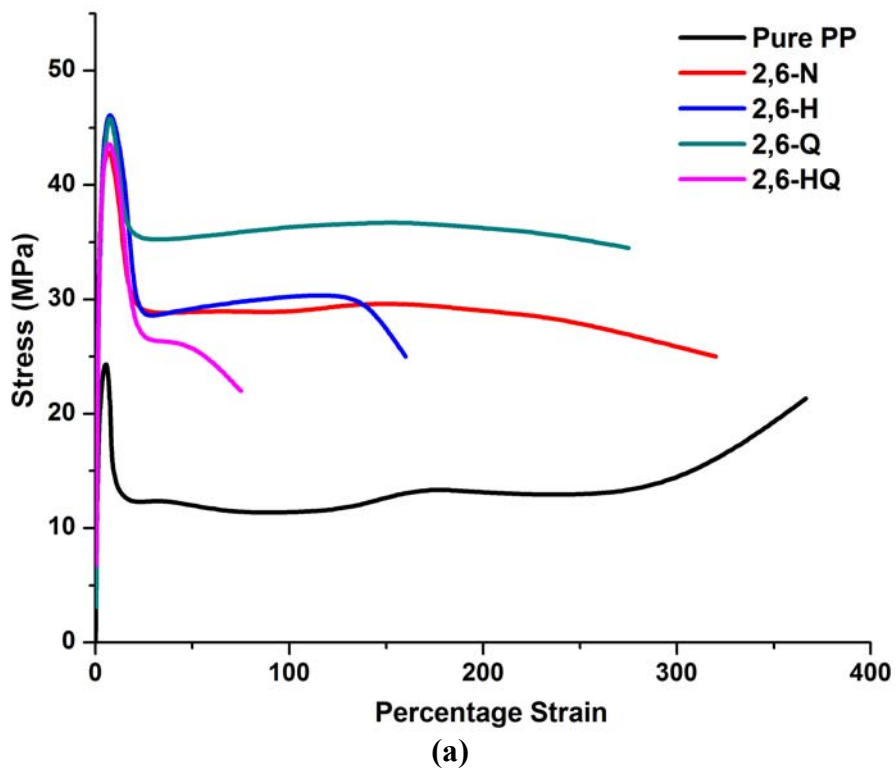


Figure D.4 Stress-strain plots of (a) 2,6, (b) 5,15 compositions

APPENDIX E

DSC THERMOGRAMS

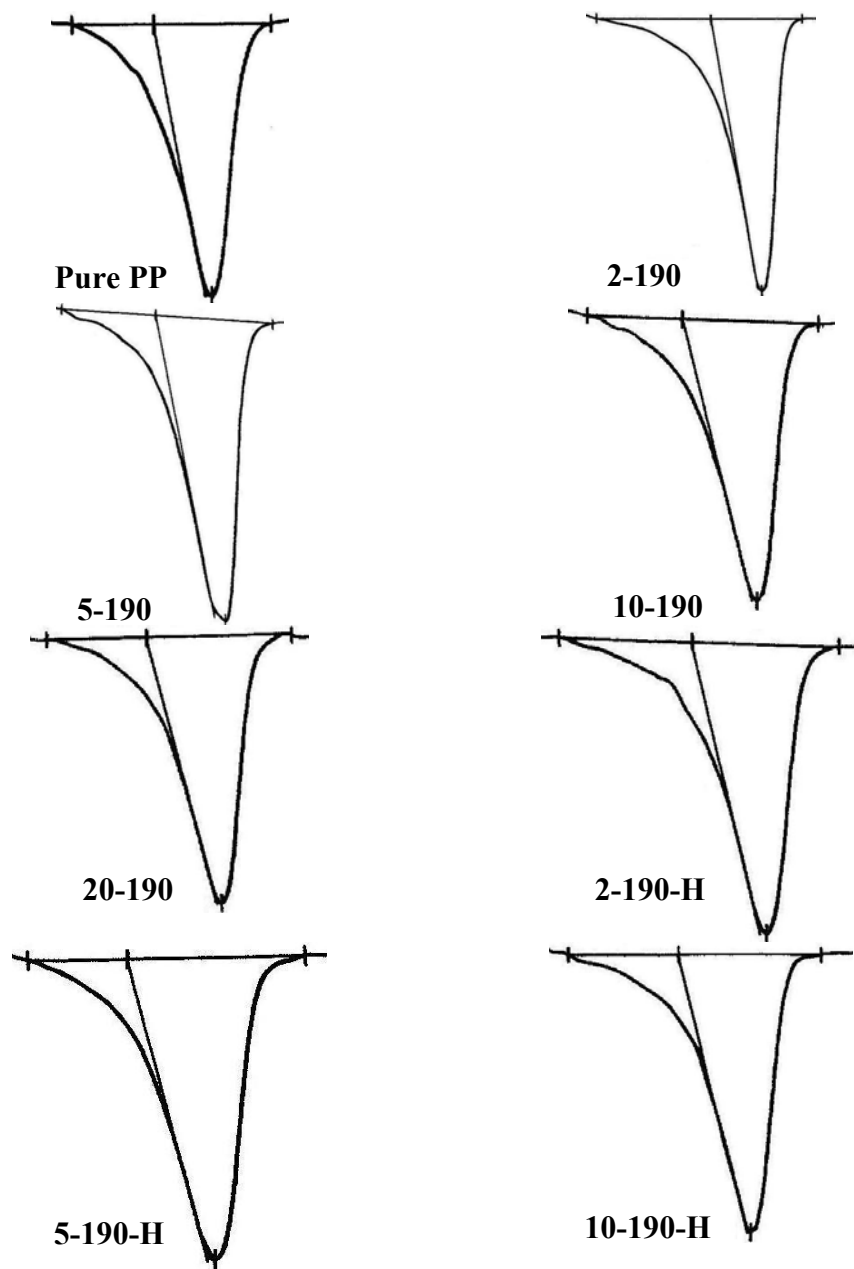


Figure E.1 DSC thermograms of group 1 compositions

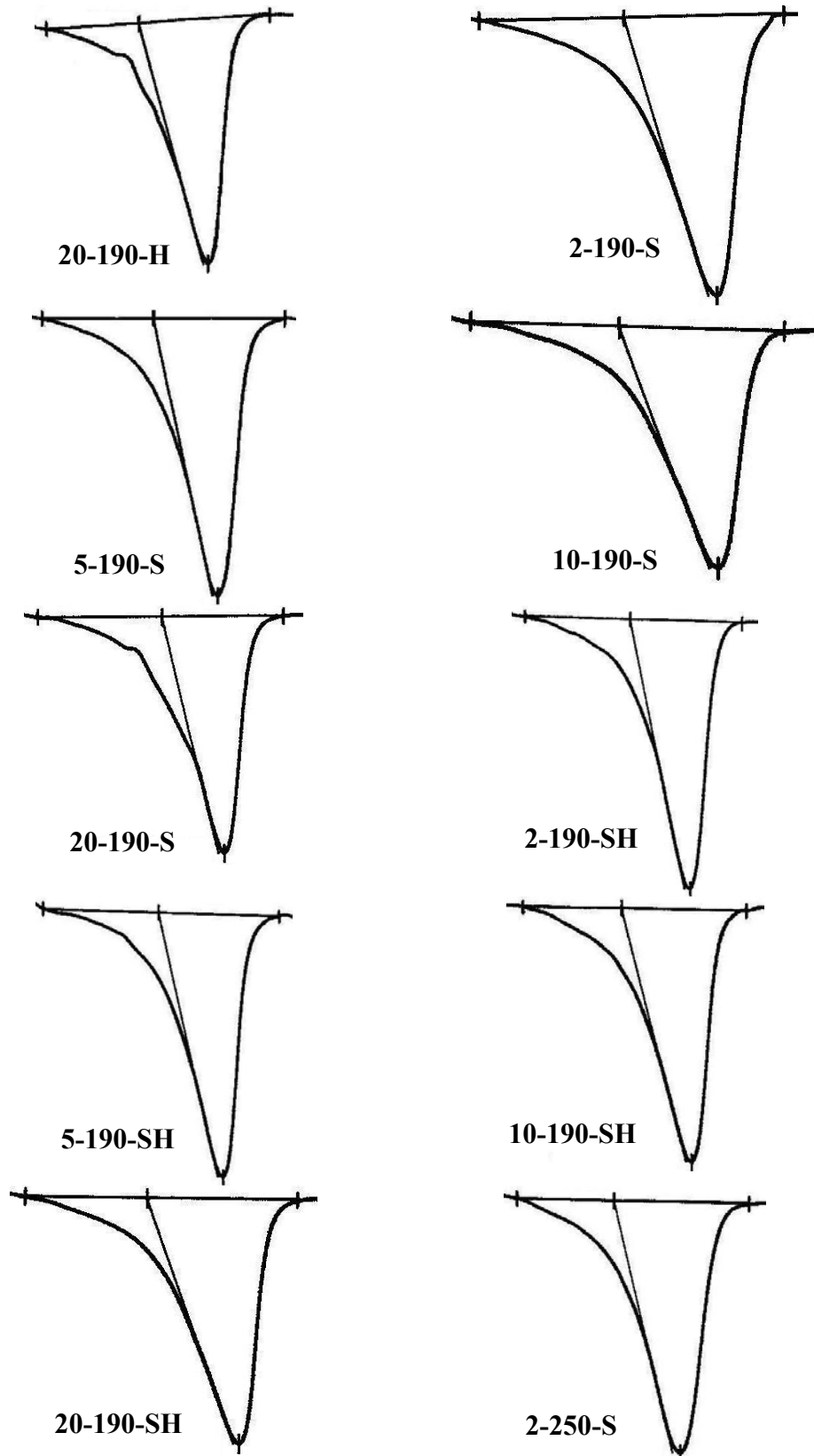


Figure E.1 (cont'd)

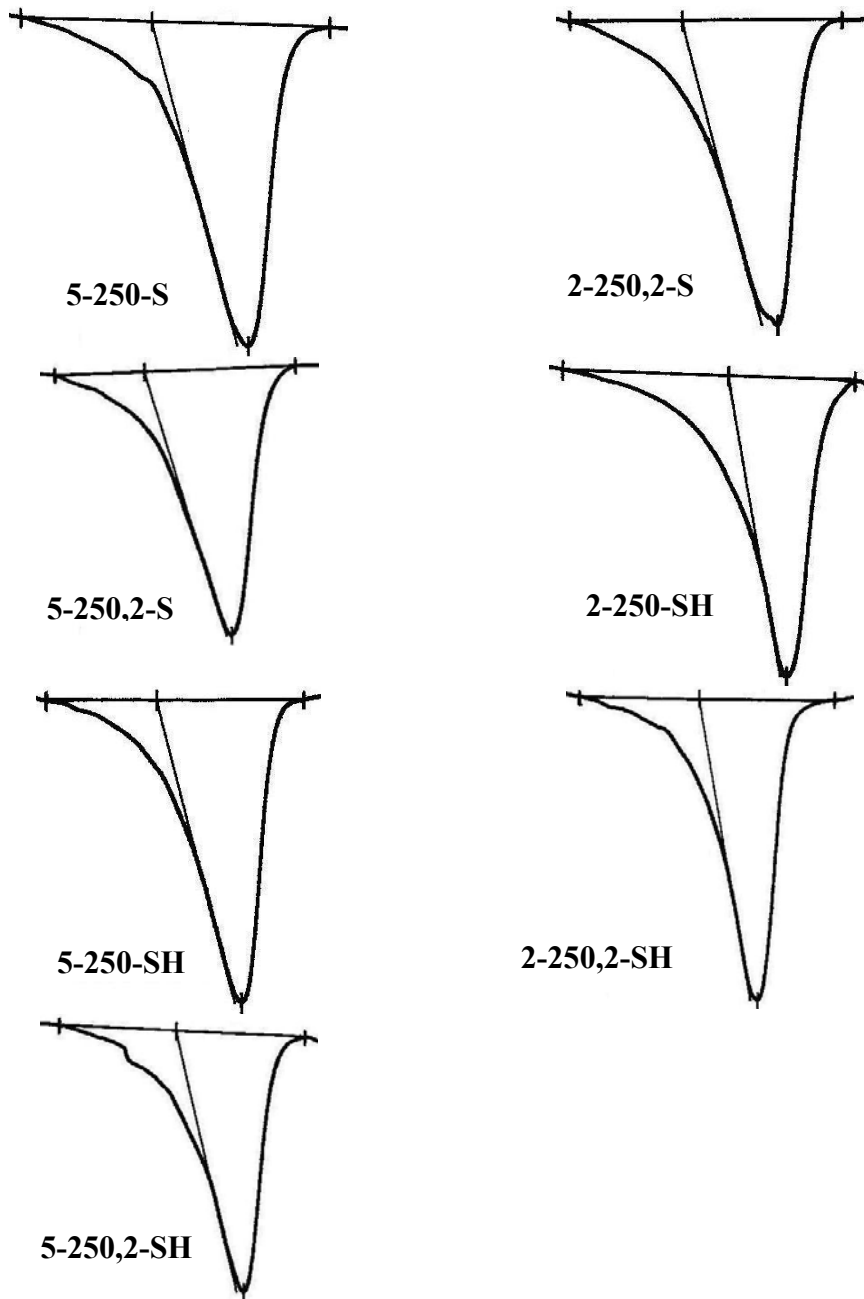


Figure E.1 (cont'd)

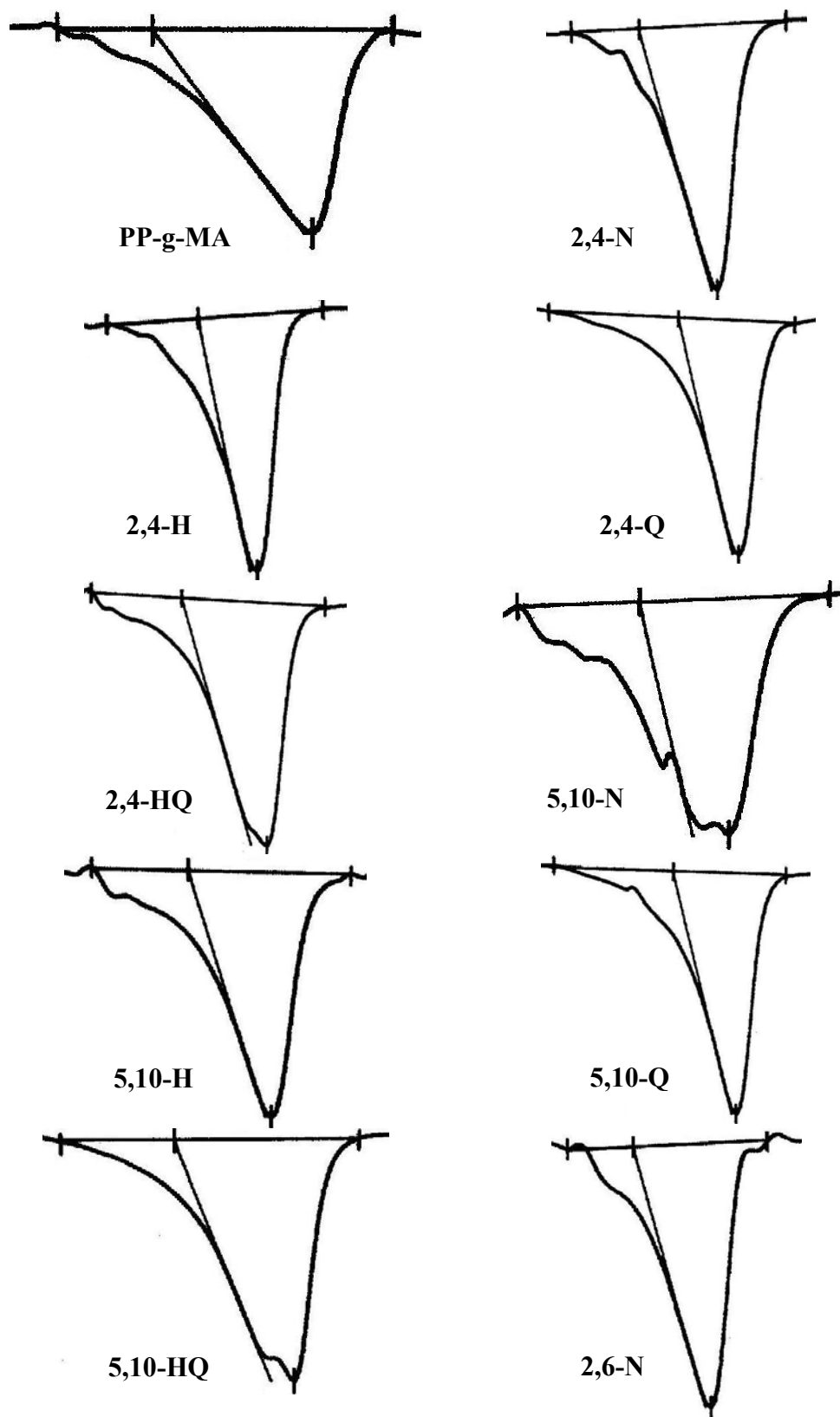


Figure E.2 DSC thermograms of group 2 compositions

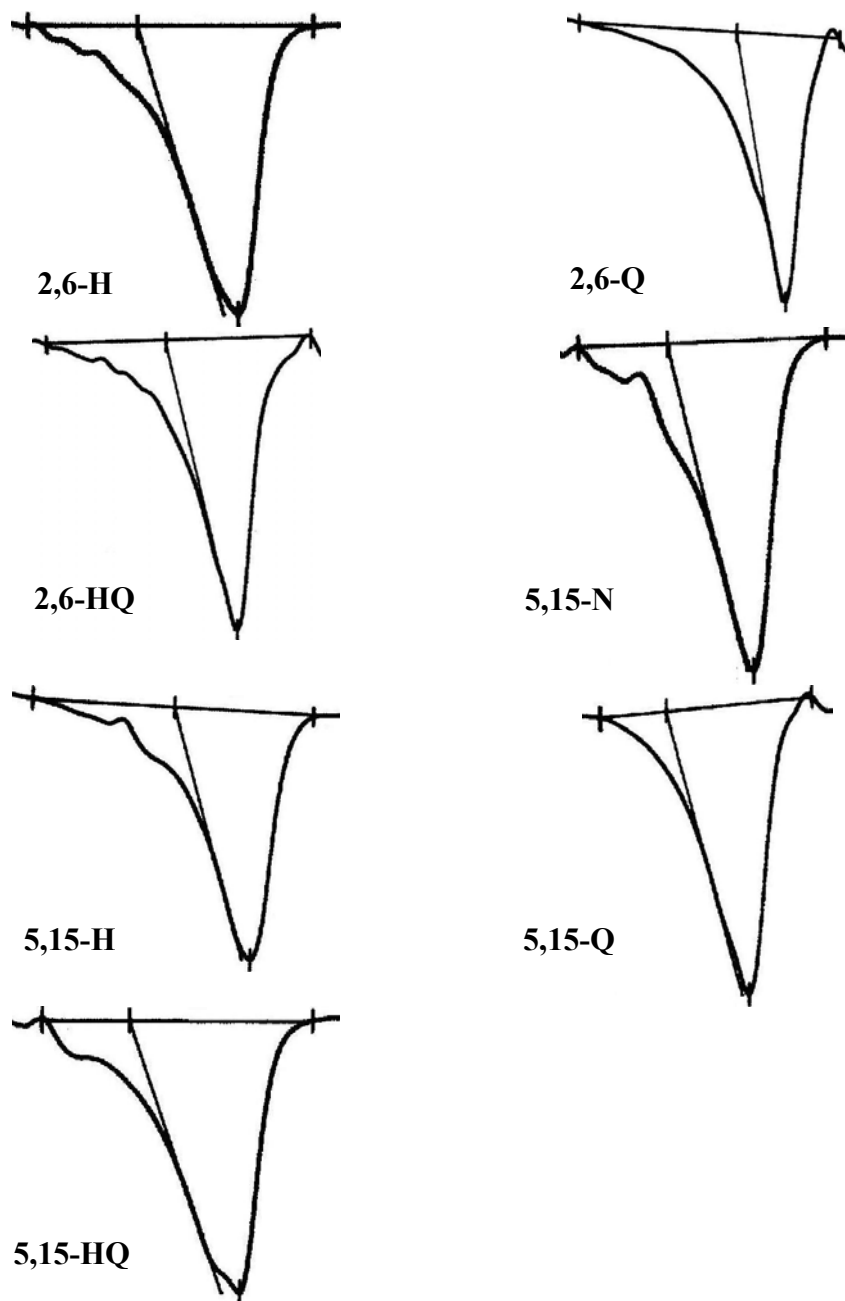
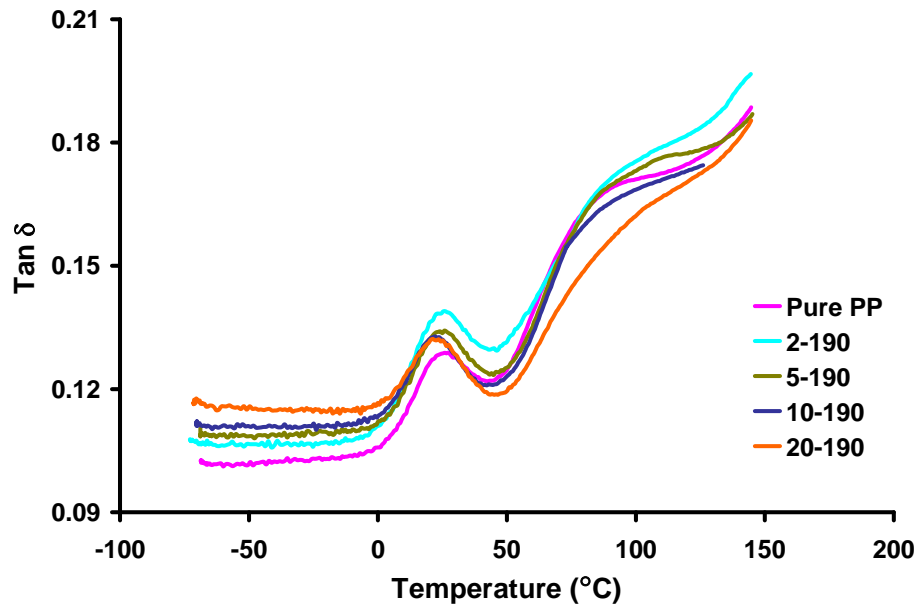


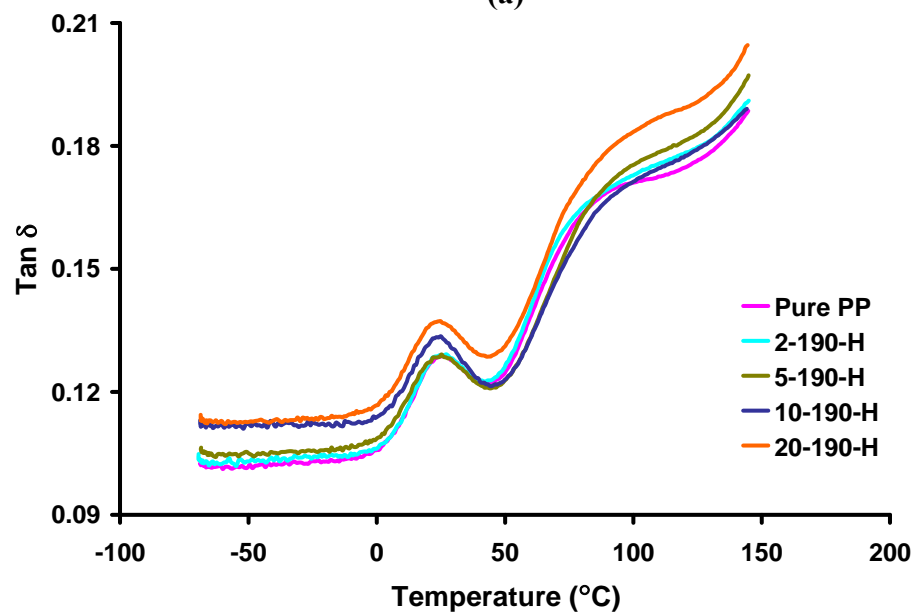
Figure E.2 (cont'd)

APPENDIX F

TAN δ vs. TEMPERATURE GRAPHS

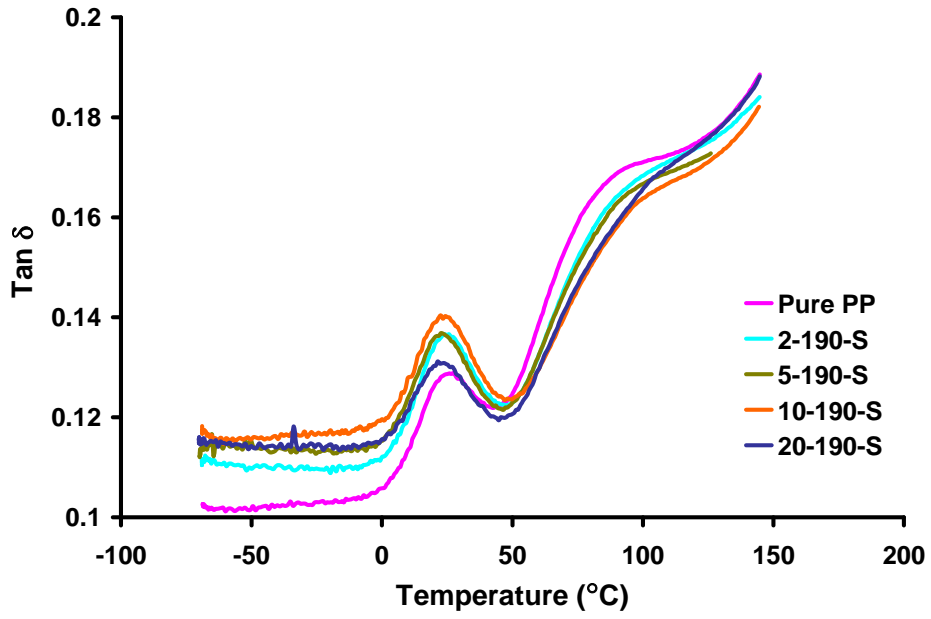


(a)

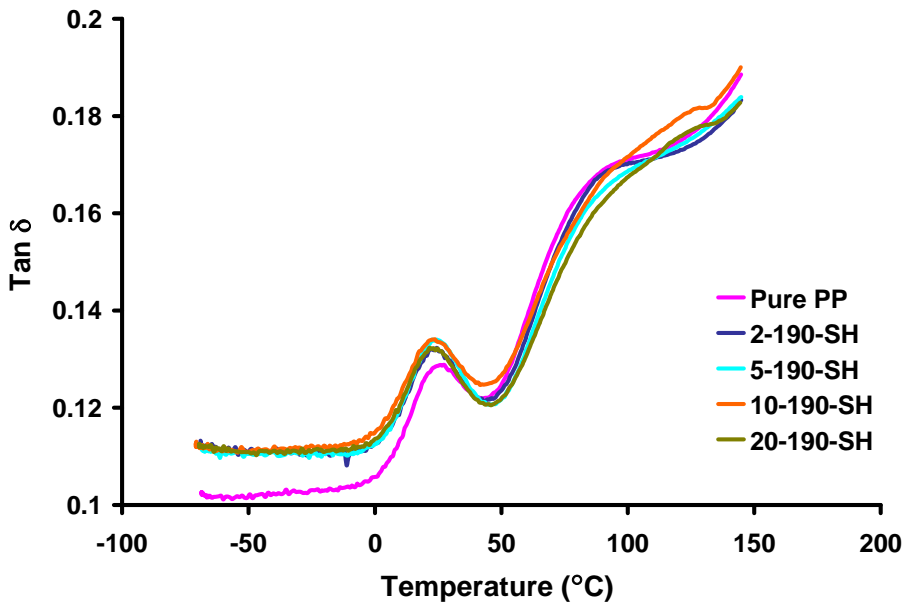


(b)

Figure F.1 Tan δ versus temperature scan for (a) N, (b) H compositions

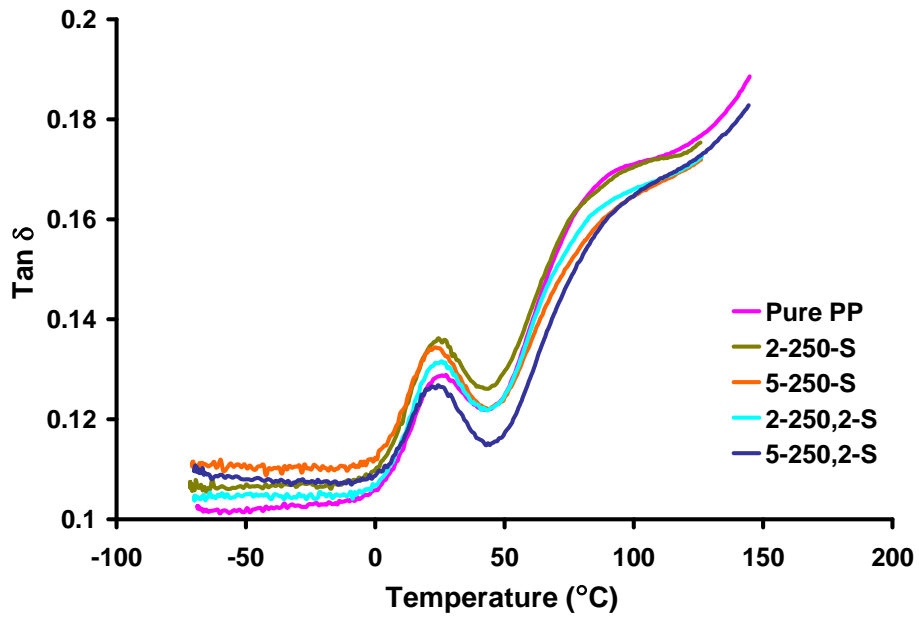


(a)

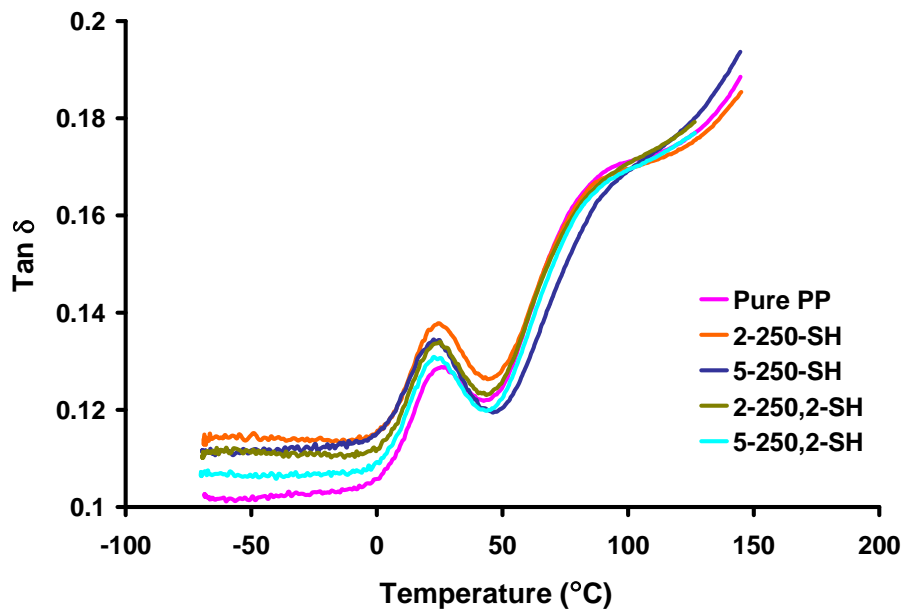


(b)

Figure F.2 Tan δ versus temperature scan for (a) S, (b) SH compositions

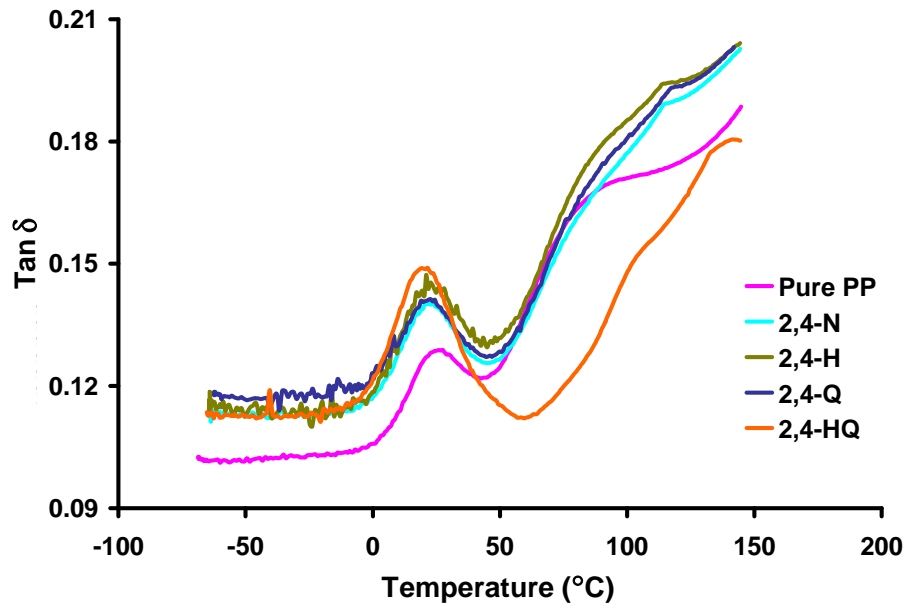


(a)

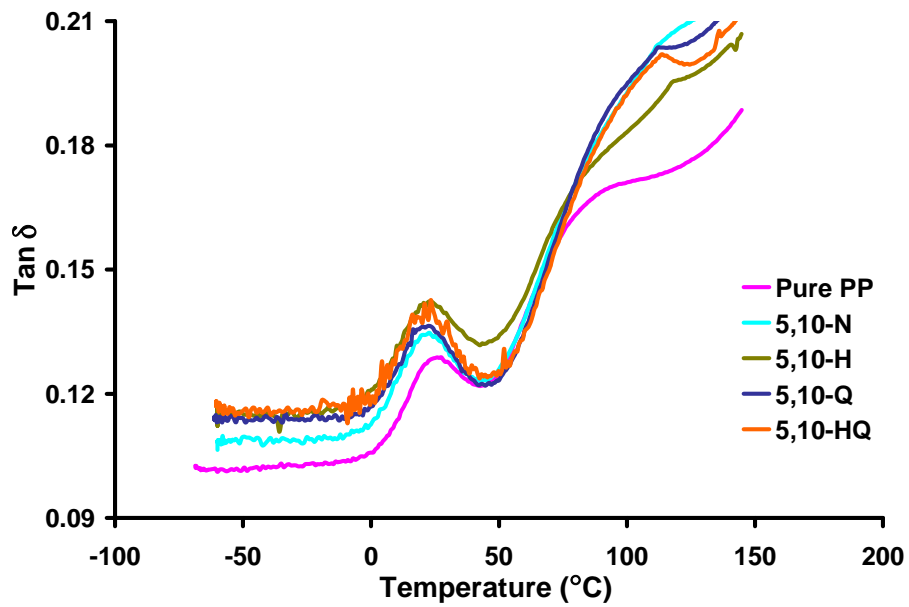


(b)

Figure F.3 $\tan \delta$ versus temperature scan for (a) S,250, (b) SH,250 compositions

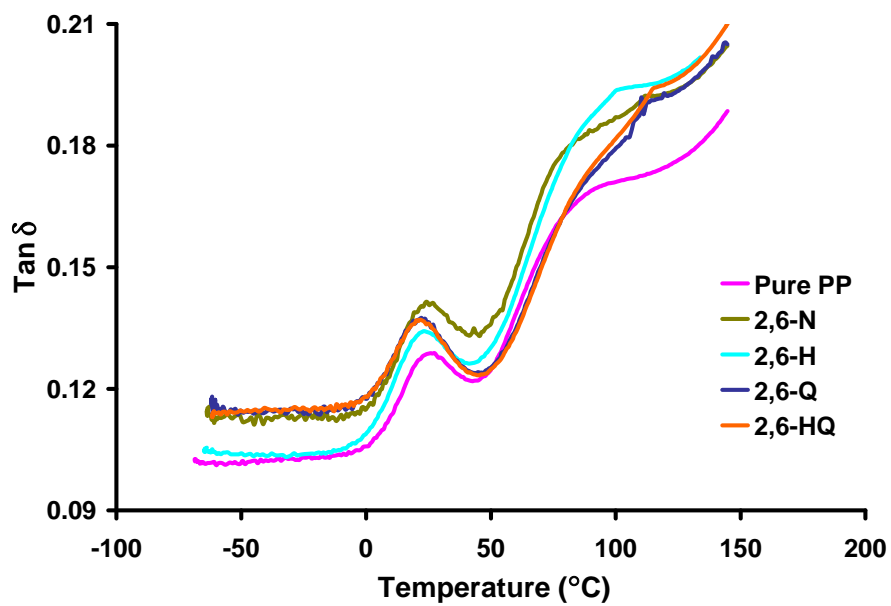


(a)

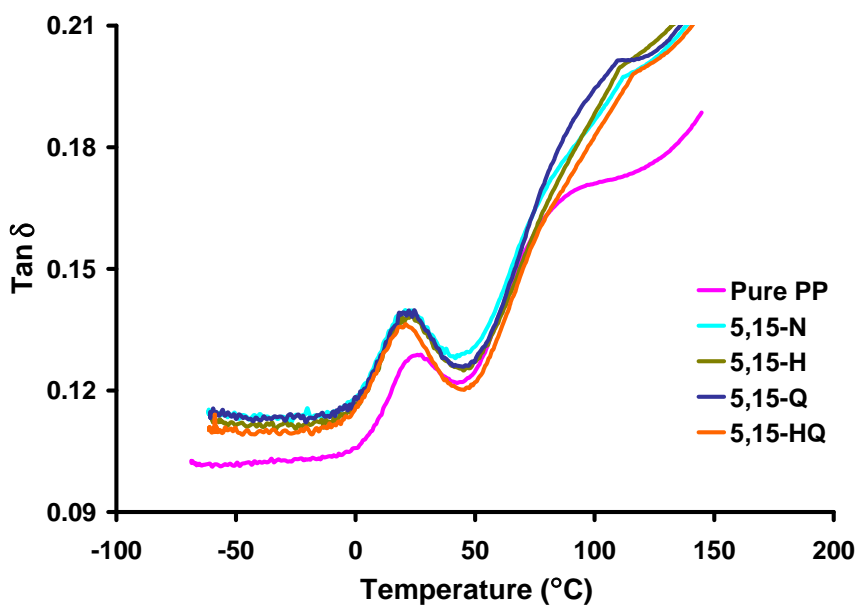


(b)

Figure F.4 $\tan \delta$ versus temperature scan for (a) 2,4, (b) 5,10 compositions



(a)



(b)

Figure F.5 Tan δ versus temperature scan for (a) 2,6, (b) 5,15 compositions

CURRICULUM VITAE

PERSONAL INFORMATION:

Name, Surname: Semra Can

Citizenship: Turkish

Date of Birth: 21.05.1977

EDUCATION:

B.S. in Chemistry (METU)

- Date of Graduation: June, 2000

Minor in Metallurgy and Materials Engineering (METU)

- Date of Graduation: June, 2000

M.S. in Polymer Science and Technology (METU)

- Date of Graduation: January 2003

CAREER RELATED EXPERIENCE:

- Project Student, 2007 April - continuing
METU, Department of Metallurgy and Materials Engineering
 - ❖ Metal Hydride Based Hydrogen Tube Production
 - ❖ Effect of Titanium Hydride Particle Size on Foaming of Aluminum
- Research Assistant, 2001 January–2007 April
METU, Department of Chemistry
- Summer Practice, Tüpraş (Turkey Petroleum Refineries) Aliğa,
İzmir/TURKEY 1999

CONFERENCE PROCEEDINGS:

- ‘Properties and Characterization of Al(OH)₃ and BaSO₄ Filled Polypropylene Copolymer’ Can S., Tinçer T., XVI. National Chemistry Congress, Selçuk University, Konya 2002 (poster presentation)
- ‘A Study on Thermal and Mechanical Properties of Mechanically Milled HDPE and PP’ Can S., Tan S., 3rd Balkan Metallurgy Conference, Ohrid, Macedonia, 2003 (oral presentation)